Complexity in financial time-series

Buonocore, Riccardo Junior

Awarding institution:
King's College London

Complexity in financial time-series

Riccardo Junior Buonocore

Department of Mathematics

King's College London

A thesis submitted for the degree of

Doctor of Philosophy

London, 2017

To my parents

Statement of Originality

I hereby declare that except where specific reference is made to the work of others, the contents of this dissertation are original and have not been submitted in whole or in part for consideration for any other degree or qualification in this, or any other university. This dissertation is my own work and contains nothing which is the outcome of work done in collaboration with others, except as specified in the text and Acknowledgements. This dissertation contains fewer than 100,000 words including footnotes.

Riccardo Junior Buonocore,

September 2017

Published and submitted papers

I list here the papers published in peer reviewed journals and in preparation that I produced during the course of my PhD and whose content has been used for this thesis:

1. R. J. Buonocore, T. Aste, T. Di Matteo, *Measuring multiscaling in financial time-series* Chaos, Solitons & Fractals 88, (2016);

2. R. J. Buonocore, N. Musmeci, T. Aste, T. Di Matteo, *Two different flavours of complexity in financial data*, Eur. Phys. J. Special Topics 225, (2016);

3. R. J. Buonocore, T. Aste, T. Di Matteo, *Asymptotic scaling properties and estimation of the Generalized Hurst Exponents in financial data*, Phys. Rev. E 95, 042311 (2017);

4. R. J. Buonocore, R. N. Mantegna, T. Di Matteo, *On the interplay between scaling properties and cross-correlation*, in preparation (2017);

5. Anshul Verma, R. J. Buonocore, T. Di Matteo, *A DBHT-driven log-volatility factor model: a deepening on the source of the volatility clustering*, in preparation (2017).

The results in paper 1 are reported in Ch. 4. The results in paper 3 are reported in Ch. 5. The results in paper 4 are reported in Ch. 6.

Acknowledgements

The journey of my PhD has been long and it is now coming to an end. I went through tough times but in some way I managed to get over the many difficulties I faced. However I have to say thank you to few people who managed to make this journey less heavy.

First of all, I would like to thank my parents: when I was younger they have always helped me to reach my goals and put me always in the position to study and focus on my personal development. I would like to thank them for their support throughout these years I spent abroad and for being always there, despite the distance.

I would also like to thank Tiziana, my supervisor, and Tomaso, her husband, whose help and humour made this experience more enjoyable.

A special thought goes to my historical group of friends from high school: Davide, Martina, Matteo, Stefano, Tommaso (in alphabetical order, so nobody complains). We almost all live abroad now, but when we manage to catch up again back in Rome, time seems to have not passed by and the very next day we have to go through some terrible interrogation at school.

I cannot avoid mentioning all the friends I made during my time spent at the university in Rome, but there is definitely not enough space to write the name of each of you; I built so many strong friendships during those years that I will never be grateful enough.

Your example always inspires me and makes me feel proud of the goals I reached in my life up to now.

A special thank goes to Nicolò for having been such a good advisor during these years at King's and also a very good friend outside. I want also to say thank you to Niccolò, Francesca and Anshul for sharing ups and downs, laughs and especially lunch times with me at King's.

I want to say thank you to the Sifu I found here in London, Austin Goh, for accepting me so warmly in his school: whenever everything seemed to turn me down, Kung Fu was always there.

At last I would like to say thank you to a new entry in the last months of my life, Alessandra 'Biscottona', for bearing with my melancholy, always managing to get a smile out of me.

Abstract

Many aspects contribute to make financial markets one of the most challenging system to understand. The aim of this thesis is to study some aspects of their complexity by focusing on univariate e multivariate properties of log-returns time-series, namely multifractality and cross-dependence.

In this thesis, we started by performing a thorough analysis of the scaling properties of synthetic time-series with different known scaling properties. This enabled us to do two things: find the presence of a strong bias in the estimation of the scaling exponents, and interpret measurement on real data which led us to uncover the true source of the multifractal behaviour of financial log-prices, which has been long debated in the literature. We addressed the presence of the bias by proposing a method which manages to filter out its presence and we validate it by applying it to synthetic time-series with known scaling properties and on empirical ones. We also found that this bias is due to the stability under aggregation of the log-returns which, due to their long memory, are processes which for high aggregation tend to a random variable which displays an exact multifractal scaling. Finally we focused the attention on linking the scaling properties of log-returns to their cross-correlation properties within a given market finding an intriguing non-linear relationship between the two quantities.

Contents

List of Figures

List of Tables

Chapter 1

Introduction

There is not a unique and commonly agreed definition of complex systems, but a common element in these systems is the presence of many parts that are interconnected, heterogeneous and often complex themselves [1, 2]. However it turns out to be quite simple to find good examples of complex systems like ecosystems, the weather, cities. According to [1], the approach for studying such systems had to change with respect to already established ones, due to technical difficulties. In particular, in a classical perspective we are interested in describing the exact trajectory of a system, given the initial position and velocity. This approach is challenged by the introduction of chaotic systems, where we can only hope to compute the probability distribution of finding the system under study in a certain state for a large evolution time [1], due to the fact that we are not able to compute with infinite precision the initial conditions. In complex systems, another layer of uncertainty is added: the uncertainty about the exact equations of motion which drive the system [1]. In such a setting, the only viable approach is to study the possible behaviour of the systems, based on a class of possible driving equations of motion [1].

In this picture, financial markets, and more in general economical systems, fit perfectly. In fact, not only we do not know what every market participant thinks in a given moment in time (initial condition), but we also do not have any idea of what will be his/her reactions to the myriads of news we are bom-

barded from nowadays (driving laws of the system). In particular, financial markets are systems where participants interact among each others with different strategies, using different technologies, at different time and volume scales and at different frequencies [3]; they are open systems where many subunits interact nonlinearly in the presence of feedback [4, 5]. Luckily beside their complexity, financial markets are the most data-rich case study among complex systems, where interactions between individuals, machines and the real world are present all at the same time. In markets all the elements contribute in different ways to the emergence of a price for each asset. These prices are the consequences of the complex interactions between all these elements and such a complexity is revealed in their behaviours that have statistical properties which change with the time-horizon, following non simple patterns.

The main motivation of this thesis is to further investigate the change of behaviour of single price time-series at different time-scales and compare them with the theoretical picture of the multifractal scaling, but also to relate the transition between different aggregation horizons with the interaction present between prices of different stocks. [1] In order to achieve these goals, we focused our attention on two different tools: the multifractal analysis, to study how the statistical properties of single time-series change by changing the time-horizon at which they are observed; and the cross-correlation analysis, to unveil the presence of dependences between different stocks in a market. In complying with this plan we pointed out that the main theoretical assumptions of the multifractal framework cannot be inherently met by the empirical data. As a consequence, multifractality measures may be affected by strong biases which manifest themselves as a transient unstable phase between the statistical properties at small and big time-scales of financial log-returns time-series. In spite of this, we show that in an asymptotic sense, financial time-series can still

[1] It is worth mentioning that an effort in this direction has already been done in [6], but the results seem to hold only in one specific market.

be regarded as multifractal, so we devised an algorithm which manages to filter out this transient for long enough time-series. Finally we found that the scaling behaviour is actually linked to the cross-dependence properties of the time-series.

The rest of the thesis is organized as follows: Chapters 2 and 3 are dedicated to the review of the main stylized facts of the financial log-returns time-series. In Chapter 2 we start by reviewing those which have been widely recognized since the early work of Mandelbrot [7]. We then describe the two main classes of models available in the literature: GARCH-type models and Stochastic Volatility models. For both classes we review univariate and multivariate models which try to implement the stylized facts discussed in the first part of the chapter. Chapter 3 is instead dedicated to a stylized fact which has been widely discussed but only in the last two decades (in the financial context): multifractality. We first give a formal definition distinguishing between a geometrical and a statistical characterization, showing that the two can actually be matched. We follow by reviewing the most widely used estimation models present in the literature highlighting strong points and drawbacks for each of them. Finally we discuss the main models which try to reproduce this statistical property.

In Chapter 4 we tackle the problem of understanding what is the true source of the multifractal scaling of financial log-returns time-series [8]. We review first the state of the art by pointing out that no agreement is present in the literature. Then, after describing the estimator we intend to use, we check its performances on time-series with known scaling properties in order to have a clear benchmark for the interpretation of the results on the empirical time-series. This preliminary analysis is in fact followed by the analysis of an empirical dataset which allows us to recognize the memory as the main

source of the multifractal behaviour, but also to identify strong biases in the estimation, due to the presence of power law tails and the memory itself.

Chapter 5 deals with the problem of defining a statistically reliable method for measuring the scaling exponents [9] by managing to filter away the bias discussed in Chapter 4. It starts by pointing out that the estimation problems of the scaling exponents arise from the discreteness in time of the data, since, according to the theoretical definition, multifractality is defined only for processes continuous in time. In particular through the comparison with a theoretical model it is inferred that the biases in the estimation arise because real processes are not stable under aggregation and reach their true scaling behaviour only asymptotically. Following this intuition, a method is devised for filtering out the transient behaviour without knowing its actual functional shape. This method is tested on synthetic multifractal series proving its unbiasedness and finally it is also applied to real empirical intraday data.

The analysis in Chapter 6 takes its steps from a recent paper where an overview of the multivariate and univariate properties of financial log-returns is given [2]. The main idea is to test whether a link exists between the scaling properties of empirical log-returns and their cross-dependence [10]. It starts by describing the dataset which is made of six different markets and also of the corresponding capitalization of each stock in each market. Then, after defining appropriate estimators for the two considered properties, a non-linear dependence between the two is found, which correlate also with the capitalization. Validation tests are carried on to prove the robustness of the result and understand its main source. Following the speculation made in Chapter 4, the source is found in the tails. The behaviour found, on one hand tells us that the stability under aggregation of single time-series depends on their cross-dependence properties, and on the other can be interpreted in terms of efficiency of the single stocks time-series.

Chapter 2

Stylized facts and models in finance: an overview

The aim of this chapter is to give a brief review of the statistical properties called in the financial jargon stylized facts. Examples of these statistical facts are shown on reference time-series like the *Standard & Poor's 500* index and also those in the *New York Stock Exchange*, *Nasdaq Stock Market* and NYSE MKT LLC. We also review the main models present in the literature dividing them in the two broad categories of GARCH family models and Stochastic Volatility models both in the univariate and multivariate case.

2.1 Introduction

The first attempt to model market stock prices dates back to the 1900, when Bachelier published his famous PhD thesis called "Theorie de la Speculation" [11]. However this field of research took its time to develop in a consistent way. In particular the next notable progress in the field was made more than 50 years later by Markovitz [12] with its asset allocation method based on optimization techniques. It took other 20 years before a systematic procedure for pricing financial products was introduced with the famous Black and Scholes formula [13]. Notably, both [12] and [13] are Nobel prize winning works and are both based on the assumption that prices (or log-prices) follow a random walk behaviour, namely the Brownian Motion (BM). It was soon understood

that the innovation of log-prices are not independent from each other and that rare events are more common that what may be expected from the BM assumption. In particular, the first who pointed this out was Mandelbrot in [7] where he proposed that prices follow an α-stable distribution and also noticed the presence of the so-called volatility clustering. The main drawback of a process with innovations drawn from an α-stable distributions is that it has increments with infinite variance, which seems not to be the case in empirical dataset (cfr. [14, 15]), and also they still neglect memory. In order to overcome the absence of memory, in the Eighties the Nobel prize winning ARCH model was introduced [16], giving rise to a massive stream of literature which tried to refine this first model by adding more parameters which should mirror empirical statistical properties both on the univariate and a multivariate level.

In this chapter we review the main statistical properties of daily data using as time-series taken from *New York Stock Exchange*, *Nasdaq Stock Market* and NYSE MKT LLC, which we will call collectively by using the acronym NYSE17 and the *Standard & Poor's 500* index. We also discuss the main models proposed in the literature able to reproduce these features. The rest of the chapter is organized as follows: in Sec. 2.2 we review the main stylized facts of financial log-returns, in Sec. 2.3 we discuss the main models available in the literature while we make a summary of the chapter in Sec. 2.4.

2.2 Main stylized facts

2.2.1 Variable of interest

Among many, the price $p(t)$ of a certain asset at time t is one of its most important properties. As an example. in Fig. 2.1 we report the daily last price of the *Standard & Poor's 500* (SPX) from the 04/03/1957 up to the 06/03/2017. However, from a statistical point of view, it is not the most appealing. The main reason rely on the fact that the price of a time-series

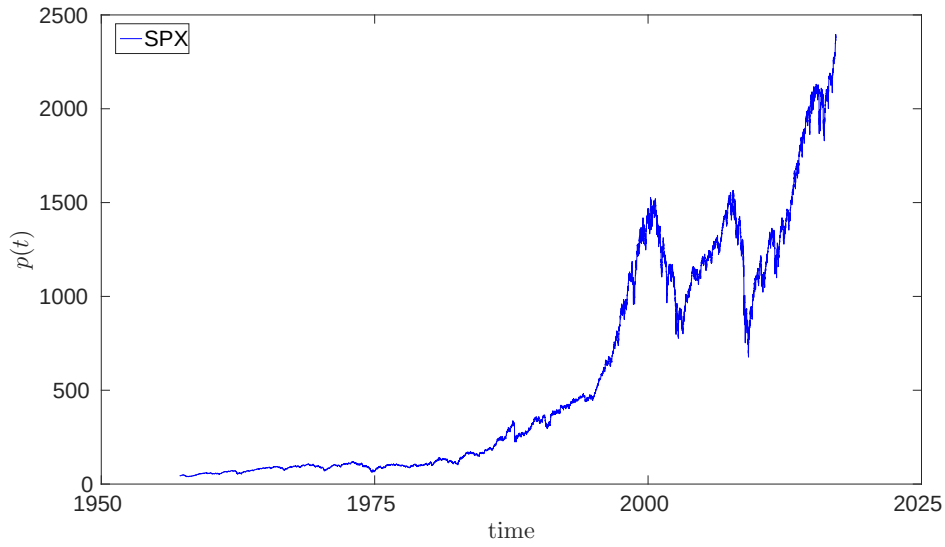

Figure 2.1: SPX Index last daily price from the 04/03/1957 up to the 06/03/2017.

is certainly not a stationary quantity. The price value, at a certain point in time, heavily depends on its previous value, also its mean and standard deviation vary in time [1]. In order to mitigate this effect, the increments of the price process might be considered. Assuming for a moment that the time t is measured in days, one possibility for the one day returns is to use

$$r_1^*(t) = \frac{p(t+1) - p(t)}{p(t)}. \tag{2.1}$$

However the most used definition for price increments is the following [18, 3]

$$r_1(t) = \ln[p(t+1)] - \ln[p(t))], \tag{2.2}$$

which are then called log-returns. Among the reasons why definition in Eq. (2.2) is preferred with respect to the one in Eq. (2.1) is that by using definition (2.3) it is easy to compute the compound return over bigger time-horizons, which we call $r_\tau(t)$. Indeed the computation consists in a sum of subsequent

[1] For a BM only the standard deviation is time dependent, while the mean is equal to zero. However for empirical prices there is evidence in the literature that they have a time changing mean [17]

one-step returns which boils down to the difference of the first and last term:

$$r_\tau(t) = \ln[p(t+\tau)] - \ln[p(t))]. \tag{2.3}$$

As for Eq. (2.1), its compound version is made of a product of many factors, which becomes bigger as the horizon we are computing the compound returns on becomes longer. Also, When the returns are small, the difference of small numbers is a fairly safe operation, while the productory of them could end up in arithmetic underflow. In Fig. 2.2 we report the log-returns time-series of the SPX dataset. The definition in Eq. (2.3) is the one we use in the rest of the thesis.

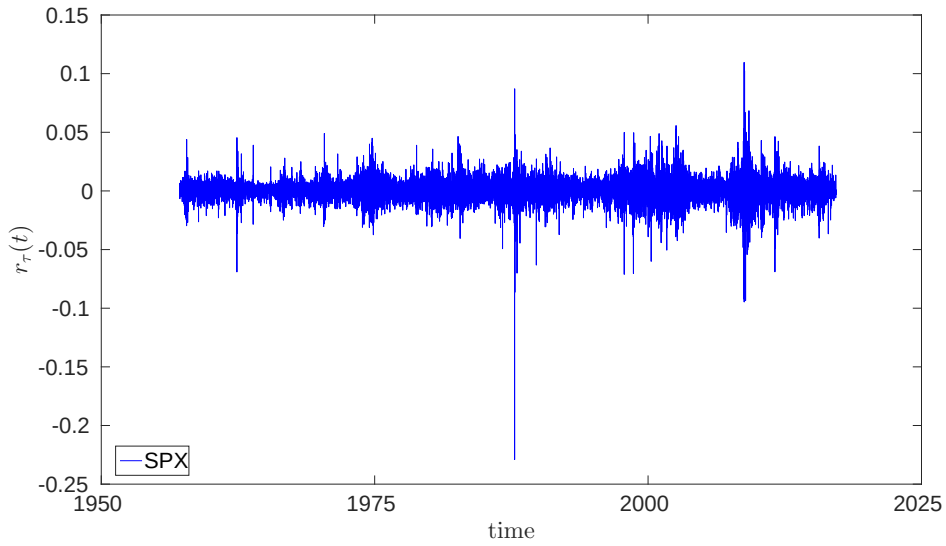

Figure 2.2: SPX Index daily log-returns from the 05/03/1957 up to the 06/03/2017.

2.2.2 A remark on stationarity

As it will be underlined in a subsequent section, log-returns are not stationary random variables as well. However they are better behaved than prices. From an operative point of view trying to reduce the non-stationarities as much as possible is paramount. If at every point in time t the statistical properties of

the time-series under study changed in an unknown way, we would not be able to make any inference about the generating process underlying financial time-series. The assumption of stationarity, which underlies any empirical analysis, allows us to substitute averages computed over the distribution with averages computed over time

$$E[f(t)] \approx \langle f(t) \rangle_t, \tag{2.4}$$

where $E[\cdot]$ is the usual expectation, f is a dummy function and $\langle \cdot \rangle_t$ is the average over time. This substitution, despite not explicitly written, will hold for the rest of the thesis when we deal with empirical data. We now review the main statistical properties of financial log-returns.

2.2.3 Fat tails

With the expression "fat tails", people refers to the tendency of extreme events to occur more often than one would expect by assuming that the logarithm of the prices follows a BM. Indeed the tails of a BM decay exponentially towards plus and minus infinity while, empirically, the tails of the financial log-returns have been found to decay as a power law [15, 14]. For example for the right tail we can write

$$P(r_\tau(t) > x) \propto x^{-\alpha_R} \qquad \text{for } x > 0. \tag{2.5}$$

With $\alpha_R \in [2, 5]$ [15]. A similar relation holds also for the left tail,

$$P(-r_\tau(t) > x) \propto x^{-\alpha_L} \qquad \text{for } x > 0. \tag{2.6}$$

with the α_L exponent lying in the same range. The two exponents α_L and α_R are usually slightly different which actually means that the log-returns unconditional distribution is skewed (see Subsec. 2.2.5). To give an example we computed and plot the decay exponents of the tails using the method proposed in [19, 20], based on Maximum-Likelihood Estimators and the Kolmogorov-

Smirnov test. The value we found are

$$\alpha_L = 3.80 \pm 0.10, \quad \alpha_R = 3.78 \pm 0.09; \tag{2.7}$$

which in this case are not different within the error bars. In Fig. 2.3 it is reported the fit of the complementary cumulative distribution of the left and the right tails in loglog scale. For the left tail on the x-axis is reported the logarithm of minus the negative returns. As a further empirical example let us

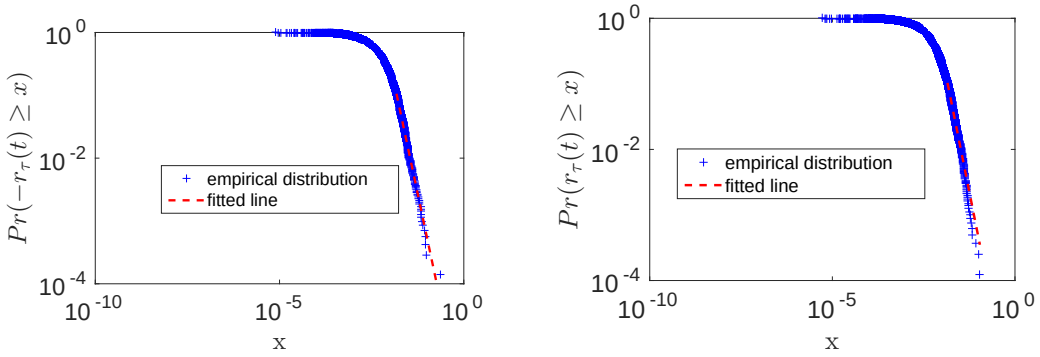

(a) (b)

Figure 2.3: (a) left tail of the SPX log-returns time-series, (b) right tail of the SPX log-returns time-series.

show in Fig. 2.4 the distribution of α_L and α_R we found on the NYSE17 dataset which is made of daily prices of the aforementioned markets from 01/01/2000 up to 12/05/2017 [2]. As we can see the variance is always finite since the values of α_L and α_R are always bigger than 2. The presence of tails implies that the core of the distribution is more peaked with respect to the Gaussian distribution, thus another measure of the presence of fat tails which weights more the values in the tails than those in the core is the kurtosis, defined as

$$\gamma_2 = \frac{E\left[(r_\tau(t) - E\left[r_\tau(t)\right])^4\right]}{E^2\left[(r_\tau(t) - E\left[r_\tau(t)\right])^2\right]}. \tag{2.8}$$

Sometimes the excess kurtosis is used, defined as $\gamma_2' = \gamma_2 - 3$, which is simply the difference between the kurtosis of the given data and the kurtosis of a

[2] Further details on this dataset are given in Ch. 6

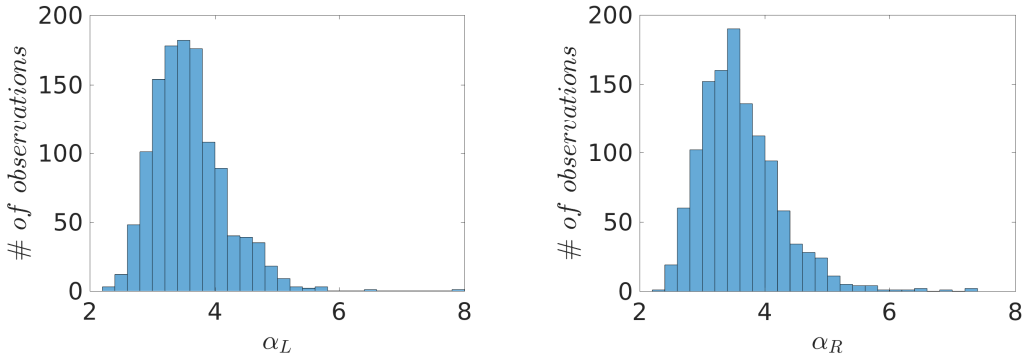

(a) (b)

Figure 2.4: (a) left tail distribution of the NYSE17 log-returns dataset, (b) right tail distribution of the NYSE17 log-returns dataset.

Gaussian distribution, which is equal to 3. As above, we show in Fig. 2.5 the distribution of the values of γ_2 for the NYSE17 dataset. We observe that extremely high values are present. This is due to the fact that not every empirical log-returns time-series has a finite fourth moment (see Fig. 2.4).

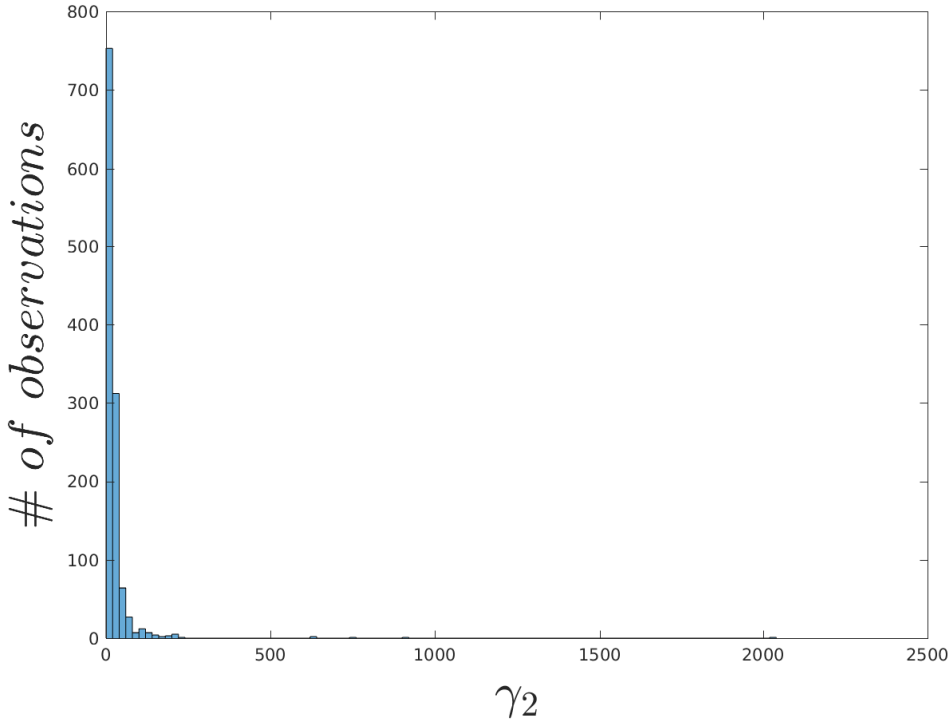

Figure 2.5: Distribution of the kurtosis coefficients for the NYSE17 dataset.

2.2.4 Memory

Daily log-returns do not exhibit autocorrelation, only in intraday data serial correlation in plain log-returns is observed but just over few minutes [14]. The reason is that serial correlation in plain log-returns would offer an easy chance to make profit for a trader. Thus, even if some tiny serial correlation is observed at a certain point in time, somebody take quickly advantage of it making it disappear. This process happens so quickly that on a daily basis, it is quite safe to consider log-returns not serially correlated *i.e.*

$$\mathrm{Corr}\left[r_\tau(t+T), r_\tau(t)\right] = 0, \qquad T \geq 1. \tag{2.9}$$

In Fig. 2.6 we report, among others, the autocorrelation function of the log-returns for SPX, which fluctuates around zero. However daily log-returns are far from being independent draws from one (or many) distribution. The empirical observation of the so-called volatility clustering is an evidence of this fact. In Fig. 2.2 this property can be spotted by noting that periods of high fluctuation alternate with periods of small fluctuations. In particular the late 80s crisis and the 2007-2008 crisis are easily recognizable. Since the paper of Engle [21], this property has been modelled by assuming that the autocorrelation function of powers of the absolute values of the log-returns decays as a power law. In particular it has been found that different powers γ of absolute log-returns have different power law decay rates with an exponent $\beta(\gamma) \in [0, 1]$ [21, 22]. We can summarise this observation as

$$\mathrm{Corr}\left[|r_\tau(t+T)|^\gamma, |r_\tau(t)|^\gamma\right] \propto T^{-\beta(\gamma)} \qquad T \geq 1. \tag{2.10}$$

Interestingly, the maximum autocorrelation is found empirically for around $\gamma = 1$ [21]. As an example, we report in Fig. 2.6 the behaviour of the auto-correlation function of few powers of absolute returns for SPX. An interesting method for computing the value of $\beta(\gamma)$ is proposed in [22]. Let us describe it

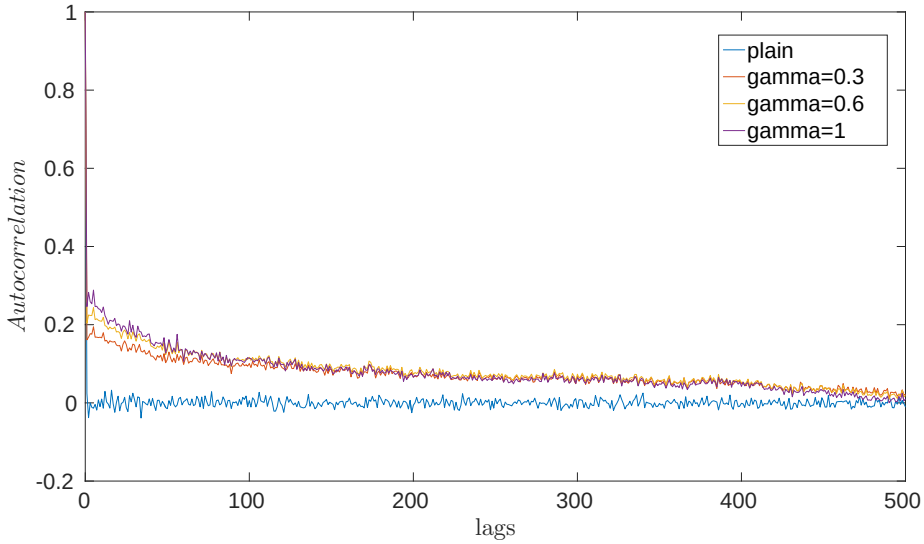

Figure 2.6: Empirical autocorrelation function computed on SPX for plain log-returns and different powers of absolute log-returns.

here briefely. The generalized cumulative absolute returns can be introduced as (cfr. [22])

$$\chi_t(L,\gamma) = \frac{1}{L}\sum_{i=0}^{L-1} |r_\tau(t+i)|^\gamma, \tag{2.11}$$

which is a sum of successive absolute returns raised to the power of γ. This quantities are defined to be non-overlapping for different values of t. It can be shown (we provide a proof of this in Appendix A) that if

$$\mathrm{Cov}\left[|r_\tau(t+L)|, |r_\tau(t)|\right] \propto L^{-\beta(\gamma)}, \qquad \beta(\gamma) \leq 1, \tag{2.12}$$

then the standard deviation, $\delta(L,\gamma)$, of $\chi_t(L,\gamma)$ goes as

$$\delta(L,\gamma) \propto L^{-\eta(\gamma)}, \qquad \text{with } \eta(\gamma) = \frac{\beta(\gamma)}{2}. \tag{2.13}$$

The distribution of the values of $\beta(1)$ we obtain through this procedure can be found in Fig. 2.7; we notice that in our dataset $\beta(1)$ does not exceed 0.5.

2.2.5 Skewness and leverage effect

The skewness and the leverage effect are two stylized facts which are linked but not equivalent. The skewness property refers to the asymmetry of the log-

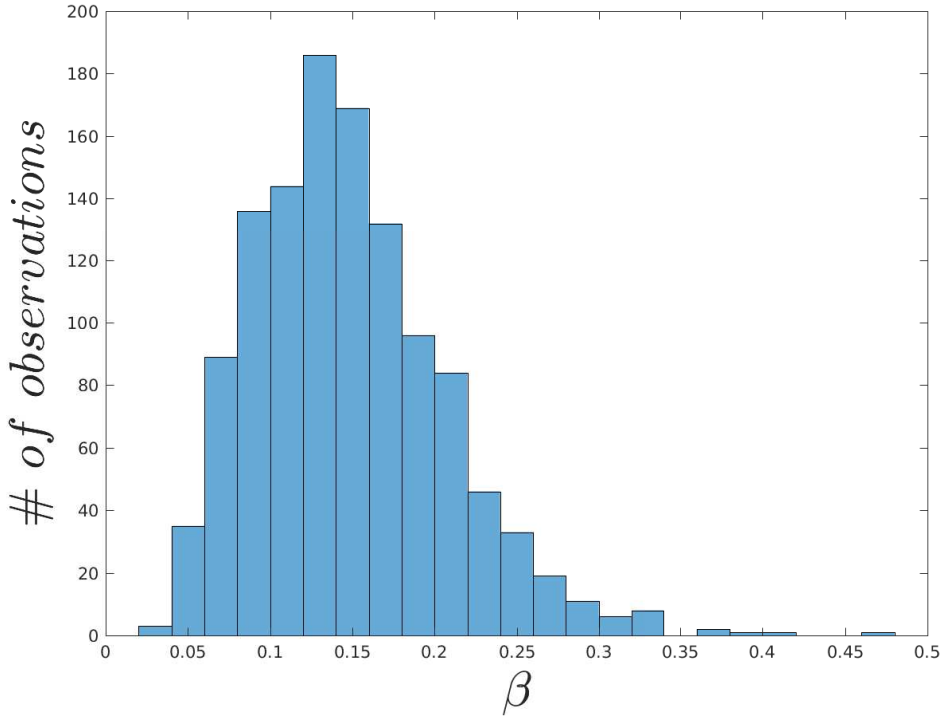

Figure 2.7: Distribution of the decay coefficient of the memory of the absolute log-returns for the for the NYSE17 dataset.

returns unconditional distribution, which usually are found to have a longer left tail and a shorter right tail. This means that the left tail is in general expected to be fatter than the right one. A way to quantify this property is via the third central moment

$$\gamma_1 = \frac{E\left[\left(r_\tau(t) - E\left[r_\tau(t)\right]\right)^3\right]}{E^{3/2}\left[\left(r_\tau(t) - E\left[r_\tau(t)\right]\right)^2\right]}. \tag{2.14}$$

When $\gamma_1 < 0$ the distribution is said left-skewed and it means that the left tail is fatter than the right one. Instead, when $\gamma_1 > 0$ the distribution is said right-skewed and it means that the right tail is fatter than the left one. To give an example, let us report in Fig. 2.8 the distribution of the skewness coefficients for the NYSE17 dataset. Another way to characterize the asymmetry of a probability density is via the non parametric skewness (see for example [23]),

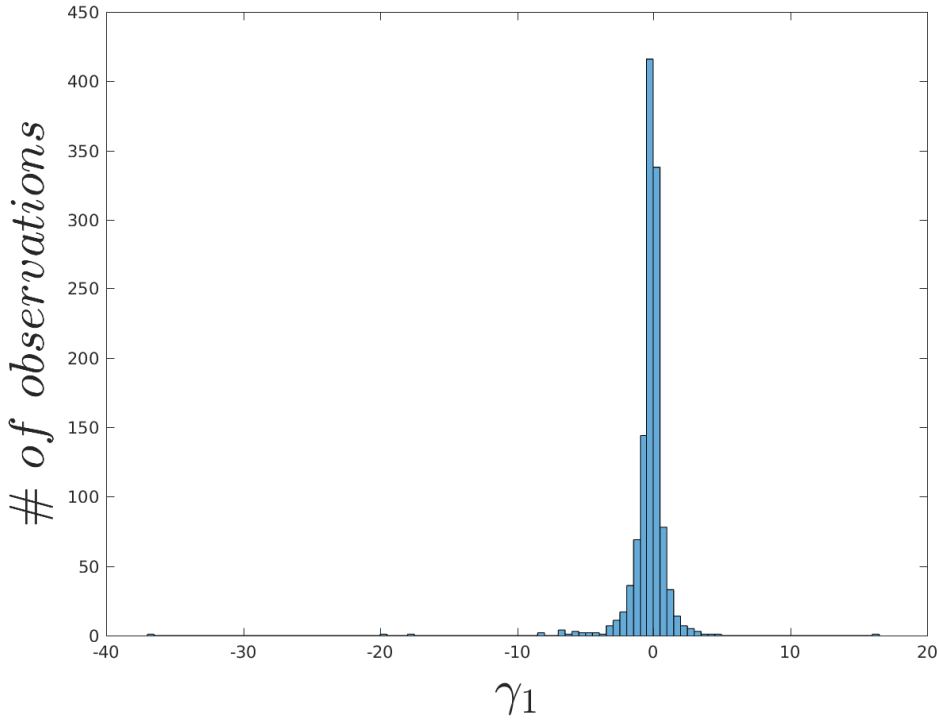

Figure 2.8: Distribution of the skewness coefficients for the NYSE17 dataset.

defined as

$$S = \frac{E\left[r_\tau(t)\right] - median\left[r_\tau(t)\right]}{\sqrt{E\left[\left(r_\tau(t) - E\left[r_\tau(t)\right]\right)^2\right]}}. \tag{2.15}$$

The interpretation of the non parametric skewness is the same as for Eq. (2.14).

Leverage effect refers to the tendency of the volatility to increase after a price drop [24, 25]. In order to quantify this effect, one can consider the lagged correlation between the log-returns and their absolute value:

$$L(T) = \mathrm{Corr}\left[r_\tau(t), |r_\tau(t+T)|\right], \tag{2.16}$$

where T is the time-lag between the two quantities. As an example we report in Fig. 2.9 the behaviour of the function $L(T)$ for SPX in a blue solid line for positive and negative lags. For negative lags $L(T)$ keeps oscillating around zero whereas for positive lags it is negative and decays exponentially to zero [25], as shown by the exponential fit in a red dashed line.

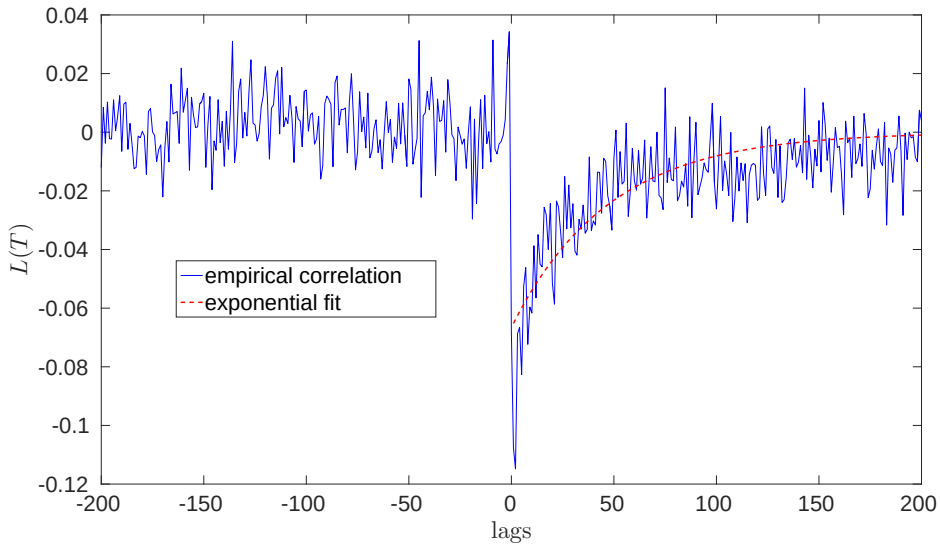

Figure 2.9: Empirical values of the function $L(T)$ in blue solid line computed on SPX along with an exponential fit in red dashed line.

In light of these observations we can say that the presence of the leverage effect implies a skewness in the probability density function, but not the other way around. In particular, the presence of skewness alone does not affect the temporal structure of a time-series.

2.2.6 Cross-dependence

An important and widely studied property of log-returns is their cross-dependence. In particular this dependence has been observed across different industries and asset classes [18, 26]. A plausible explanation of this behaviour is that traders react simultaneously to new information and also share accidentally same trading strategies [18]. It is worth noting that, despite the presence of these dependencies does not necessarily imply arbitrage [18], some authors managed to take advantage of their presence in order to build profitable strategies, thus challenging the Efficient Market Hypothesis (EMH) [27].

The main measure of cross-dependence is the cross-correlation matrix which, given the log-returns time-series of two different stocks $r_i(t)$ and $r_j(t)$, reads

as

$$\Sigma ij = \mathrm{Corr}\left[r_i(t), r_j(t)\right]. \tag{2.17}$$

As it appears evident, Eq. 2.17 tests only for linear dependence between stock i and j, nonethelss interest in the cross-correlation matrix has grown since the introduction of the Nobel prize winning Markovitz portfolio selection [12], which is based on it. Despite the simplicity of its formula, the proper estimation of the cross-correlation matrix is not an easy task, due to the presence of statistical fluctuations and redundancies [28]. In light of this a sweeping amount of papers have been published dealing with the problem of de-noising the cross-correlations matrix (see for example [29, 30, 31, 32, 33, 34, 35, 36, 37, 38, 39, 40, 41, 42, 43]). One of the most popular tools introduced in order to achieve this task are the information filtering networks [5, 18, 44, 45]. They are based on the intuition that a cross-correlation matrix can be mapped into a sparse graph which retain only a subset of the information enclosed in the original matrix according to some filtering criterion. For example for the Minimum Spanning Tree (MST) [44] the filtering criterion consists in building a graph without creating loops among the nodes, whereas for Embedded Graphs [30, 32, 46] the filtering criterion is to map the matrix into a topological surface with a fixed genus. When the genus is equal to zero, the surface becomes a plane and the result of the filtering technique is called Planar Maximally Filtered Graph (PMFG) [29, 30]. Once the graphs are built, hierarchical clustering techniques can be applied. Among many, we report that the Linkage family of clustering techniques are applied to MST type of graph [47], for example Single Linkage, Average Linkage and Complete Linkage [48]. As for the PMFG, the recently proposed Directed Bubble Hierarchical Tree (DBHT) was proposed as its natural clustering method [35, 34]. Finally let us mention that in [49] an empirical relationship between the volatility cross-correlation and the volatility clustering was found, while in [50] a model based on the DBHT

was proposed to explain this phenomenon.

2.3 Models

In the econometric literature, models for the log-returns can be divided in two broad categories: GARCH-type models and Stochastic Volatility (SV) models, both univariate and multivariate. Their main aim is to reproduce the main stylized facts of financial log-returns usually introducing a set of (or just one) *ad hoc* parameters for each of them. Despite at a first glance they might look similar, they have a fundamental difference: in GARCH-type models the conditional volatility is a deterministic function of the previous innovations, while in the SV models the conditional volatility is random but drawn from a known distribution. Before giving an overview of these two families, let me briefly describe three fundamental models: the autoregressive model (AR), the moving average model (MA), the autoregressive moving average (ARMA) model (see for example [51]), which encloses features of both AR and MA models.

1. An AR(p) model, where p is the order, is a model where the current value of the process X_t depends linearly on its past p realizations. It can be specified as
$$X_t = c + \sum_{i=1}^{p} \varphi_i X_{t-i} + \varepsilon_t, \tag{2.18}$$
where c is a constant, $(\varphi_i)_{i\in[1,p]}$ is a vector made of p components which defines the impact of past events on the new one (from which the name comes from) and ε_t is white noise.

2. A MA(q) model, where q is the order, is a model where the current value of the process X_t depends linearly on the present and also on the past q values of the random shocks. It can be specified by
$$X_t = \mu + \sum_{i=0}^{q} \vartheta_i \varepsilon_{t-i}, \tag{2.19}$$

where μ is the mean of the process X_t, $(\vartheta_i)_{i\in[1,q]}$ is a vector of $(q+1)$ components with $\vartheta_0 = 1$ and ε_t is white noise.

3. Finally, a time-series X_t which follows an ARMA(p,q) model can be written as

$$X_t = c + \varepsilon_t + \sum_{i=1}^{p} \varphi_i X_{t-i} + \sum_{i=1}^{q} \vartheta_i \varepsilon_{t-i}, \tag{2.20}$$

where c is a constant, $(\varphi_i)_{i\in[1,p]}$ and $(\vartheta_i)_{i\in[0,q]}$ are vectors of, respectively p and q components and ε_t is white noise. This model is a mixture of both an AR and an MA since it depends linearly on either the p past realizations of the process and on the q past realizations of the shocks, plus the current value of the shocks. If $q = 0$ the model reduces to a AR(p), it becomes a MA(q) if $p = 0$.

It is worth noting that in order to make the AR(p) and the ARMA(p,q) models weakly stationary, the polynomial given by $1 - \sum_{i=1}^{p} \varphi_i z^i$ must have all its root outside the unit circle [51].

2.3.1 GARCH-type models

2.3.1.1 Univariate case

AR, MA and ARMA models are not good candidates for describing the behaviour of log-returns. The main reason is because their innovations are correlated, whereas financial log-returns are not. GARCH-type models are designed such that they manage to keep their innovations uncorrelated but still introducing non linear correlations. In the GARCH-type familiy fall models like the Nobel prize winning autoregressive conditional heteroscedasticity (ARCH) model [16], the generalized autoregressive conditional heteroskedasticity (GARCH) model [52] and its further generalizations.

A time-series x_t, follows an ARCH(q) process if its innovations are defined as

$$x_t = \sigma_t \varepsilon_t, \tag{2.21}$$

where ε_t is white noise and σ_t is the volatility time series which is in turn modelled as [16]

$$\sigma_t^2 = \alpha_0 + \sum_{i=1}^{q} \alpha_i x_{t-i}^2, \tag{2.22}$$

with $\alpha_0 > 0$ and $\alpha_i \geq 0$, $\forall i > 0$. In order to make the covariance stationary and the unconditional variance finite the condition $\sum_{i=1}^{q} \alpha_i < 1$ has to be added [16]. The ARCH process manages to reproduce the fat tails and volatility clustering [16]. In particular, it is easy to see that the kurtosis of a generic ARCH process exceeds three:

$$\gamma_2 = \frac{E\left[(x_t - E[x_t])^4\right]}{E^2\left[(x_t - E[x_t])^2\right]} = \frac{E\left[(x_t)^4\right]}{E^2\left[(x_t)^2\right]} = 3\frac{E\left[(\sigma_t)^4\right]}{E^2\left[(\sigma_t)^2\right]} > 3, \tag{2.23}$$

where the second equality follows from $E[\varepsilon_t] = 0$ and the last inequality from the Jensen inequality. However, in order to achieve long memory by using the ARCH approach, one has to increase the order q to a relatively large number of terms [52]. But increasing the number of terms in the expansion in Eq. 2.22, means also having more parameters to be estimated, which should be avoided in practical situations. In order to circumvent this problem, the GARCH model was introduced [52]. The innovations of a GARCH(p, q) model are defined as those of Eq. (2.21), but the definition of variance process encloses also an autoregressive part, namely

$$\sigma_t^2 = \alpha_0 + \sum_{i=1}^{q} \alpha_i x_{t-i}^2 + \sum_{i=1}^{p} \beta_i \sigma_{t-i}^2, \tag{2.24}$$

where α and β are vectors of respectively q and p parameters. For the overall increment process to be stationary the condition $\sum_{i=1}^{q} \alpha_i + \sum_{i=1}^{p} \beta_i < 1$ must hold. The chain of equalities in Eq. (2.23) holds for the GARCH model as well, proving that it reproduces qualitatively the fat-tails. As for the long memory, it manages to have longer memory than the ARCH model with a smaller number of parameters, since a GARCH(p, q) model, can be seen as an infinite order ARCH(∞). Let us show this for the case of the GARCH$(1, 1)$;

the conditional variance of a GARCH$(1,1)$ takes the form

$$\sigma_t^2 = \alpha_0 + \alpha x_{t-1}^2 + \beta \sigma_{t-1}^2, \tag{2.25}$$

which implies that

$$\sigma_{t-1}^2 = \alpha_0 + \alpha x_{t-2}^2 + \beta \sigma_{t-2}^2. \tag{2.26}$$

Repeating this procedure n times and substituting the expressions of σ_{t-*} in Eq. 2.25, one obtains

$$\sigma_t^2 = \alpha_0 \sum_{i=0}^{n} \beta^i + \alpha \sum_{i=1}^{n} \beta^{i-1} x_{t-i}^2 + \beta^n \sigma_{t-n}^2. \tag{2.27}$$

Performing the limit for $n \to \infty$ Eq. 2.27 becomes

$$\sigma_t^2 = \frac{\alpha_0}{1-\beta} + \sum_{i=1}^{\infty} \alpha \beta^{i-1} x_{t-i}^2, \tag{2.28}$$

which holds for $\beta < 1$. Eq. 2.28 is indeed a infinite order ARCH(∞).

A sweeping amount of modifications of the basic GARCH(p,q) have been developed in order to have more refined models which accomodate other statistical propoerties of finacial time-series aside of fat-tails and volatility clustering, like the leverage effect. For example NAGARCH ([53]), QGARCH ([54]), GJR-GARCH ([55]) all introduce the leverage effect giving all different recipes. The EGARCH ([56]) instead models the logarithm of the variance and also introduces terms which estimate separately the effect of the sign and of the amplitude of past returns.

2.3.1.2 Multivariate case

Multivariate GARCH models are of three types [57]: generalisations of the univariate GARCH, linear combination of univariate GARCH and non linear combination of univariate GARCH. They can all be written in general as [57]

$$x_t = H_t^{1/2} \varepsilon_t, \tag{2.29}$$

where x_t is a vector of length N representing the stocks being modelled, ε_t is a length N vector of normally distributed variables with independent components and H_t is a $N \times N$ positive definite matrix which represents the conditional variance of the process. Despite the models we describe below can depend on an arbitrary number of shocks (noise values) and innovations in the past, like their univariate counterpart, we limit ourself to describe their simplest version, which depends only on one lag in the past of both the innovation process and the noise.

The first multivariate GARCH model proposed is the VEC model [58], which is a straightforward generalization of the univariate GARCH model. The VEC(1, 1) model, can be written in the following way [58]

$$vech\left(H_t\right) = C + Avech\left(\varepsilon_t \varepsilon_t'\right) + Bvech\left(H_{t-1}\right), \tag{2.30}$$

where *vech* is the operator which rearranges the lower triangular part of the input matrix into a vector, A and B are square matrices of parameters and C is a parameter vector. If we apply this model to a set of $N = 3$ stocks, this model has 78 parameters to be estimated[57]. In order to circumvent this problem, in [58] was already proposed to put constraint to the definition of the matrices A, B and C. In particular the DVEC model [58, 57] is defined as in Eq. (2.30) but with the matrices A and B being diagonal. Also, an even stronger simplification has been proposed with the a scalar model in [59], by setting A and B as scalars.

All these models have to deal with the positive definiteness of the matrix H_t, which can be achieved only via strong restrictions on the parameters [57]. In order to circumvent this problem, a different parametrization of the VEC model was proposed, which is less flexible than the original one, but achieves a positive definite matrix H_t more easily. This model is called the BEKK model

[60], and it is defined in the following way:

$$H_t = C^{*T}C^* + \sum_{k=1}^{K} A_k^{*T}\varepsilon_{t-1}\varepsilon_{t-1}^T A_k^* + \sum_{k=1}^{K} B_k^{*T}H_{t-1}B_k^*, \tag{2.31}$$

where, A^*, B^* and C^* are matrices, C^* is upper triangular and $\cdot^T$ is the transposition symbol. Also for this model a diagonal version can be formulated as for the DVEC. A simplification to the structure of the BEKK model came from the intuition behind the factor models [61] that stocks comovements are driven by a small number of common factors. In [62] the authors proposed a factor version of the BEKK model called F-GARCH$(1, 1, K)$ (factor GARCH), which reads exactly as the model in Eq. (2.31) but with A^* and B^* being rank one matrices with the same left and right eigenvectors. Factor models inspired also another type of multivariate GARCH models, called OGARCH [63, 64] which means orthogonal GARCH. In these models the log-returns are modelled as an orthogonal transformation of univariate GARCH time-series (and/or its modifications), which represent the common latent factors of the market.

In the spirit of the parameters reduction, in [65] the author proposed to constraint the conditional cross correlation matrix to be constant, while the cross-covariance matrix being time-dependent only through the univariate volatilities of each stock. This model is called CCC and it is defined as follows

$$H_t = D_t R D_t, \tag{2.32}$$

with R a symmetric positive definite matrix satisfying $R_{ii} = 1 \quad \forall i$, $D_t = diag(h_{1t}^{1/2} \dots h_{Nt}^{1/2})$ and the h_{it} defined as univariate GARCH models. However assuming a constant conditional cross-correlation turned out to be unrealistic in many applications, thus a dynamical conditional correlation (DCC) model was proposed in [66, 67] allowing the conditional cross-correlation matrix to evolve as a GARCH model itself:

$$R_t = (1 - \Theta_1 - \Theta_2)R + \Theta_1\Psi_{t-1} + \Theta_2 R_{t-1}, \tag{2.33}$$

with $\Theta_1, \Theta_2 > 0$, $\Theta_1 + \Theta_2 < 1$, R a symmetric positive definite matrix, $R_{ii} = 1 \quad \forall i$ and Ψ_{t-1} being the cross correlation matrix of the ε_t computed over M steps in the past. Finally we report that also copulas [68] have been included in the GARCH literature through the introduction of the copula-GARCH models [69, 70]. In these models the conditional variances of each stock follow a GARCH model, the noises follow a certain marginal distributions whose parameters may vary in time and the conditional dependence is captured by a time-varying copula.

2.3.2 Stochastic Volatility models

In this section we review the main SV models, limiting ourself to the discrete-time case.

2.3.2.1 Univariate case

The first SV model was proposed in [71] and it is given by

$$y_t = \varepsilon_t e^{h_t/2}, \tag{2.34}$$

$$h_t = \mu + \phi(h_{t-1} - \mu) + \eta_t, \tag{2.35}$$

where y_t models a log-returns time-series, $\varepsilon_t \sim N(0,1)$ and h_t is the so-called log-volatility which follows an AR(1) process with $\eta_t \sim N(0, \sigma_\eta^2)$ and parameters μ, $|\phi| < 1$. Moreover, the unconditional mean and variance of h_t are respectively $\mu_h = \mu$ and $\sigma_h^2 = \dfrac{\sigma_\eta}{1-\phi^2}$. As for the fat tails, the same chain of equalities in Eq. (2.23) holds here as well, so SV models exhibit fat-tails.

As pointed out in [72, 73], the tails of the model in Eq. (2.34) are too thin with respect to observed ones, so that extreme events are too rare compared to real log-returns time-series. Thus modifications have been put in place to generalize it. A first modification proposed was to define ε_t to follow a t-Student distribution [72, 73]. Another way to take into account rare events is via the inclusion of jumps into the log-returns process. In [74, 73] the

authors propose to add to the process in Eq. (2.34) a Gaussian variable, whose contribution to the innovations is controlled by a Bernoulli random variable with a certain probability. It is also worth mentioning that some authors proposed to add jumps in the log-volatility process and proved their importance [75, 76, 74].

Other modifications to the standard model in Eq. (2.34) concern the introduction of a dependence between log-volatility innovations h_t and log-returns innovations y_t in order to take into account the leverage effect. This has been done either by writing h_t explicitly in the definition od y_t, as in the SV-in-mean model [77], or via the introduction of a correlation between u_t and η_{t+1}, as in [78, 79, 80]. Further generalizations deal with the introduction of long-memory, since a finite amount of lags in the log-volatility process ends up in its autocorrelation function decaying geometrically [81]. In order to overcome this, integrated processes were introduce to describe the the log-volatility process [81, 82, 83, 84].

2.3.2.2 Multivariate case

The first multivariate SV proposed in the literature, can be regarded as the stochastic volatility counterpart of the CCC model, discussed above. In particular it assumes that the conditional cross-correlation of the time-series is constant. This model was proposed in [85] and it reads as

$$y_{it} = e^{h_{it}/2}\varepsilon_{it}, \tag{2.36}$$

$$h_{it} = \gamma_i + \phi_i h_{it-1} + \eta_{it}, \tag{2.37}$$

with ε_{it} and η_{it} being N-dimensional multivariate Gaussian processes, independent among each other and also serially independent, having cross-covariance structure given by the $N \times N$ matrices $\mathrm{Cov}\left[\varepsilon_{it}, \varepsilon_{jt}\right] = \Sigma^{\varepsilon}_{ij}$ and $\mathrm{Cov}\left[\eta_{it}, \eta_{jt}\right] = \Sigma^{\eta}_{ij}$. The quantities $\{\gamma_i\}$ and $\{\phi_i\}$ are instead N-dimensional vectors.

The factor models approach has also been applied to multivariate SV models. The first and simplest specification was given in [86], where, say, $K < N$ factors are driven by a univariate standard SV model and a matrix mix them to give the N-dimensional process. In particular the model is defined as follows

$$\mathbf{y_t} = \mathbf{B}\mathbf{f_t} + \omega_\mathbf{t}, \tag{2.38}$$

$$f_{it} = e^{h_{it}/2}\varepsilon_{it}, \tag{2.39}$$

$$h_{it} = \gamma_i + \phi_i h_{it-1} + \eta_{it}, \tag{2.40}$$

where $\mathbf{y_t}$ is a N-dimensional vector, $\mathbf{B}$ is a $N \times K$ matrix, $\mathbf{f_t}$ is a K-dimensional vector which represents the factors, the f_{it}s are the components of $\mathbf{f_t}$ each following the standard SV model with $i \in [1, K]$ and $\omega_\mathbf{t} \sim N(\mathbf{0}, \mathbf{\Omega})$ is a multivariate N-dimensional Gaussian process where each component has zero mean and cross-correlation matrix $\mathbf{\Omega}$. Since in this model shocks in the modelled time-series can be explained only via systemic changes, in [87, 88] the authors proposed to allow each component of the vector $\omega_\mathbf{t}$ to be a standard SV process independent from the others.

2.4 Summary

In this chapter we discussed the main stylized fact of the financial daily log-returns. We found that source of complexity can be found either on the univariate and on the multivariate level. On the univariate level GARCH family models and SV models seem both to point out that the memory of the volatility plays a role in the heaviness of the unconditional tails of real process, however it seems that this heaviness cannot be all ascribed to the effect of the memory. On the multivariate level instead cross-dependence properties are the source of complexity of the financial systems, which are a challenge either for their estimation and for their modelling. We reviewed the main model present in the literature able to reproduce univariate and multivariate properties explaining

what empirical observation motived the introduction of each of them.

Chapter 3

Multifractality in time-series analysis

The aim of this chapter is to discuss the main features of the multifractal scaling in the context of time-series analysis and to pinpoint its importance in the literature. We review its main theoretical properties related to financial log-returns, describing then the the most important estimation methods for univariate and bivariate processes. We conclude by reviewing the most important models able to reproduce this empirical property along with the others described in the previous chapter.

3.1 Introduction

The theoretical background of the multifractal measures stems from an early work of Mandelbrot [89] on turbulent flows. The concepts and ideas in this paper worked as an input for the subsequent statistical Physics literature by opening new scenarios (see for example [90, 91, 92, 93, 94, 95, 96]). Some authors also started to observe that the multifractal picture could have been relevant to the financial modelling [97, 98, 99, 100]. Now, the multifractal behaviour of financial time-series is one of the acknowledged stylized facts in the literature (see: [18, 3, 101, 102, 14]). Many works have been dedicated to its empirical characterization [103, 104, 105, 106, 107, 108, 109, 110, 111, 112, 113, 114, 115, 116, 117, 118, 119, 120], reporting strong evidence of its

presence in financial markets and several models have been proposed [121, 122, 123, 124, 125, 126, 127, 128, 129, 130] to reproduce these empirical facts.

Multifractality proved also to be a very valuable tool. From a theoretical point of view models with a multifractal nature display also power law tails and volatility clustering, leading to consider these well-known stylized facts as consequences of the multifractal nature of financial time-series [125]. From a practical point of view multifractal models proved to be valuable tools for volatility and Value-at-Risk forecasting [122, 123, 124, 125, 131, 132] and also for monitoring the stability of firms and markets [133, 134, 115].

The rest of the chapter is organized as follows: in Sec. 3.2 we give a geometrical and statistical definition of multifractality, in Secs. 3.3 and 3.4 we respectively review the main univariate and bivariate estimation methods of multifractality available in the literature, in Sec. 3.5 we review the main multifractal models proposed in the literature, finally a summary of this chapter is given in Sec. 3.6.

3.2 Formal definition

In this subsection we give an overview on what is multifractality from a mathematical point of view giving its geometrical and statistical characterization.

3.2.1 Geometrical characterization

Let $X(t)$ be a process continuous in time with stationary increments. The notion of local Hölder exponent $h(t)$ can be introduced via the following expression [135]

$$|X(t+\Delta t) - X(t)| \sim C(t)(\Delta t)^{h(t)} \qquad \text{when } \Delta t \to 0, \tag{3.1}$$

where $C(t)$ is a function of t and Δt is an infinitesimal quantity which tends to zero. Also, in order to assure that stationarity holds almost surely, the set on which $C(t)$ and $h(t)$ vary has zero Lebesgue measure. Intuitively the local

Hölder exponent quantifies the local degree of singularity of a time-series [135]. The set of all local Hölder exponents thus expresses the degree of singularity of the whole process $X(t)$ associating a number with every point in time. In order to characterize how a certain singularity affects the behaviour of the process, following [136], we can compute the number of intervals $N(h, \Delta t)$ of size Δt which cover all the points in time which share the same degree of singularity h, as

$$N(h, \Delta t) \propto (\Delta t)^{-D(h)} \qquad \text{for } \Delta t \to 0, \tag{3.2}$$

where $D(h)$ is the Hausdorff or fractal dimension of the set. The quantity $D(h)$ is also called *Singularity Spectrum* and in general, for a certain value $\bar{h}$, can be defined as (cfr. [135, 137, 138, 139])

$$D(\bar{h}) = D_H\{t : h(t) = \bar{h}\}. \tag{3.3}$$

If only one Hölder exponent, say h_0, characterizes the process, then the process is said to be mono or uni-fractal and the Singularity Spectrum reads as [136]

$$D(h) = \begin{cases} 1 & h = h_0 \\ -\infty & \text{otherwise,} \end{cases} \tag{3.4}$$

so the spectrum reduces to a single point. A process is said to be multifractal if it has a range of values of h over which $D(h) \geq 0$ [135, 136].

3.2.2 Statistical characterization

It turned out that the geometrical properties of a process can be linked to its statistical ones. In particular the so called Multifractal Formalism was introduced [137, 138, 139] and can be applied in the context of the stochastic processes [135]. The process $X(t)$, continuous in time, is said to be multifractal also if the following scaling relation holds [140]

$$E[|X(t+\tau) - X(t)|^q] = K(q)\tau^{\zeta(q)}, \tag{3.5}$$

where τ is the time-horizon of the increments, both $K(q)$ and $\zeta(q)$ are functions of q and $\zeta(q)$ is concave [121] and codifies the scaling exponents of the process.

Using this definition, a process is said to be unifractal when the function $\zeta(q)$ is linear, *i.e.* $\zeta(q) = qH$, where H is the so called Hurst exponent [102].

3.2.3 Matching the two characterizations

As underlined in [121], multifractality defined by Eq. 3.5 is a global property because τ is not constrained to tend to zero, whereas the definition given in Eq. (3.1) is local. Let us now describe the heuristic argument which links the two characterizations. For this purpose, let us consider the following proxy of Eq. (3.5)

$$\frac{\Delta t}{T}\sum_{i=1}^{T/\Delta t}|X\left((i+1)\Delta t\right) - X(i\Delta t)|^q \propto (\Delta t)^{\zeta(q)}, \tag{3.6}$$

where T is the whole length of the time-series under consideration. The following chain holds [136]

$$\begin{aligned}\frac{\Delta t}{T}\sum_{i=1}^{T/\Delta t}|X\left((i+1)\Delta t\right) - X(i\Delta t)|^q &\propto \frac{\Delta t}{T}\sum_{i=1}^{T/\Delta t}(\Delta t)^{h(i\Delta t)q} \\ &= \frac{\Delta t}{T}\int dh(\Delta t)^{hq}(\Delta t)^{-D(h)} \\ &\propto \int dh(\Delta t)^{1+hq-D(h)} \\ &\simeq (\Delta t)^{\inf_h(1+hq-D(h))},\end{aligned} \tag{3.7}$$

where in the first step we used Eq. (3.1), in the second one we rewrote the sum over times as an integral over all the possible values of h weighted with the number of points sharing that certain h value and in the fourth one we used the steepest descent method to solve the integral for $\Delta t \to 0$ [138, 139, 136, 137]. Comparing Eq. (3.6) with Eq. (3.7) we obtain the well-known relation [135, 14])

$$\zeta(q) = 1 + \inf_h\{qh - D(h)\}, \tag{3.8}$$

which states that the scaling exponents and the Singularity Spectrum are linked via a Legendre transform. Thanks to the involution property we can also write

$$D(h) = 1 + \inf_q\{hq - \zeta(q)\}. \tag{3.9}$$

The request of concavity is crucial for this result since otherwise the Legendre Transform would not be well-defined. From this computation, it appears evident that the relation between the two approaches relies heavily on the continuity in time of the underlying time-series since the local regularity can be characterized only when the box size Δt tends to zero. It is also worth stressing that another key point is that Eq. (3.5) must hold also for small value of Δt.

3.2.4 Few more remarks

In practice one does not deal with processes continuous in time. As a consequence, it was shown [14, 137] that the straightforward estimation of $D(h)$ cannot be practically achieved. In light of this, the importance of relations (3.8) and (3.9) relies in the fact that they allow to estimate a geometrical quantity (the Singularity Spectrum) via statistical measurements. In particular one usually assumes that a real process (for example a log-price) is a discretized version of an underlying unobservable process continuous in time, which are sharing the same statistical properties. Thus, while geometrical arguments cannot be applied to the discrete version, statistical ones are. Usually the function $\zeta(q)$ is rewritten as $\zeta(q) = qH(q)$, with $H(q)$ called the Generalized Hurst Exponent [102, 133, 134]. In particular, from Eq. (3.9) (in order to find the minimum) we obtain the following chain of equalities

$$h = \frac{d\zeta(q)}{dq} = H(q) + q\frac{dH(q)}{dq}, \tag{3.10}$$

which shows that the Hölder exponent is equal to the Hurst exponent only when the latter does not depend on q, which is the case of unifractal time-series where $\zeta(q)$ reduces to a straight line. The two most notable unifractal processes are the Brownian Motion (BM) and the Fractional Brownian Motion (fBM), which satisfy respectively $\zeta(q) = q/2$, thus $H(q) = 0.5$, and $\zeta(q) = qH$, thus $H(q) = H$ (see for example [102]).

3.3 Estimation methods

In this section we review the main numerical estimation methods available in the literature for determining the multifractal spectrum of both empirical and synthetic time-series, underlining their main strengths and weak points.

3.3.1 Generalized Hurst Exponent Method

The Generalized Hurst Exponent Method (GHE) method was introduced in [133, 134, 102][1] which relies on the measurement of the direct scaling of the qth-order moments of the distribution of the increments of the time-series under study. It has been shown to be one of the most reliable estimators when dealing with time-series with infinite variance[141]. The GHE method considers the following function of the increments

$$\frac{E[|X(t+\tau)-X(t)|^q]}{E[|X(t)|^q]} \propto K(q)\tau^{qH(q)}, \tag{3.11}$$

Where τ, $K(q)$ and $H(q)$ have the same meaning as in the previous subsection. The denominator on the left hand side of Eq. (3.11) is add with respect to Eq. (3.5) for numerical stability reasons. In particular, GHE considers the logarithm of Eq. (3.11)

$$\ln\left(\frac{E[|X(t+\tau)-X(t)|^q]}{E[|X(t)|^q]}\right) \propto qH(q)\ln(\tau) + \ln\left(K(q)\right), \tag{3.12}$$

and, if linearity with respect to $\ln(\tau)$ holds, it computes the slopes of the straight lines at different q. The slopes are computed in the following way: for every q, several linear fits are computed taking $\tau \in [\tau_{min}, \tau_{max}]$, with usually $\tau_{min} = 1$ and several values of τ_{max} typically between $[5, 19]$; the output estimator for $H(q) = \dfrac{\zeta(q)}{q}$ is the average of these values for a given q. This method gives also the errors which are the standard deviations of these values. The main strength of GHE is that it computes directly the scaling of the moments

[1] The code can be found at http://www.mathworks.com/matlabcentral/fileexchange/30076-generalized-hurst-exponent.

with respect to the aggregation horizon without relying on any pre-processing of the data, however the measurements are aggregation horizon dependent.

3.3.2 Multifractal Detrended Fluctuation Analyisis

The Multifractal Detrended Fluctuation Analyisis (MFDFA) method, introduced first in [142], is an evolution of the Detrended Fluctuation Analysis [143] and is based on the scaling of the so-called fluctuation function. Its most appealing feature is the possibility to deal with non-stationary time-series. We review it here briefly. Let us call X_k a discrete time-series of length N and compute its profile

$$Y(t) = \sum_{k=1}^{i} \left[X_k - \bar{X}\right], \qquad t \in [1, N], \tag{3.13}$$

where $\bar{X} = \frac{1}{N}\sum_{k=1}^{N} X_k$. Next, starting from the beginning, the profile $Y(t)$ is split into $N_s = \left\lfloor \frac{N}{s} \right\rfloor$ intervals of length s, where $\lfloor\cdot\rfloor$ means rounding down to the lower integer. The overall length N is in general not expected to be a multiple of s, so the division is repeated starting from the end of the profile, ending up in $2N_s$ intervals overall. Next the algorithm deals with the non-stationarities by removing the local polynomial trend from each of the $2N_s$ intervals, and then by computing the variance of the residuals with respect to the trend in each interval. Explicitly, let us first consider the segments starting from the beginning of the profile $Y(t)$, the variance is ([142])

$$F^2(\nu, s) = \frac{1}{s}\sum_{i=1}^{s} \left\{Y[(\nu-1)s + i] - y_\nu(i)\right\}^2, \tag{3.14}$$

where y_ν is the trend in the ν interval, with $\nu \in [1, N_s]$. The same operation is repeated for the intervals starting at the end of the profile giving ([142])

$$F^2(\nu, s) = \frac{1}{s}\sum_{i=1}^{s} \left\{Y[N - (\nu - N_s)s + i] - y_\nu(i)\right\}^2, \tag{3.15}$$

where now $\nu \in [N_s + 1, 2N_s]$. The next step consists in finding the q^{th} order fluctuation function defined as ([142])

$$F_q(s) = \left\{ \frac{1}{2N_s} \sum_{\nu=1}^{2N_s} \left[F^2(s,\nu) \right]^{q/2} \right\}^{1/q}, \tag{3.16}$$

for different value of s. If the analysed is long ranged correlated with a power law decay, than also $F_q(s)$ is with respect to s,

$$F_q(s) \sim s^{h(q)}, \tag{3.17}$$

with $h(q) = H(q)$ being the Generalized Hurst Exponent. The main strength of this technique is that it is applicable to non-stationary time-series, however the choice of the detrending polynomial is arbitrary.

3.3.3 Wavelet Transform Modulus Maxima

The Wavelet Transform Modulus Maxima (WTMM) method relies on the Wavelet Transform (WT) formalism, which allows to decompose a signal into elementary contributions in a space-scale plane via the translation and the dilation of a so-called analysing wavelet ψ ([144]). In general, the analysing wavelet is required to have zero mean, but in the context of multifractal analysis, it is also required to be orthogonal to polynomials with degree m below a certain value n_ψ [144], *i.e.*

$$\int_{-\infty}^{+\infty} x^m \psi(x) dx = 0, \qquad 0 \leq m < n_\psi. \tag{3.18}$$

A common choice for the analysing wavelet is to pick the n^{th} derivative of the gaussian function, for a given value of n:

$$\psi^{[n]}(x) = \frac{d^n}{dx^n} e^{-x^2/2}. \tag{3.19}$$

Once the analysing wavelet is defined, the WT of a function f at the space value b and scale $a > 0$ can be defined as [145, 146, 144]

$$T_\psi[f](b,a) = \frac{1}{a} \int_{-\infty}^{+\infty} \psi\left(\frac{x-b}{a} \right) f(x) dx. \tag{3.20}$$

The next step consists in considering only the modulus maxima of the WT defined as $|T_\psi[f](b,a)|$ for a given scale value a. These modulus maxima are arranged as lines on the (b,a) half plane [144]. In particular one can define $\mathfrak{L}(a_0)$ as the set of maxima lines at scale value $a \leq a_0$. The multifractal analysis can be performed by defining the partition function $Z(q,a)$ as [144, 147, 148]

$$Z(q,a) = \sum_{l \in \mathfrak{L}(a)} \left(\sup_{(b,a') \in l} |T_\psi[f](b,a)|^q \right), \tag{3.21}$$

and by considering its scaling properties with respect to a [144]

$$Z(q,a) \sim a^{\zeta(q)-1}. \tag{3.22}$$

The main strength of this method is that it has a deep mathematical formulation which makes a parallelism with the thermodynamic, however the choice of the analysing wavelet function is arbitrary.

3.4 Bivariate measures of scaling

In the last decade interest has grown in the detection of long range dependence in the scaling of cross correlations. Many methods have been proposed and also applied to datasets not only coming from the financial world (see for example [149, 116, 150, 151]). The first method proposed is a straightforward generalization of the DFA [143] called Detrended Cross Correlation Analysis (DCCA) [149]. Consider two stationary discrete time-series $\{X_k\}$ and $\{X'_k\}$ and assume that their correlation behaves asymptotically as a power law

$$\text{Corr}\left[X_k, X'_{k+n}\right] \propto n^{-\gamma_\times}, \tag{3.23}$$

with $0 < \gamma_\times < 1$. The purpose of the DCCA is to measure the bivariate scaling exponent $\gamma_\times$. In order to achieve this, in [149] the authors notice that by defining the integrated profile time-series Y_k as for the MFDFA (see [142] and Subsubsec. 3.3.2),

$$\begin{array}{l} Y_k = \sum_{i=1}^{k} X_i, \\ Y'_k = \sum_{i=1}^{k} X'_k, \end{array} \tag{3.24}$$

their covariance behaves asymptotically as [149]

$$\mathrm{Cov}\,[Y_n, Y'_n] \propto n^{2\lambda}, \tag{3.25}$$

with $\lambda = 1 - \frac{\gamma_\times}{2}$. Eq. 3.25, can be used only when data are stationary. In order to remove the non-stationarites, calling N the length of both time-series, the authors propose to divide the time-span of the integrated profiles in $N-n$ overlapping segments made of $n+1$ values and compute the linear local trend $\bar{Y}_{k,i}$ and $\bar{Y}'_{k,i}$ in each of them, with $i \leq k \leq i+n$. By removing the trend from the signals the residuals of both time-series are obtained and the covariance of the residual in each box can be computed [149],

$$f^2_{DCCA}(n,i) = \frac{1}{n-1}\sum_{k=i}^{i+1}(Y_k - \bar{Y}_{k,i})(Y'_k - \bar{Y}'_{k,i}). \tag{3.26}$$

Finally, the detrended covariance by averaging over all the boxes:

$$F^2_{DCCA}(n) = \frac{1}{N-n}\sum_{i=1}^{N-n} f^2_{DCCA}(n,i). \tag{3.27}$$

It is worth noticing that this method boils down to the simple DFA [143] when $\{X_k\} = \{X'_k\}$.

A bivariate generalization of the MFDFA was proposed in [116], where the Multifractal Detrended Cross-Correlation Analysis (MFDXA) was introduced. Let us consider again two time-series, $\{X_k\}$ and $\{X'\}$, with zero mean made of N points. As for the DCCA the time-domain is divided into N/s non-overlapping intervals of size length s. The profiles of $\{X_k\}$ and $\{X'\}$ are computed in each interval and, for, say, the n^{th} they read as [116]

$$\begin{array}{c} Y_n(k) = \sum_{i=1}^{k} X_i[(n-1)s+i], \\ Y'_k = \sum_{i=1}^{k} X'_i[(n-1)s+i], \end{array} \tag{3.28}$$

with $i \in [1,s]$. In each interval local trends, which we call respectively $\bar{Y}_n(k)$, $\bar{Y}'_n(k)$, can also be defined using for example polynomials [116]. From the profiles in Eq. (3.28) and the local trends, the detrended covariance in each

interval reads as

$$F_n(s) = \frac{1}{s}\sum_{k=1}^{s}\left[Y_n(k) - \bar{Y}_n(k)\right]\left[Y'_n(k) - \bar{Y}'_n(k)\right], \tag{3.29}$$

which in turn allows to define the q^{th}-order detrended covariance as

$$F_{XX'}(q,s) = \left(\frac{1}{\lfloor N/s \rfloor}\sum_{n=1}^{\lfloor N/s \rfloor} F_n(s)^{q/2}\right)^{1/q} \propto s^{h_{XX'}(q)}, \tag{3.30}$$

with $h_{XX'}$ being the bivariate scaling exponent.

Another measure proposed in the literature concerning the scaling of the cross correlation function is the one in [150], where the authors measures the cross correlation of the returns both with respect to its scaling and with respect the relative lags of the considered time-series. In order to do so they consider the following expression for the cross-correlation [150]

$$C_{XX'}(t,\tau) = E\left[(X(t) - \mu_X(t))(X'(t+\tau) - \mu_{X'}(t+\tau))\right], \tag{3.31}$$

where X and X' are the two considered time-series and $\mu_X(t)$ and $\mu_{X'}(t)$ are the time-dependent means. The explicit presence of the time as an argument of each variable underlines the possible non-stationarity of the data. In order to deal with this, authors propose to substitute the time-dependent means with moving averages over a certain time-period n, namely [150]

$$\begin{aligned} \mu_X(t) &\mapsto \frac{1}{n}\sum_{k=0}^{n} X(t-k), \\ \mu_{X'}(t) &\mapsto \frac{1}{n}\sum_{k=0}^{n} X'(t-k). \end{aligned} \tag{3.32}$$

In this way the time-dependence in Eq. 3.31 is assumed to be removed. In the case of two fBM the correlation at lags $\tau = 0$ behaves as [150]

$$C_{XX'}(\tau = 0) \propto n^{H_X + H_{X'}}, \tag{3.33}$$

where H_X and $H_{X'}$ are the self-similarity exponents of the two fBMs.

The last method we briefly review here is the Multifractal Height Cross-Correlation Analysis (MFHXA) [151]. Consider two time-series X_t and X'_t recorded at resolution ν. If the original time-series have length T, let us define $T^* = \nu \left\lfloor \frac{T}{\nu} \right\rfloor$. We next call the τ order difference of, say, the X_t time series as $\Delta_\tau X_t = X_{t+\tau} - X_t$ and the component-wise product of the two τ order difference of the series as $\Delta_\tau X_t X'_t = \Delta_\tau X_t \Delta_\tau X'_t$. Using these definitions, the height-height cross covariance function as [151]

$$K_{XX',q}(\tau) = \frac{\nu}{T^*} \sum_{t=1}^{T^*/\nu} |\Delta_\tau X_t X'_t|^{q/2} \propto \tau^{qH_{XX'}(q)}, \tag{3.34}$$

with $H_{XX'}(q)$ being the generalized bivariate Hurst exponent.

3.5 Multifractal models

In this section we review the main multifractal models available in the literature.

3.5.1 Markov-Switching Multifractal Model

The Markov-Switching Multifractal Model (MSM) model was first introduced in [122]. The name comes from the definition of the volatility of this process, which is modelled as a Markov-Switching process in discrete time. In this model, the log-returns are defined as [122]

$$r_t = \varepsilon_t \sigma_t, \tag{3.35}$$

where $\varepsilon \sim N(0,1)$ and σ_t is the volatility modelled as

$$\sigma_t^2 = \sigma^2 \prod_{i=1}^{k} M_t^i. \tag{3.36}$$

The M_t^is are the volatility components which are independent for different value of i i at a given time t, non-negative and satisfy $E[M_t^i] = 1$. At each time step, the values of M_t^i is either renewed with a certain probability γ_i, or

stays the same. It is worth stressing that the different values of γ_i define a hierarchy of the volatility components, from the component which changes its value more frequently to the one which changes more rarely. In the literature, different choices of the distribution of the M_t^is have been made; for example in [131] the authors chose a Binomial distribution, while in [126, 123] the authors considered also a log-normal specification.

This model has also been extended to include skewness and leverage effect in [152]. In particular the authors introduced a correlation between the signs of the process in order to reproduce the skewness and also, inspired by [153], a kernel term which introduces a dependence between volatility shocks and past signs.

3.5.2 Multifractal Random Walk

The Multifractal Random Walk (MRW) was first introduced in [127]. Its most appealing property is that it has exactly computable scaling exponents in the continuous time limit. In order to describe this model let us consider a discretized time-line with steps of length Δt. The returns of this model over an horizon τ can be written as

$$r_\tau(t) = X(t+\tau) - X(t) = \sum_{k=\frac{t}{\Delta t}+1}^{\frac{t+\tau}{\Delta t}} \epsilon_{\Delta t}(k) e^{\omega_{\Delta t}(k)}, \tag{3.37}$$

with $\epsilon_{\Delta t} \sim N(0, \sigma^2 \Delta t)$, $\omega_{\Delta t} \sim N(-\lambda^2 \ln(L/\Delta t), \lambda^2 \ln(L/\Delta t))$, where λ is called intermittency parameter, L is the autocorrelation length and σ is the variance of the overall process [127].

What charaterizes this model is that autocorrelation structure, in particular the $\epsilon_{\Delta t}(k)$ are i.i.d and the $\omega_{\Delta t}(k)$ are not, having autocovariance (see [127]):

$$Cov(\omega_{\Delta t}(k_1), \omega_{\Delta t}(k_2)) = \lambda^2 \ln \rho_{\Delta t}(k_1 - k_2), \tag{3.38}$$

with

$$\rho_{\Delta t}(k_1 - k_2) = \begin{cases} \dfrac{L}{(|k_1 - k_2| + 1)\Delta t} & |k_1 - k_2| < L/\Delta t, \\ 1 & \text{otherwise.} \end{cases} \tag{3.39}$$

The scaling exponents of this model in the continuous time limit $\Delta t \to 0$ are (see [127]):

$$\zeta(q) = qH(q) = -\frac{\lambda^2}{2}q^2 + (\lambda^2 + \frac{1}{2})q. \tag{3.40}$$

According to its definition, this model has uncorrelated returns, but it has been shown (cfr. [127, 154]) to exhibits both power law tails and volatility clustering. In particular, the tails decay with an exponent proportional to λ^2 (see [154]), as it is the decay of the autocorrelation function of the absolute powers of the returns (see [127]).

Alternative specifications of this model have been proposed with different scaling exponents by changing the distribution of the variable $\omega_{\Delta t}$ [129]. Also for this model the leverage effect was introduced first in [153] where a kernel was introduced to link past values of the variable $\varepsilon_{\Delta t}$ to new volatility shocks. However as pointed out by the authors themselves, this specification leads to a model which in the continuous time limit boils down to the symmetric model (3.37). So in [130] the authors proposed a model which keeps its asymmetry and the leverage effect also in the continuous time limit by introducing a correlation between $\varepsilon_{\Delta t}$ and $\omega_{\Delta t}$.

3.5.3 Bivariate MSM

The MSM was extended also to the bivariate case in [155]. Let us consider two stocks α and β and let us denote r_t a bivariate log-returns vector whose components are r_t^α and r_t^β. Following [155], the process r_t satisfies

$$r_t = [M_{1,t} * ... * M_{k,t}]^{1/2} * \varepsilon_t, \tag{3.41}$$

where $*$ is the element-wise product, $M_{i,t}$ are k 2×1 matrices and $\varepsilon_t \sim N(0, \Sigma)$ is a bivariate Gaussian process with cross-covariance Σ having non-zero diago-

nal elements. A further element of cross dependence comes from the definition of the bivariate volatility components $M_{i,t}$. As in the univariate case at each time t the value of $M_{i,t}$ is independent from the previous one, however, let us call $1_{i,t} = \left(1^{\alpha}_{i,t}, 1^{\beta}_{i,t}\right)$ the arrival vector, with, say, first (second) coordinate equal to one if a change in the ith volatility component of the α (β)stock happens, zero otherwise. Then

$$\mathbb{P}(1^{\alpha}_{i,t} = 1) = \gamma_k, \tag{3.42}$$

$$\mathbb{P}(1^{\beta}_{i,t} = 1 | 1^{\alpha}_{i,t} = 1) = (1 - \lambda)\gamma_k + \lambda, \tag{3.43}$$

where $\mathbb{P}(\cdot)$ is the probability of the event $\cdot$, and λ is the correlation between the coordinates of $1_{i,t}$ [155].

A modification of this model can be found in [156] where a certain number of volatility components are allowed to be in common between the stocks while the remaining ones are independent. A generalization, instead, of the MSM model can be found in [157], where a time-dependent correlation of the residuals is considered.

3.5.4 Multivariate Multifractal Random Walk

The Multivariate Multifractal Random Walk (MMRW) is a straight forward extension of the MRW discussed above and it was introduced first in [158]. Let us consider an N-dimensional vector of returns $r_\tau(t)$ over a certain horizon τ, then the MMRW, in its discretized version is defined as

$$r_\tau(t) = \sum_{k=\frac{t}{\Delta t}+1}^{\frac{t+\tau}{\Delta t}} \epsilon_{\Delta t}(k) * e^{\omega_{\Delta t}(k)}, \tag{3.44}$$

Let us describe in detail every term (cfr. [158]). The vector $\epsilon_{\Delta t}(k)$ is a multivariate N-dimensional Gaussian process with cross-covariance matrix equal to $\mathrm{Cov}\left[\varepsilon_{i,\Delta t}(k+\ell), \varepsilon_{j,\Delta t}(k)\right] = \delta(\ell)\Sigma_{ij}\Delta t$, with Σ being the cross-correlation matrix between each element of $\varepsilon_{\Delta t}(k)$ and the authors call it the Markovitz

matrix. The vector $\omega_{\Delta t}(k)$ is again an N-dimensional Gaussian process but with covariance given by $\mathrm{Cov}\left[\omega_{i,\Delta t}(k+\ell), \omega_{j,\Delta t}(k)\right] = \Lambda_{ij} \ln\left(T_{ij}/(\Delta t + |\ell|)\right)$ for $\Delta t + |\ell| < T_{ij}$ and zero elsewhere, with Λ_{ij} called the multifractal matrix. Also in this case $E[\omega_{\Delta t}(k)] = -Var[\omega_{\Delta t}(k)]$. This model, despite being multivariate, has exactly computable scaling exponents, which read as [158]

$$\zeta(q_1, ..., q_N) = \sum_{i=1}^{N} \zeta_i(q_i) - \sum_{1 \le i < j \le N} \Lambda_{ij} q_i q_j, \tag{3.45}$$

where ζ_i is the spectrum of the ith component of $r_\tau(t)$.

3.6 Summary

In this chapter we reviewed different aspects of multifractality in time-series analysis. We covered in detail theoretical features which can be related directly to log-returns financial time-series focusing then on the main estimation methods available in the literature either for univariate and for bivariate time-series. Finally we discussed the main models proposed in the literature which are able to reproduce this stylized fact along with many others. In the next chapters, we build on all this theoretical background by presenting the original contribution of this thesis.

Chapter 4

Empirical multifractality in financial time-series: source and estimation issues

In this chapter we discuss the origin of the multifractal behaviour of financial time-series and investigate how to best quantify it. Our methodology consists in separating the different sources of measured multifractality by analysing the multi/uni-scaling behaviour of synthetic time-series with known properties. We use the results from the synthetic time-series to interpret the measure of multifractality of real log-returns time-series. The main findings are the true source of the multifractal scaling of financial log-return time-series and that the aggregation horizon of the returns can introduce a strong bias effect on the measure of multifractality. The latter can become especially important when returns distributions have power law tails with exponents in the range $(2, 5)$. We discuss the right aggregation horizon to mitigate this bias.

4.1 Introduction

The origin of the measured multifractal behaviour of financial log-returns time-series has been debated in the literature. This question has been raised first in [142, 116] where the authors pointed out that the power law tails and the auto-correlation of the analysed time-series must be the two sources of the measured

multifractality. In the first case, the multifractal behaviour is a consequence of the broadness of the unconditional distribution of the returns; while in the second case, the multifractal behaviour is associated with the causal structure of the time-series. It was also reported in [159] that a spurious multifractality may arise in processes with a long range autocorrelated volatility. After [142], many papers have investigated the relative contribution of these two sources to the measured multifractality ([160, 161, 162, 163, 164]), however no agreement exists. For example in [160] the author points out that the autocorrelation structure has a minor impact on the measured multifractality while the power law tails are the major source of it. In [161] they also report that the power law tails give the major contribution, but they also point out that the presence of unknown autocorrelations might introduce a negative bias effect in the quantification of multifractality. Conversely, in [162] the authors find that the autocorrelation gives the major contribution while for a specific time-series the "extreme events are actually inimical to the multifractal scaling". This lack of agreement motivated our work, leading us to investigate what the source of the measured multifractality is and how it can be detected.

In this chapter we quantify the two contributions by using synthetic times series where the two contributions can be separated. Specifically, we analyse Brownian Motion with innovations drawn from a t-Student distribution, Multifractal Random Walk and normalized version of the Multifractal Random Walk. The measured multifractality on these synthetic series are compared with measures on both real financial log-returns and on a normalized version of the real log-returns where the heavy tails are removed. Results show that the aggregation horizon has a strong effect on the quantification of multifractality. We verify however that there are regions of the aggregation horizon that can be used in practice to extract reliable multifractality estimators.

The rest of the chapter is organized as follows: in Sec. 4.2 we perform a

brief literature review discussing the results from previous works, in Sec. 4.3 we review the theoretical models we use, in Sec. 4.4 we define the multifractality estimators that shall be used throughout the chapter, in Secs. 4.5 and 4.6 are dedicated respectively to the analysis of artificial and real financial data, in Sec. 4.7 we discuss the results and in Sec. 4.8 we draw conclusions.

4.2 Source of multifractality in financial data: state of the art

As already mentioned in Sec. 4.1, there is a debate in literature concerning what property of the financial time-series contributes mostly to their observed multiscaling behaviour. Let us here discuss some findings present in the literature. In [160] the author studied the Dow Jones Industrial Average taken on a daily basis and processed the data in four different ways in order to uncover the source of the multiscaling behaviour. The methods used were ([160]):

1. shuffling the data in order to check the impact of the shape of the unconditional distribution;

2. building up surrogate data with the same unconditional distribution and linear correlation of the empirical one but with any non linear correlation removed;

3. cutting the tails by substituting the more extreme events with resampled ones from the core of the distribution;

4. generating surrogate power law-tailed time-series, namely double Weibull and t-Student, preserving the temporal structure of the empirical time-series.

The author found that, on one hand the temporal structure, both linear and non linear, has a minor impact. On the other hand, the fatter the tails are,

the stronger the multiscaling. And this result was confirmed both by cutting the extreme events and changing the unconditional distribution.

In [162] the authors studied again the Dow Jones Industrial Average taken on a daily basis plus the Dow Jones Euro Stoxx 50 sampled at one minute. In this case three analyses were performed:

1. shuffling the whole dataset;
2. dividing the dataset into intervals and shuffling them in order to keep short memory contributions then repeating the analysis changing the length of the intervals;
3. cutting the extreme events.

The authors found that when shuffled, the dataset loses its multiscaling behaviour ([162]). The shuffling of the intervals showed that the linearity of the scaling of the fluctuation functions worsen when the length of the interval is small and improves increasing it, thus according to the authors this should be regarded as a sign that .temporal correlations are the source of multiscaling. For what concerns the cut of the most extreme events they found that for the Dow Jones Industrial Average extreme events have no particular impact, while for the Dow Jones Euro Stoxx 50 they cause a distortion in the Singularity Spectrum ([162]).

Finally in [161] an extensive analysis was conducted on several empirical time-series including stock market indexes, exchange rates and interest rates. In order to unveil the source of the empirical multiscaling, the shuffling method was used plus a comparison with synthetic data. The authors also found an increase of the measured multiscaling of the shuffled time-series which then led them to draw two conclusions: first that the major source of the multifractality comes from the power law tails of the distribution; second that the presence of time correlations decreases the multifractality. These conclusions

are consistent with the analysis of the Markov Switching Multifractal Model ([123]). Further analyses have been conducted by means of fractional Brownian motions, random walks with steps drawn from a Levy distribution and ARFIMA processes, all confirming the results found on the empirical datasets ([161]).

4.3 Benchmark models

In this section we describe the analytical properties of the benchmark models we used for our analysis. As already mentioned in the introduction of this chapter, one of our goal is to measure the uni-multifractal on time-series with known scaling properties but also separating the contribution of the tails form the contribution of the autocorrelation. In light of this, in order to understand the contribution of the power-law tails alone, our reference model is a Brownian motion with t-Student innovations (tBM). This process is uniscaling with independent increments drawn from a t-Student distribution. Introducing the dummy variable t, the probability density of a t-Student distribution is given by ([165])

$$p(t) = \frac{\Gamma(\frac{n+1}{2})}{\sqrt{n\pi}\Gamma(\frac{n}{2})}\left(1+\frac{t^2}{n}\right)^{-\left(\frac{n+1}{2}\right)}, \tag{4.1}$$

where n is the number of degrees freedom which can be non-integer. According to Eq. (4.1) the variable t has mean zero if $n > 1$ and infinite otherwise. The variance is instead equal to $\frac{n}{n-2}$ if $n > 2$, infinite if $1 < n < 2$ and undefined otherwise. The spectrum of a tBM can be computed analytically in both cases, either if n is bigger or smaller than two. For $n < 2$ the t-Student distribution of Eq. (4.1) behaves as a stable distribution with skewness parameter equal to zero and stability parameter equal to n, so the scaling exponents are (see

[142, 166, 167])[1]

$$\zeta(q) = qH(q) = \frac{q}{n} \quad \text{if } q < n. \tag{4.2}$$

For $n > 2$ and finite aggregation horizon τ it can be shown that

$$E[|X(t+\tau) - X(t)|^q] = f(q)\tau^{\frac{q}{2}}. \tag{4.3}$$

Thus

$$\zeta(q) = qH(q) = \frac{q}{2} \quad \text{if } n > 2. \tag{4.4}$$

It is expected then that for $n > 2$ the scaling exponents are identical to the one of a BM up to $q = n$. For $n = 2$, it can be proved rigorously that the scaling exponents, in the continuous time limit, behave like Eq. (4.4) (cfr. [168]). According to these analytical observations a tBM is a unifractal process both for $n < 2$ and $n \geq 2$ and $\zeta(q)$ behaves as a straight line.

As for the contribution of the autocorrelation to the multifractal scaling, we chose to use the MRW reviewed in Subsec. 3.5.2 which is a true multifractal model. As pointed out in Subsec. 3.5.2, this model exhibits both volatility clustering and power law tails thus it seems to be unsuitable for our purpose of separating the contributions in synthetic time-series. In order to circumvent this problem we use a numerical technique, which we describe in detail below, which allows to remove the contribution of the tails from this model.

4.4 Multifractality proxy

In order to understand the behaviour of the scaling exponents $\zeta(q)$, among the estimators available in the literature (see for example Sec. 3.3) we chose to use a method inspired by the GHE method (cfr. Subsec. 3.3.1). As discussed in Subsec. 3.3.1, the GHE method, for a given value of q, computes several linear fits using different nested scaling regions, $[\tau_{min}, \tau_{max}]$, and outputs a value of the

[1] In [142] is reported the shape of the scaling exponent for $q > n$ to be equal to one. However, as underlined in [166] and [167], this so called bifractal behaviour is a pure finite size sample effect.

scaling exponent $\zeta(q)$ given by the average of the slopes measured. In particular it holds the value of τ_{min} fixed, increasing the value of τ_{max}. However, in what follows we do not perform any average over different nested scaling regions but we instead consider just one linear fit for a given range $\tau \in [\tau_{min}, \tau_{max}]$. In particular we focus our attention on two ranges, namely $\tau \in [1, 19]$, following the prescription of other works ([134, 133, 115]), and $\tau \in [30, 250]$. The reason for this simplification is that, given a range of τ, we did not want to weight more the small values with respect to the big values. This point will be further stressed later. Let us also note that due to the presence of the power law tails in the empirical datasets (see for example [14, 15]), the value of q should be less than the tail exponent of the analysed time-series, since the moments are not finite for large q. Moreover, the existence of a moment does not guarantee its measurement on finite samples to be reliable when its variance is not finite. Following these observations, along with the fact that the decay exponents of the empirical power law tails typically range between two and five ([14]), in our analyses we limited ourselves to $q \leq 1$. In particular we took a range of q between 0.1 and 1 every 0.1 units, having 10 points in total[2].

Once a method to measure the scaling exponents is defined, in order to assess the presence of a statistically meaningful curvature in the scaling exponents, thus multiscaling, we performed a parabolic fit over the range $q \leq 1$ and then we took the coefficient of the second degree term as a multiscaling estimator, *i.e.*

$$\zeta(q) = qH(q) \simeq Bq^2 + Aq + const, \tag{4.5}$$

where then $\hat{B}$ is the multifractality estimator[3] we adopted in this paper. It must have negative (multiscaling behaviour) or zero (uniscaling behaviour) expectation value (due to concavity). The expected value of the parameter

[2]We checked that increasing the number of points over the interval does not change the results.

[3]The notation of the hat means the estimator of the quantity under it.

const is zero and in our measurements of $\zeta(q)$ we always checked this condition for consistency. Note that in [169] the authors fit the Singularity Spectrum, with a fourth degree polynomial which implies necessarily a fourth degree polynomial functional form for $\zeta(q)$. However, for the purposes of this chapter, a second degree fit is enough and we verified that the inclusion of the terms up to the fourth degree does not modify our results. For completeness we also report the values of $H(0,1)$, $H(0,5)$, $H(1)$.

4.5 Analysis of artificial data

We started our analysis simulating 10^4 MRW processes, specified in Subsec. 3.5.2, made of 10^6 steps Δt with parameters $\lambda^2 = 0.03$, $L = 1000$, $\sigma = 1$ and computing the mean and the standard deviation of $\hat{B}$, $\hat{H}(0.5)$ and $\hat{H}(1)$ over the realizations. We then repeated the measure over the shuffled version of the time-series. The convergence of the estimators has been always checked. The values of λ^2 and L have been chosen according to empirical analyses conducted in other works (see for example [170]), while the length has been chosen to reduce as much as possible the finite size sample errors keeping reasonable computational times. The results are reported in Tabs. 4.1 and 4.2 with respectively $\tau \in [1, 19]$ and $\tau \in [30, 250]$. The theoretical values are reported in boldface within brackets under the measured values.

MRW	Plain	Shuffled
$\hat{B}$	-0.0090 ± 0.0006 $(\mathbf{-0.015})$	-0.0273 ± 0.0006 $(\mathbf{0})$
$\hat{H}(0.5)$	0.514 ± 0.001 $(\mathbf{0.5225})$	0.541 ± 0.001 $(\mathbf{0.5})$
$\hat{H}(1)$	0.509 ± 0.001 $(\mathbf{0.515})$	0.527 ± 0.001 $(\mathbf{0.5})$

Table 4.1: Comparison between $\hat{B}$, $\hat{H}(0.5)$ and $\hat{H}(1)$ for a plain and a shuffled MRW with $\tau \in [1, 19]$.

MRW	Plain	Shuffled
$\hat{B}$	-0.014 ± 0.002 $(\mathbf{-0.015})$	-0.002 ± 0.002 $(\mathbf{0})$
$\hat{H}(0.5)$	0.521 ± 0.005 $(\mathbf{0.5225})$	0.503 ± 0.005 $(\mathbf{0.5})$
$\hat{H}(1)$	0.514 ± 0.005 $(\mathbf{0.515})$	0.502 ± 0.005 $(\mathbf{0.5})$

Table 4.2: Comparison between $\hat{B}$, $\hat{H}(0.5)$ and $\hat{H}(1)$ for a plain and a shuffled MRW with $\tau \in [30, 250]$.

It is evident from the Tables that in the region $\tau \in [1, 19]$ also for MRW the non linearity of the scaling exponents increases after shuffling confirming the results of [161], while in the region $\tau \in [30, 250]$ this effect disappears and the shuffled process seems statistically indistinguishable from a BM. According to its definition (see Sec. 3.5.2), a shuffled MRW is an uncorrelated, symmetric time-series with power law tails. In light of this, a model which might give us some further indication is a tBM. In the next subsection we focus on this model.

4.5.1 The effect of the power law tails

Let us here report the estimators $\hat{B}$, $\hat{H}(0.5)$ and $\hat{H}(1)$ in the presence of power law tails. In Fig. 4.1 we report the results of the computation of the scaling exponents $\zeta(q)$ for $\tau \in [1, 19]$ of single realizations of processes with t-Student innovations made of 10^6 steps, for various values of n: $n \in [1, 5]$ every 0.5 units (cfr. Eq. 4.1). In blue solid line the measured scaling exponents of the synthetic time-series are reported, whereas in dashed red line the theoretical expectation (see Eqs. (4.2) and (4.4)). It is evident that as soon as n moves away from 1, a curvature of $\zeta(q)$ arises. But it is also evident that, as the tail index increases above $n = 2$ the graphs become more linear with apparent linearity almost recovered above $n = 5$. It is worth noting that the empirically measured tail indexes fall exactly in the range $[2, 5]$, which

is the most numerically biased. In order to make a quantitative assessment, for each value of $n = 3, 4, 5$, which roughly covers the range of empirically observed tails, we simulated 10^4 tBM made of 10^6 steps and we computed the mean and the standard deviation of $\hat{B}$, $\hat{H}(0.5)$ and $\hat{H}(1)$ for all values of n. Tabs. 4.3 and 4.4 report the numerical results for respectively $\tau \in [1, 19]$ and $\tau \in [30, 250]$ (theoretical values in boldface within brackets under measured values).

tBM	$n = 3$	$n = 4$	$n = 5$
$\hat{B}$	-0.0364 ± 0.0007 ($\mathbf{0}$)	-0.0251 ± 0.0005 ($\mathbf{0}$)	-0.0186 ± 0.0005 ($\mathbf{0}$)
$\hat{H}(0.5)$	0.570 ± 0.001 ($\mathbf{0.5}$)	0.544 ± 0.001 ($\mathbf{0.5}$)	0.531 ± 0.001 ($\mathbf{0.5}$)
$\hat{H}(1)$	0.552 ± 0.001 ($\mathbf{0.5}$)	0.531 ± 0.001 ($\mathbf{0.5}$)	0.522 ± 0.001 ($\mathbf{0.5}$)

Table 4.3: Mean and standard deviation of $\hat{B}$, $\hat{H}(0.5)$ and $\hat{H}(1)$ computed on t-Students time-series with $n = 3, 4, 5$ and $\tau \in [1, 19]$.

tBM	$n = 3$	$n = 4$	$n = 5$
$\hat{B}$	$(-9 \pm 2) \cdot 10^{-3}$ ($\mathbf{0}$)	$(-4 \pm 2) \cdot 10^{-3}$ ($\mathbf{0}$)	$(-2 \pm 2) \cdot 10^{-3}$ ($\mathbf{0}$)
$\hat{H}(0.5)$	0.517 ± 0.005 ($\mathbf{0.5}$)	0.506 ± 0.005 ($\mathbf{0.5}$)	0.503 ± 0.005 ($\mathbf{0.5}$)
$\hat{H}(1)$	0.513 ± 0.005 ($\mathbf{0.5}$)	0.504 ± 0.005 ($\mathbf{0.5}$)	0.502 ± 0.005 ($\mathbf{0.5}$)

Table 4.4: Mean and standard deviation of $\hat{B}$, $\hat{H}(0.5)$ and $\hat{H}(1)$ computed on t-Students time-series with $n = 3, 4, 5$ and $\tau \in [30, 250]$.

Let us note that in the range $\tau \in [1, 19]$ with a significance level of 1%, a multiscaling behaviour is found due to the presence of power law tails in all cases, while in the range $\tau \in [30, 250]$ only the case $n = 3$, keeps its concavity at 1% significance level, but still very lowered with respect to the other region. Thus the measurements in the latter region seem to agree better with the theoretical uniscaling behaviour.

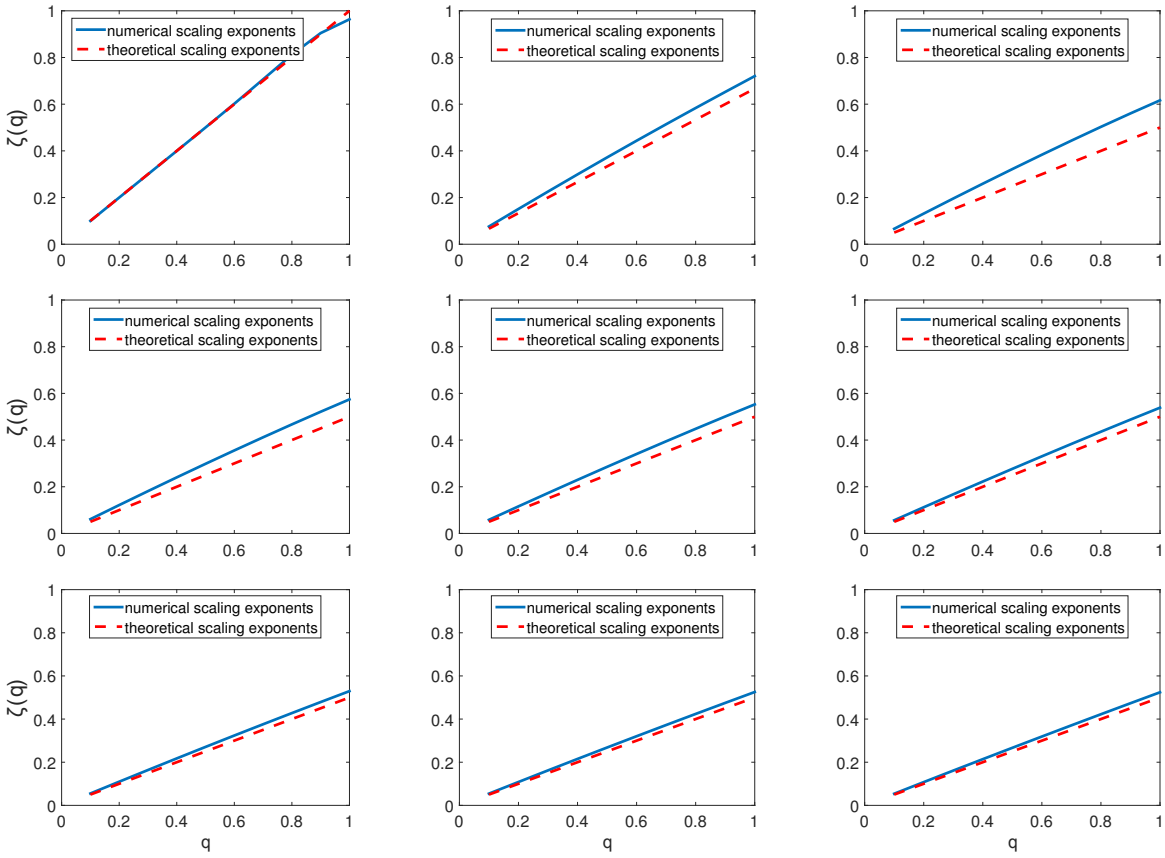

Figure 4.1: Numerical values of $\zeta(q)$ (blue solid line) against their theoretical values (red dashed line) for a tBM with $n = [1, 1.5, 2, 2.5, 3, 3.5, 4, 4.5, 5]$ taken every 0.5 units, in increasing order from left to right and top to bottom.

4.5.2 Effect of autocorrelations

In order to isolate the contribution of the autocorrelation and eliminate the effect of the tails, we applied a normalization procedure to the MRW. The method consists in changing the unconditional distribution of a time-series into a desired one preserving its causal structure as proposed in [160]. In particular, let us consider a first (empirical) time-series with a certain casual structure. Let us now consider a second synthetic time-series made of i.i.d. numbers drawn from given probability distribution. The method proposed in [160] consists in ordering the second synthetic time-series by using the ranking of the first (empirical) one, thus making the second time series inherit the causal

structure of the first one. We need however to stress a detail. If the empirical time-series has power law tails while the surrogate is normally distributed, the autocovariance of the second one has the same functional form of the first one, but its strength is lowered. This can be simply ascribed to the fact that the extreme events give a big contribution in the computations of the averages, thus normalizing them reduces the strength of the correlations at each lag. This effect can be easily seen by plotting in semilog scale on the same figure the function proposed in [154] for the estimation of the model parameters computed on a MRW and on its normalized version (nMRW). This is shown in Fig. 4.2 in semilog scale where we observe that the autocovariance of the original time-series follows well the theoretical behaviour ([154])

$$C(T) = Cov\left[\ln|r_\tau(t+T)|, \ln|r_\tau(t)|\right] = \lambda^2 \ln\left(\frac{L}{T+1}\right), \tag{4.6}$$

whereas the normalized one has a smaller effective value of λ. It is evident that the slope of the line relative to the normalized process is smaller than the slope of the line relative to the plain one (in absolute value). The behaviours of the scaling exponents $\zeta(q)$ for $\tau \in [1, 19]$ of single realizations of nMRWs made of 10^6 steps for different degree of autocorrelation λ, specified in the captions, $L = 1000$ and $\sigma = 1$ are reported in Fig. 4.3. As noted before the effective value of λ after the normalization is a bit lower than the one reported in the captions, so the theoretical line is plotted recomputing the value of λ over the normalized processes.

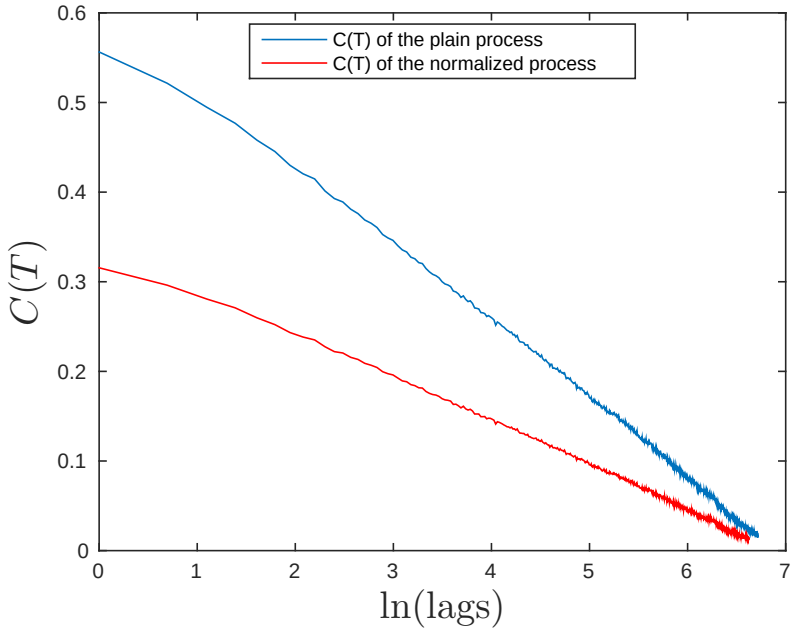

Figure 4.2: Autocovariance function of the log absolute returns for a plain (top blue) and normalized (bottom red) path drawn from a MRW made of 10^6 steps with $\lambda = 0.3$, $L = 1000$, $\sigma = 1$.

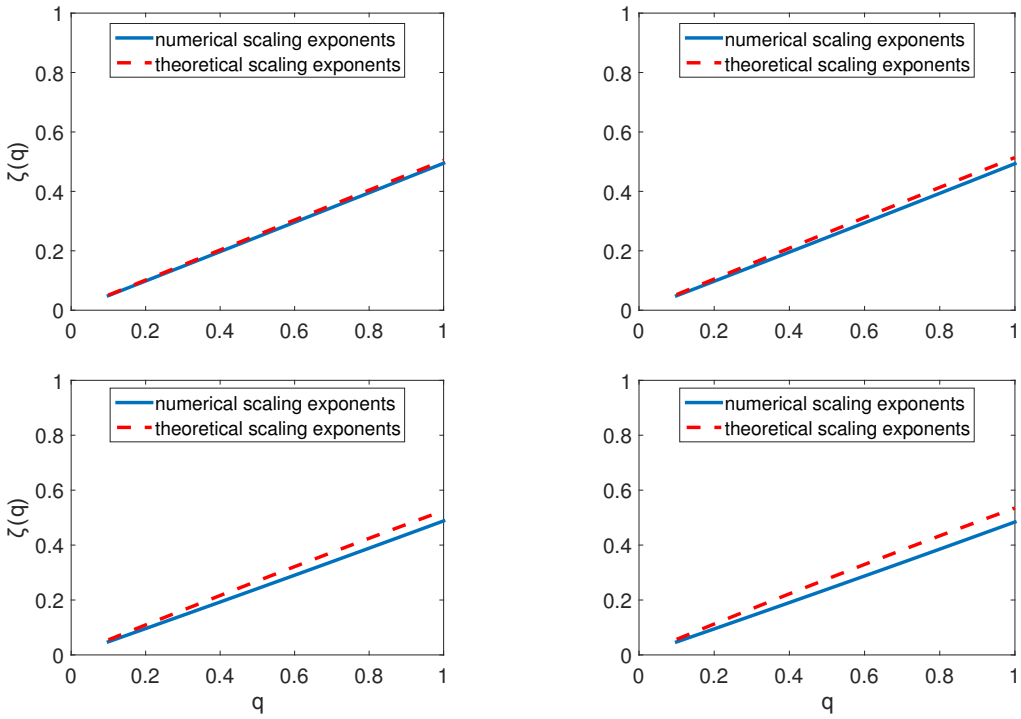

Figure 4.3: Numerical values of $\zeta(q)$ (blue solid line) against their theoretical values (red dashed line) for a nMRW with $\lambda = [0.1, 0.2, 0.3, 0.4]$, in increasing order from left to right and top to bottom.

We observe that, in all cases, the function $\zeta(q)$ changes its concavity. In order to make a quantitative assessment, for each value of $\lambda^2 = 0.03, 0.04, 0.05$, we simulated 10^4 MRWs made of 10^6 steps, we normalized them and we computed the mean and the standard deviation of $\hat{B}$ along with $\hat{H}(0.5)$ and $\hat{H}(1)$. Tabs. 4.5 and 4.6 report the numerical results for $\tau \in [1, 19]$ and $\tau \in [30, 250]$ together with the theoretical expected values in boldface under the measured ones. The effective value of λ, called λ_{eff} in the table, which affects $\hat{B}$, $\hat{H}(0.5)$ and $\hat{H}(1)$, was obtained from Eq. (4.6) by fitting the autocovariance of each normalized time-series, computing then the mean and the standard deviation.

	$\lambda^2 = 0.03$	$\lambda^2 = 0.04$	$\lambda^2 = 0.05$
λ^2_{eff}	0.0223 ± 0.0005	0.0279 ± 0.0007	0.0330 ± 0.0008
$\hat{B}$	0.0075 ± 0.0005 ($\mathbf{-0.0111 \pm 0.0003}$)	0.0085 ± 0.0005 ($\mathbf{-0.0139 \pm 0.0003}$)	0.0093 ± 0.0006 ($\mathbf{-0.0165 \pm 0.0004}$)
$\hat{H}(0.5)$	0.489 ± 0.001 ($\mathbf{0.5167 \pm 0.0004}$)	0.487 ± 0.001 ($\mathbf{0.5209 \pm 0.0005}$)	0.486 ± 0.001 ($\mathbf{0.5247 \pm 0.0006}$)
$\hat{H}(1)$	0.492 ± 0.001 ($\mathbf{0.5111 \pm 0.0003}$)	0.491 ± 0.001 ($\mathbf{0.5139 \pm 0.0003}$)	0.490 ± 0.001 ($\mathbf{0.5165 \pm 0.0004}$)

Table 4.5: Mean and standard deviation of $\hat{B}$, $\hat{H}(0.5)$ and $\hat{H}(1)$ computed on nMRWs with $L = 1000$, $\sigma = 1$ and $\tau \in [1, 19]$.

	$\lambda^2 = 0.03$	$\lambda^2 = 0.04$	$\lambda^2 = 0.05$
λ^2_{eff}	0.0223 ± 0.0005	0.0279 ± 0.0006	0.0330 ± 0.0008
$\hat{B}$	-0.007 ± 0.002 ($\mathbf{-0.0111 \pm 0.0003}$)	-0.009 ± 0.002 ($\mathbf{-0.0139 \pm 0.0003}$)	-0.010 ± 0.002 ($\mathbf{-0.0165 \pm 0.0004}$)
$\hat{H}(0.5)$	0.511 ± 0.005 ($\mathbf{0.5167 \pm 0.0004}$)	0.513 ± 0.005 ($\mathbf{0.5209 \pm 0.0005}$)	0.515 ± 0.005 ($\mathbf{0.5247 \pm 0.0006}$)
$\hat{H}(1)$	0.507 ± 0.005 ($\mathbf{0.5111 \pm 0.0003}$)	0.508 ± 0.005 ($\mathbf{0.5139 \pm 0.0003}$)	0.509 ± 0.005 ($\mathbf{0.5165 \pm 0.0004}$)

Table 4.6: Mean and standard deviation of $\hat{B}$, $\hat{H}(0.5)$ and $\hat{H}(1)$ computed on nMRWs with $L = 1000$, $\sigma = 1$ and $\tau \in [30, 250]$.

These results confirm the change of the concavity of the scaling exponents in the region $\tau \in [1, 19]$. Indeed, we observe in Tab. 4.6 that, within the 1% significance level, all $\hat{B}$ stay positive. Positive values of $\hat{B}$ imply the convexity

of the function $\zeta(q)$, which, in the multifractal picture, is supposed to be concave.

The region $\tau \in [30, 250]$ is instead much more well-behaved having in all three cases concave scaling exponents within the 1% significance level, despite for $\lambda^2 = 0.05$ only (the most correlated) the measured $\hat{B}$ falls slightly outside the 1% significance level from the expected value.

4.6 Analysis of real data

4.6.1 Dataset

The dataset we focused our attention on is the log-price of the *Dow Jones Industrial Average* (DJIA) from 02/01/1900 to 29/12/2000 taken on a daily basis, made of 25,366 points. We report in Fig. 4.4 the scaling of the moments (cfr. Eq. (3.5)) respectively, for $\tau \in [1, 19]$ and $\tau \in [30, 250]$ in blue solid lines along with their linear fit in red dashed lines.

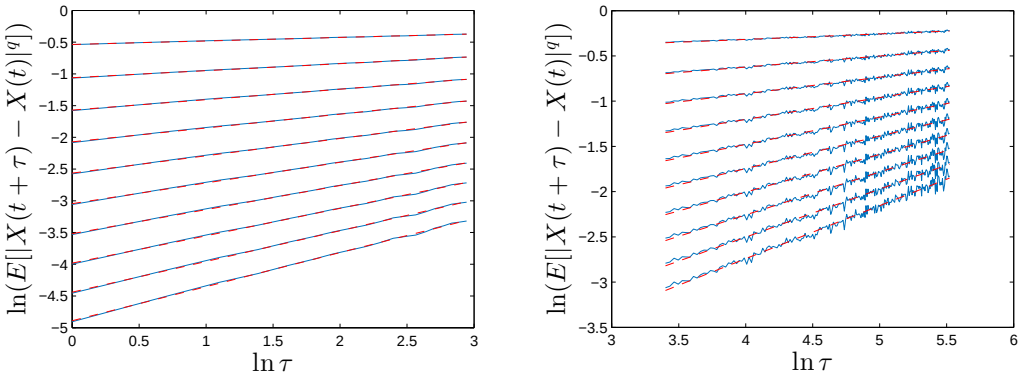

Figure 4.4: Left panel: scaling of the moments of the DJIA time-series with $\tau \in [1, 19]$. Right panel: scaling of the moments of the DJIA time-series with $\tau \in [30, 250]$. The values of q are taken in the interval $[0.1, 1]$ every 0.1 units, increasing from top to bottom in both panels.

In Fig. 4.5 the scaling exponents $\zeta(q)$ are reported again in both regions of τ, (blue crosses); as it appears evident, the parabolic shape of Eq. 4.5 (red dashed lines) seems to fully capture the empirical behaviour.

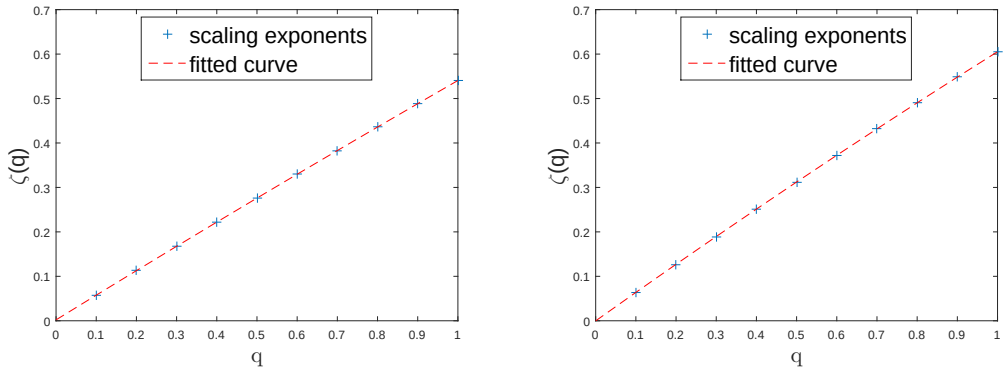

Figure 4.5: Left panel: scaling exponents $(qH(q))$ of the DJIA time-series with $\tau \in [1, 19]$. Right panel: scaling exponents $(qH(q))$ of the DJIA time-series with $\tau \in [30, 250]$

This time-series exhibits power law tails and we computed the decay exponents of the tails using the method proposed in [19, 20], based on Maximum-Likelihood Estimators and the Kolmogorov-Smirnov test. Fig. 4.6 reports the fit of the complementary cumulative distribution of the left and the right tails in loglog scale. For the left tail on the x-axis is reported the logarithm of minus the negative returns. The estimated values of the tails exponents are

$$\alpha_{left} = 3.20 \pm 0.05 \quad \alpha_{right} = 3.61 \pm 0.06; \tag{4.7}$$

they are different within the errors and so the time-series exhibits skewness. We verified that however skewness has no effects on the measured multifractality.

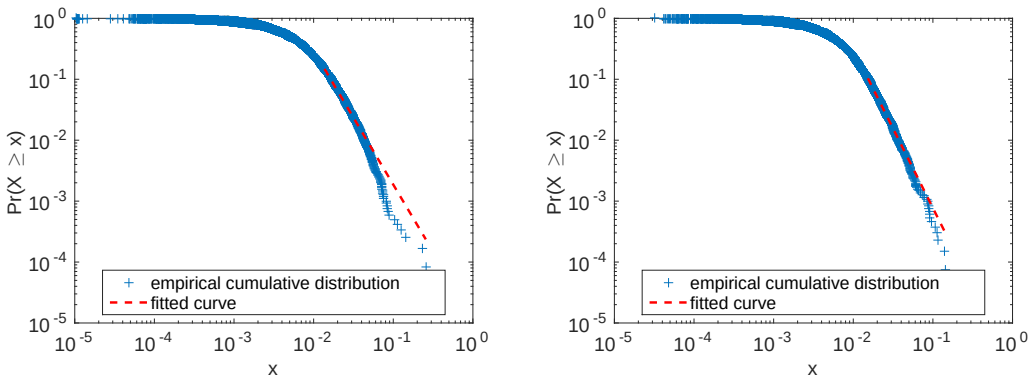

Figure 4.6: Left panel: left tail of the DJIA time-series. Right panel: right tail of the DJIA time-series.

4.6.2 Effect of power law tails and autocorrelation in real data

In order to uncover the source of the multiscaling behaviour of our dataset we used the following two procedures: the shuffling (cfr. [161]), in order to isolate the effects of the power law tails, and the normalization (cfr. [160]), in order to isolate the effects of the autocorrelation. We focused first on the region $\tau \in [1, 19]$. A first test we made is a comparison of the scaling exponents of the DJIA and a tBM, in order to check whether the empirical measured multiscaling behaviour after shuffling could be all ascribed to the presence of the power law tails or not. In order to do so, we took the DJIA time-series and shuffled it 10^4 times. On every time-series obtained we computed $\hat{B}$, $\hat{H}(0.5)$ and $\hat{H}(1)$, this allowed us to associate a mean and a standard deviation coming from the shuffling procedure. We then compared these values with the ones obtained computing $\hat{B}$, $\hat{H}(0.5)$ and $\hat{H}(1)$ on 10^4 tBM with the same length of the DJIA time-series and tails equal to the heavier empirical one, namely α_{left}. A second test regards checking the behaviour of the DJIA time-series after normalization in order to test if the change of concavity holds for empirical data. We normalized then our time-series 10^4 times, computing the mean and the standard deviation of $\hat{B}$, $\hat{H}(0.5)$ and $\hat{H}(1)$. The results are reported in Tab. 4.7 along with the value of $\hat{B}$, $\hat{H}(0.5)$ and $\hat{H}(1)$ computed on the plain time-series.

	DJIA	$\text{DJIA}_{shuffled}$	$\text{DJIA}_{normalized}$	tBM
$\hat{B}$	-0.019	-0.039 ± 0.003	0.0026 ± 0.0005	-0.034 ± 0.004
$\hat{H}(0.5)$	0.552	0.572 ± 0.007	0.5082 ± 0.0008	0.563 ± 0.007
$\hat{H}(1)$	0.541	0.551 ± 0.006	0.5092 ± 0.0006	0.546 ± 0.007

Table 4.7: Plain, shuffled and normalised DJIA time-series and a tBM with $\tau \in [1, 19]$.

According to these simulations we confirm previous results that after shuf-

fling the measured multiscaling behaviour of real data increases for $\tau \in [1, 19]$ (see [161]). Moreover it appears evident that this increased value is statistically indistinguishable from the one of the tBM, which is uniscaling. This result led us to infer that the multiscaling measured on shuffled empirical time-series should be ascribed only to the presence of power law tails.
The normalised time-series changes its concavity after normalization (stays positive within the 1% significance level), showing the same issue observed previously for the MRW.

Let us now turn our attention to the region $\tau \in [30, 250]$; results are reported in Tab. 4.8.

	DJIA	$\text{DJIA}_{shuffled}$	$\text{DJIA}_{normalized}$	tBM
$\hat{B}$	-0.038	-0.01 ± 0.01	-0.0036 ± 0.0007	-0.014 ± 0.007
$\hat{H}(0.5)$	0.624	0.53 ± 0.03	0.6244 ± 0.0006	0.52 ± 0.02
$\hat{H}(1)$	0.605	0.52 ± 0.03	0.6229 ± 0.0005	0.52 ± 0.02

Table 4.8: Plain, shuffled and normalised DJIA and a tBM time-series with $\tau \in [30, 250]$.

We observe first that the results change considerably. Secondly, within the 1% significance level the shuffled time-series can be considered uniscaling, as it happens for the tBM, so there is not an increase in multifractality. Thirdly the normalized time-series keeps its concavity, thus it is not affected anymore by the negative bias mentioned previously. This therefore demonstrates that a statistically significant multiscaling behaviour is present in financial time-series.

4.7 Discussion

Our analyses provide clear evidence that the estimation of the scaling exponents is affected by the aggregation horizon. We chose two regions: (1) $\tau \in [1, 19]$, which is in line with previous works and (2) $\tau \in [30, 250]$. We

observed that the analyses on the region $\tau \in [1, 19]$ do not reproduce the theoretical expectations on time-series exhibiting power law tails or autocorrelation structures like the empirical ones. We also found an unexpected concavity of the scaling exponents $\zeta(q)$ on tBMs and nMRWs. These results are in line with previous observations on real time-series and actually enable us to give them an explanation. In particular in [161] the authors argue that the presence of autocorrelations in real data can induce a negative bias in the estimation of the scaling exponents. According to our interpretation, the change of concavity of $\zeta(q)$ (reported in Tab. 4.7) is exactly the effect of the negative bias. In light of this, the increased multiscaling behaviour measured in [161] after shuffling has to be ascribed to the fact that the causal structure of a shuffled time-series is destroyed along with the negative bias itself and only the power law tails effect is left resulting in an apparent increase of multiscaling.

For what concerns the region $\tau \in [30, 250]$ we observed that the spurious multiscaling found on tBM processes and on the DJIA time-series is lower with respect to the measurements performed in the $\tau \in [1, 19]$ region, being even statistically absent for $n = 4, 5$ and for the DJIA as well. Furthermore, the convexity of $\zeta(q)$ returns to a concavity, almost removing the negative bias effect. We conclude therefore that GHE measurements of multifractality in the region $\tau \in [30, 250]$ are reliable and reveal that some degree of multifractality is present in real financial log-return time-series and it has to be ascribed to the effect of the causal structure of the process.

We report that a similar distinction between small scales and big scales regions was reported also in [171]. At this point a question to address is why there is a so big difference in the two regions of τ. For what concerns the effect of the tails we explain this difference via the speed of convergence of the Central Limit Theorem (CLT). In particular, for processes exhibiting increments with power law tails, with tails index bigger than two, it is well-known that

under aggregation they behave, in the asymptotic limit, as a BM. The speed of convergence depends on how heavy the tails are but if the aggregation is finite, whatever the tails index is, there will always be a region in the final part of the tails of the probability density which will have a power law behaviour. The effect of increasing the aggregation horizon is to push this region further in the tail. This explains why, increasing the aggregation horizon, the spurious power law tails concavity tends to disappear, reconciling with the theoretical expectations. Counter-intuitively processes with increments exhibiting tails with exponents less than two are less affected by this problem, since their convergence under aggregation is ruled by a generalized Central Limit Theorem and they keep their power law nature in the tails of the distribution so the convergence is faster. Concerning the autocorrelation we postpone the whole discussion to the next chapter where at thorough analysis of the scaling behaviour is performed.
In light of these results we argue that in order to make a reliable measure of multifractality, regions of τ with a small aggregation horizon should be taken with care. Let us however stress that the region $\tau \in [30, 250]$ has not been chosen optimizing the performance of the multifractal estimator. However it proved to be sufficient to give us valuable insights and improved our estimation of the scaling parameters.

Let us make few other observations concerning the measurements. Since the measures, as proposed here (cfr. Subsec. 4.4), depend on two parameters, τ_{min} and τ_{max}, we report that in general, τ_{min} rules the precision while τ_{max} the accuracy. So a bigger value of τ_{min} would reflect in measured values nearer to expected ones. On the other hand taking bigger values of τ_{max} ends up in including more oscillating values in the analysis, thus in a larger standard deviation. However for a process like the MRW, attention must be paid, since, if τ_{min} becomes bigger than the autocorrelation length, no multifractal behaviour

holds anymore, since the increments of the process become independent. So the range of τ must be taken large enough to reduce as much as possible the power law tails effect, but not too much to exceed the time-span where the correlations are relevant. Finally, we notice that it appears evident that at small ranges of τ the power law tails concavity has a bigger impact to the measures with respect to the convexity induced by the autocorrelation.

4.8 Summary

In this chapter we studied the multiscaling behaviour of financial time-series by studying synthetic and real datasets at different aggregation horizons. We started by analysing the MRW, finding that, for small aggregation horizons, the multiscaling behaviour after shuffling, appears to increase, in agreement with previous works on empirical datasets. However for larger aggregation horizons this effect disappears. Since the shuffling procedure destroys the temporal structure of a time-series, but preserves its unconditional distribution, we focused our attention on the scaling properties of another process, the tBM which is a unifractal process. It turned out that for small aggregation horizons the presence of power law tails induces a concavity in the scaling exponents, indicating therefore a multiscaling behaviour which is however not predicted by the theory. We turned then our attention to the causal structure of a time-series. In this case we observed that, at small aggregation horizons, the presence of autocorrelation introduces a negative bias, *i.e.* a reduced concavity which ended up in a convexity of the scaling exponents, both for synthetic and real time-series. These numerical findings explain well the puzzling increase in multifractality found in previous works after shuffling: as long as both power law tails and autocorrelation are kept, the spurious multiscaling contribution of the tails is lessen by the presence of the autocorrelation, while after shuffling, only the tails effect is present. We pointed out that the aggregation of

the returns is crucial. Indeed for higher aggregation horizons all these issues disappear or at least strongly lessen. For what concerns the tails we interpret this effect as a consequence of the Central Limit Theorem and its speed of convergence on time-series with power law tails and finite variance. In particular the range of tail exponents between two and five turned out to affect the most the measurements. This is due to the fact that under aggregation a residual of the power law tail is always present in the unconditional distribution and the nearer the exponent is to two, the stronger the effect. We finally note that, choosing higher values of aggregations can reduce this effect but this requires to have longer time-series. Before concluding, let us highlight that the considerations which follow the results reported in this chapter do not apply only to the analysis of financial time-series, but to any time-series where a (uni)multifractal signal is looked for.

Chapter 5

Asymptotic scaling properties and estimation of the Generalized Hurst Exponents in financial data

In this chapter we propose a new method to measure the Hurst exponents of financial time-series. The scaling of the absolute moments against the aggregation horizon of real financial processes and of both uniscaling and multiscaling synthetic processes converges asymptotically towards linearity in log-log scale. In light of this we found appropriate a modification of the usual scaling equation via the introduction of a filter function. We devised a measurement procedure which takes into account the presence of the filter function without the need of directly estimating it. We verified that the method is unbiased within the errors by applying it to synthetic time-series with known scaling properties. Finally we show an application to empirical financial time-series where we fit the measured scaling exponents via a second or a fourth degree polynomial, which, thanks to theoretical constraints have respectively only one and two degrees of freedom. We found that on our dataset there is not clear preference among the second or fourth degree polynomial. Moreover the study of the filter functions of each time-series shows common patterns of convergence depending on the momentum degree.

5.1 Introduction

In Sec. 3.3, among others, we reviewed the most important methods for estimating the univariate multifractal spectrum of synthetic and empirical time-series, namely MFDFA [142], GHE [102, 133, 134, 141] and WWTM [144]. As pointed out in Sec. 3.3 all of them have advantages and drawbacks. Moreover they deal with the study of the scaling of a certain quantity against another one but none of them gives a prescription on how to properly choose the scaling region and why certain regions should be discarded.

The aim of this chapter is to propose a new method for the estimation of the scaling behaviour of the moments of real financial time-series with respect to the aggregation horizon, without the need of free parameters and which gives a precise prescription of the scaling region which has to be considered. In the previous chapter, solving an ongoing debate in the literature (see for example [160, 161, 162]), it has been clarified that the true source of the multifractal behaviour found in empirical financial time-series is their autocorrelation structure. However it was also shown that the measure of multifractality performed via the scaling of the moments in log-log scale is aggregation horizon dependent and that the true multifractal scaling should be measured in the limit of infinite aggregation horizon. In particular, already for processes with i.i.d. increments but with power law tails in their distribution with exponents between 2 and 5, which is the range empirically observed [15], due to the slow convergence of the Central Limit Theorem the small aggregation horizon is affected by strong biases [8]. In light of this, we now face the problem of building up an estimation procedure able to address these issues and to reduce as much as possible these biases by proposing a reliable proxy of the asymptotic multifractal behaviour of real financial time-series. For reason that are detailed later in the chapter the method is well-suited for intraday high frequency data, in particular we focus on tick-by-tick data.

The structure of the chapter is as follows: in Sec. 5.2 we discuss the effect of the discreteness of processes on scaling measures, in Sec. 5.3 we introduce the method, in Sec. 5.4 we show a step by step application of the method on a synthetic process with known multifractal properties, in Sec. 5.5 we perform first a step by step application of the method to one real financial time-series then we apply it to different real time-series and in Sec. 5.6 we draw the conclusions.

5.2 The curse of the discretization

As underlined in Subsec. 3.2.4 the introduction of the multifractal formalism allows to study the geometrical fractal properties of a process by analysing its discrete version. However, as shown in the previous chapter, the estimation of the scaling exponents turns out to be strongly biased. Convergence issues arise for both power law-tailed and autocorrelated discrete processes, both for synthetic and real data. In this section we discuss in more detail these two features in the case of synthetic processes, which in turn will justify our choice of introducing the filter function in Sec. 5.3. The need of the filter function also for real financial process will become evident in Sec. 5.5 where we apply our method to real data.

5.2.1 Effect of the CLT

In the previous chapter we pointed out that for processes with independent increments, power law tails and finite variance the asymptotic convergence is obviously ruled by the CLT. We want here to show results showing the actual numerical behaviour of this convergence. Let us then consider a discrete process with independent increments x_i i.i.d. distributed according to a certain pdf $p(x_i)$ for all i such that

$$E[x_i] = 0, \quad Var[x_i] = \sigma^2 \Delta t < \infty, \tag{5.1}$$

for some constant σ, where Δt is the time interval between two increments. Let us stress that we are not making any assumption on $p(x_i)$ which can be skewed, power law-tailed or both as long as the variance is finite. For example it could be the density of a shuffled empirical time-series. We now introduce the quantity

$$S_N = \sum_{i=1}^{N} x_i, \tag{5.2}$$

which is an the aggregated sum of N returns, thus

$$E[S_N] = 0, \quad Var[S_N] = \sum_{i=1}^{N} Var[x_i] = \sigma^2 N \Delta t, \tag{5.3}$$

so the variance grows linearly with time as expected. We stress now that the quantity we use to measure the scaling of empirical time-series is exactly $E[|S_N|^q]$. In this case we are considering it for a shuffled/independent process. The scaling properties of S_N are a straightforward consequence of the CLT. It can be shown (see B for an explicit computation) that

$$E[|S_\infty|^q] = \lim_{\substack{\Delta t \to 0 \\ N \to \infty \\ N\Delta t = \tau}} E[|S_N|^q] = \sigma^q \frac{2^{\frac{q}{2}} \Gamma(\frac{q+1}{2})}{\sqrt{\pi}} \tau^{\frac{q}{2}}. \tag{5.4}$$

Eq. 5.4 proves rigorously that any i.i.d. process with finite variance aggregates asymptotically into a unifractal process and in particular it scales as a BM (we underline that it holds also for shuffled empirical financial time-series). As a corollary, this also shows that empirical multifractality can arise only from a non trivial causal structure.

5.2.1.1 First example: power law tails

We apply here Eq. (5.4) to the case of tBM (cfr. Sec. 4.3). For our purposes we chose the number of degrees of freedom (DoF) to be equal to $n = 3$ and, in order to reduce the statistical fluctuation as much as possible, we generated a time-series made of 10^7 steps. For a tBM Eq. (5.4) tells us everything about

its asymptotic behaviour. In particular, with $n = 3$ and $q = 1$,

$$E[|S_\infty|] = \sqrt{\frac{6}{\pi}}\tau^{\frac{1}{2}}, \tag{5.5}$$

thus

$$\ln\left(E[|S_\infty|]\right) = \frac{1}{2}\ln(\tau) + \ln\left(\sqrt{\frac{6}{\pi}}\right). \tag{5.6}$$

In Fig. 5.1 we superpose the theoretical behaviour of Eq. (5.6) with the numerical one. As appears evident the linearity is achieved only asymptotically

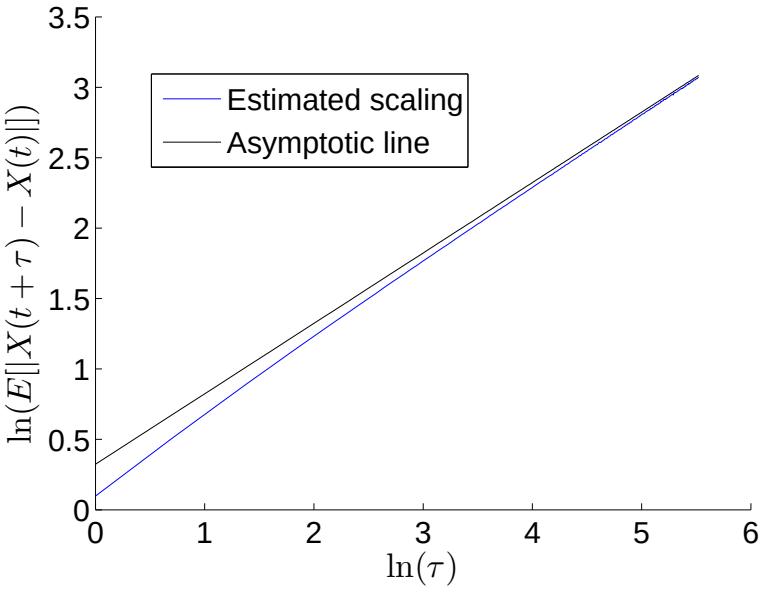

Figure 5.1: Blue solid line: numerical scaling of $E[|S_N|]$ for a tBM with $n = 3$ (cfr. Eq. (B.3) with $q = 1$). Black solid line: theoretical expectation in the continuous time limit.

(cfr. the effect of the productory in Eq. (B.3)).

5.2.1.2 Second example: shuffled MRW

In this subsection we apply Eq. (5.4) in the case of shuffled MRW. We set the parameters to $\lambda = 0.3$, $L = 5000$ and $\sigma = 1$ (because of the shuffling the choice of the values of λ and L may be arbitrary while σ is simply a scale) and again we generated a time-series made of 10^7 steps to remove as much noise as possible. In Fig. 5.2 we superpose the theoretical behaviour of Eq. (5.4)

with the numerical one for $q = 1$. As appears evident the linearity is achieved

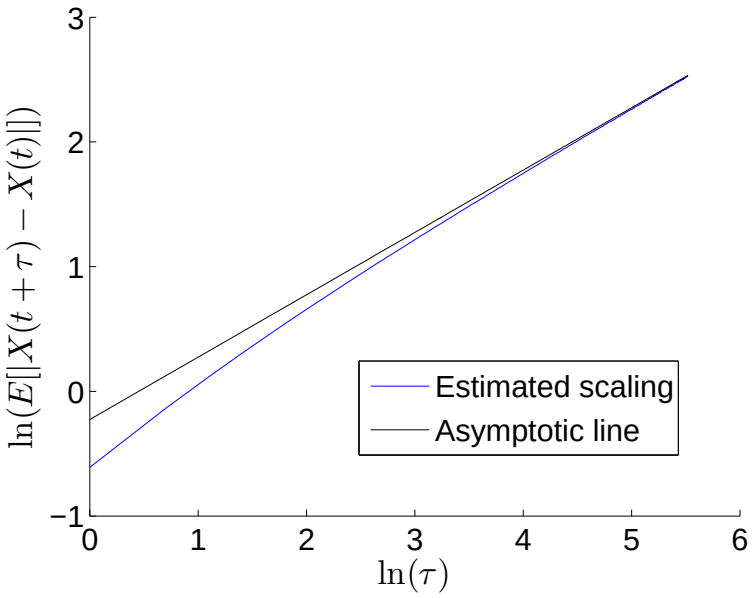

Figure 5.2: Blue solid line: numerical scaling of $E[|S_N|]$ for a shuffled MRW (cfr. Eq. (B.3) with $q = 1$). Black solid line: theoretical expectation in the continuous time limit.

again only asymptotically (cfr. the effect of the productory in Eq. (B.3)).

5.2.2 Effect of the autocorrelation

In the previous chapter it is proven numerically that the autocorrelation is the true source of the empirical multifractality. In the same direction is the result of Subsec. 5.2.1 which proves that the shape of the distribution plays no role in the asymptotic scaling as long as the variance is finite. However for small aggregation horizons scaling measures are strongly biased also when the effect of the tails is removed (see Chapter 4). These observations lead to the puzzling conclusion that the causal structure is, from the theoretical point of view, the source of the multifractal nature of a process, but, from a numerical point of view, also the source of a bias. In order to reconcile these results let us consider the case of the MRW. A first observations is that Eq. (3.40) holds in

the continuous time limit whereas synthetic and real processes are inherently discrete in time. A second observation is that the innovations of the discretized version of the MRW, shown in Eq. (3.37), are conditionally Gaussian, whereas the distribution of the innovations in the continuous time limit has power law tails (cfr. [132]). It is worth noting that in this case continuous time limit means aggregating an infinite number of conditionally Gaussian variables with a certain memory structure given by Eq. (3.38). Thus, for the MRW, the mismatch arises because the discrete process in Eq. (3.37) is not a multifractal process described by the scaling exponents in Eq. (3.40), but its infinite aggregation limit (continuous time limit) is.

We propose that the same feature also holds for real financial processes, by arguing that the distribution of the returns at their smallest considered scale (for example tick-by-tick) is different from their distribution at large aggregations. For instance, one evident difference between returns taken on a tick-by-tick basis and, say, daily returns, is the role of the tick size ([172]). In the first case the returns have discrete values, while in the second case they can be safely modelled as continuous. We now want to give an empirical proof to this observation via a simple analysis. In order to do so, we need to build a proxy which gives us information about how dense the returns are on their domain, which is an interval of the real line. We manage to do so by defining the following quantity:

$$\Delta(\tau) = \min_{\tau} \left(\left\{ \frac{|r_\tau(t)|}{\sqrt{\tau}} \right\} / \{0\} \right), \tag{5.7}$$

which is the value of the minimum return in absolute value (smaller log-price change without the sign) found at a certain level of aggregation, excluding the value zero and scaled with the square root of the aggregation itself. The reason for dividing by the square root relies on the fact that in order to compare the value of returns at different aggregations the effect of the growth of the variance with the aggregation must be removed, in particular, since after few

lags the plain returns are uncorrelated, the variance grows linearly with the aggregation. We show here this analysis carried on two intraday time-series, namely American International Group (AIG) and Procter & Gamble (PG), taken between 12/10/2015 and 11/11/2015 on a tick-by-tick basis and traded on the NYSE. In Fig. 5.3 it is shown the behaviour in loglog scale of $\Delta(\tau)$ for AIG and PG. It is quite clear that for both time-series the quantity $\Delta(\tau)$ follows a power law which then converges asymptotically to zero. The spikes found at higher aggregations are due to the finiteness of the samples, still their power law baseline is clearly visible. This proves that the distribution of real financial returns converges asymptotically to a process continuous in value. As

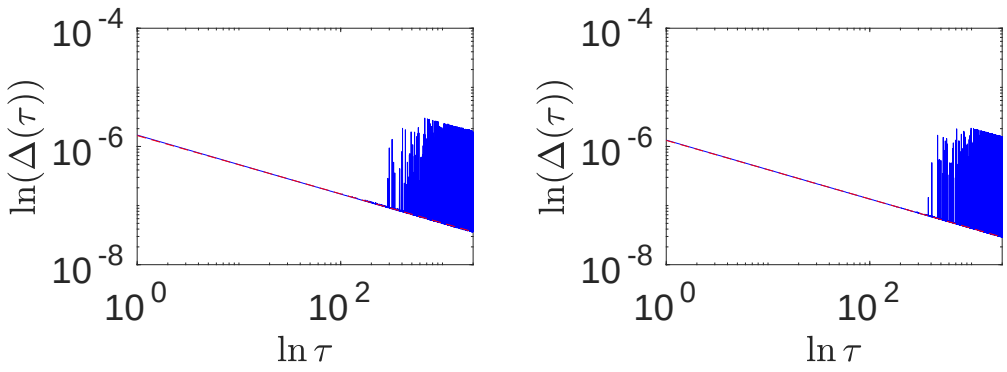

Figure 5.3: Left panel: in blue solid line the behaviour of $\Delta(\tau)$ for AIG while in red dashed line the liner fit. Right panel: in blue solid line the behaviour of $\Delta(\tau)$ for PG while in red dashed line a liner fit.

a corollary of these observations, we observe that for the BM and the fBM the convergence issues are not present because the distribution of the increments in the discrete version of the processes are Gaussian as the distribution of the increments in the continuous time limit *i.e.* they are described by a distribution stable under aggregation.

5.3 Building a scaling exponents proxy

In this section we provide a procedure to estimate the scaling exponent of a given time-series. It is made up of two parts: the first consists in giving a reliable parameter free estimate of the set of scaling exponents taking into account the convergence issues discussed above, in the second, a fit of the measured scaling exponents is performed, allowing then to smooth them according to the theoretical prescriptions of the multifractal picture.

5.3.1 Taking into account the convergence issues

As shown in the previous section, the scaling properties of a time-series are completely uncovered only in the limit of infinite aggregation. In practical situations this condition is obviously unrealistic. In particular, for a process continuous in time, the condition of infinite aggregation of the increments is already satisfied at any finite aggregation horizon, while for a discrete time-series the infinite aggregation request translates into infinite aggregation horizon. It thus seems that the multifractal properties of a discrete time-series are theoretically uncovered only asymptotically. Let us consider then the logarithm of Eq. (3.5)

$$\ln\left(E[|X(t+\tau)-X(t)|^q]\right) = \zeta(q)\ln(\tau) + \ln\left(K(q)\right). \tag{5.8}$$

In the previous chapter it was proven that the scaling measures are horizon dependent, in other words the results change with τ, reconciling with the theoretical expectations for large values of τ. It means in particular that the scaling is not exactly linear. In light of this we argue that for discrete processes the right hand side of Eq. (5.8) is an oblique asymptote. In other words, Eq. (5.8) holds exactly for every τ only for processes continuous in time, while for discrete ones a correction is needed due to the convergence issues. Let us define then $x = \ln(\tau)$ and $f(x) = \ln\left(E[|X(t+\tau)-X(t)|^q]\right)$ for a given value

of q. Using these variables the usual fit performed in order to unveil the scaling structure of a time-series is

$$f(x) = mx + z \tag{5.9}$$

where then $m = \zeta(q)$ is the quantity we are interested in and z is the logarithm of the q-moment for $\tau = 1$. We propose now instead to take into account the convergence issues by generalizing Eq. (5.9) as

$$f(x) = g(x) + mx + z \tag{5.10}$$

where $g(x)$ is a correction function which we call filter function, which models the convergence toward the asymptotic behaviour. Coherently with the previous section, Eq. (5.10) has to satisfy the condition $g(x) \xrightarrow[x\to\infty]{} 0$. For real time-series, determining the actual shape of $g(x)$ is a hard task, however we developed a data driven method which allows to take into account the presence of $g(x)$ without computing it explicitly.

5.3.2 Taking advantage of the convergence issues

The first step is considering the integral of the signal. This implies that the scaling is now supposed to be given by the integral of Eq. (5.10), namely

$$F(x) = \int_0^x (g(x') + mx' + z)\, dx' = \int_0^x g(x')dx' + \frac{m}{2}x^2 + zx, \tag{5.11}$$

which is a parabola plus the integral of the filter function. Let us now assume that the filter function has a finite integral over the positive real axis[1], *i.e.*

$$\int_0^\infty g(x)dx = const, \tag{5.12}$$

which we will prove numerically in the next sections during applications. So it follows that

$$F(x) \xrightarrow[x\to\infty]{} \frac{m}{2}x^2 + zx + const. \tag{5.13}$$

[1] We recall that $g(x) \xrightarrow[x\to\infty]{} 0$ by definition, which is a necessary but not sufficient condition for the convergence of its integral.

We fit then the integrated empirical scaling with a parabolic shape, namely

$$p(x) = ax^2 + bx + c. \tag{5.14}$$

Theoretically it should be in perfect agreement with the empirical scaling in the interval[2] $[\tau^*, \infty)$ with $\tau^* \gg 1$. Varying then τ^* between 1 and ∞ we expect the term of degree zero in Eq. (5.14) *i.e.* $c(\tau^*)$, to reach asymptotically a plateau since it represents the area between the empirical scaling and the asymptotic linear scaling. Three scenarios are possible: if the empirical scaling tends to the asymptote from above, we expect $c(\tau^*)$ to be positive since the integral of the filter function is a positive number, if the empirical scaling tends to the asymptote from below, we expect $c(\tau^*)$ to be negative since the integral of the filter function is a negative number, if the empirical scaling oscillates around the asymptote before converging on it, we expect $c(\tau^*)$ to present maxima and minima.

5.3.3 Finding the maximum value of the aggregation

However due to the finiteness of empirical samples a maximum value of aggregation, τ_{max}, has to be found. Moreover, from a theoretical point of view the multifractal scaling holds only as long as the causal structure plays a role (cfr. [8]). In light of this we infer that a good proxy for the value of τ_{max} is the autocorrelation length. It is known (cfr. [173, 21]) that, given an iid discrete process of length T, say $|r_\tau(t)|^q$, its autocorrelation function behaves asymptotically as a normally distributed noise, $N(0, 1/T)$. In light of this, the most common choices for cutting its autocorrelation profile are:

1. the first lag when the autocorrelation function of $|r_\tau(t)|^q$ reaches the 99%th of the noise distribution,

2. the first lag when the autocorrelation function of $|r_\tau(t)|^q$ reaches the 95%th of the noise distribution,

[2] We recall that $x = \ln(\tau)$.

3. the first lag when the autocorrelation function of $|r_\tau(t)|^q$ reaches the 50%th (zero level) of the noise distribution.

Since fixing one of these criteria would be arbitrary, for empirical data we apply all three prescriptions running our algorithm for all of them, deciding afterwards the best of the three using a criterion we discuss in a following subsection based on the root-mean-square error. We however report that in general, given a certain value of τ_{max}, it is always a good habit to check the empirical scaling in loglog scale and, if linearity does not hold, reduce τ_{max} accordingly.

5.3.4 Finding the minimum value of the aggregation

Let us now describe how the value of τ_{min} is fixed. Going back to the function $c(\tau^*)$, fixing a maximum value means that now finite size effects occur. In particular we found that when τ^* approaches τ_{max}, $c(\tau^*)$ starts to wildly oscillate because the number of points over which the fit is performed becomes too small. Thus we need to understand which value of $c(\tau^*)$ gives us a good approximation of its asymptotic behaviour, which in turn would give us information about τ_{min}. In principle we do not know if the empirical scaling will settle on its asymptote from above or below (maybe oscillating before), however we expect a good approximation of its asymptotic behaviour to be given either by one of its maxima, if it finally settles from above, or by one of its minima, if it finally settles from below. In order to make a statistically meaningful decision, we prescribe to take, among the set of all maxima and minima of $c(\tau^*)$, the one which attains the maximum value of the adjusted coefficient of determination [174]. We call the value of τ^* where this maximum/minimum occurs τ_{min}. In order to avoid the method to detect spurious maxima/minima) due to noise in the scaling we add the condition that the τ_{min} have to be such that $H(q) = 2a(\tau_{min})/q > 0.5$ to ensure the concavity

of the function $\zeta(q)$. Once both the values of τ_{min} and τ_{max} are fixed, the best linear fit of the scaling of the considered moment can be performed in the range $[\tau_{min}, \tau_{max}]$, where the slope gives the value of scaling exponent itself.

5.3.5 Fitting the scaling exponents

The procedure described up to now is completely parameter-free and allows to estimate single scaling exponents. In order to smooth the measured scaling exponents coherently with the multifractal picture requirement and to make a quantitative assessment about the overall shape of the empirical functions $\zeta(q)$, we decided to perform a polynomial robust fit, using the least absolute residuals method (see [175]), with q between -0.9 and 1 every 0.1 units, extending then the prescription given in [8]. In particular we used a second and a fourth degree polynomials[3]. Let us first consider the latter, namely

$$\zeta(q) = Dq^4 + Cq^3 + Bq^2 + Aq + const. \tag{5.15}$$

In its most general form Eq. (5.15) has 5 degrees of freedom, however, the function $\zeta(q)$ must satisfy few conditions, in particular

$$\begin{cases} \zeta(0) = 0 \\ \zeta(2) = 1 \\ \zeta''(q) < 0. \end{cases} \tag{5.16}$$

The first condition follows directly from the definition of the scaling exponents (see Subsec. 3.2.2), the second one, which implies $H(2) = 0.5$, follows from the absence of autocorrelation in the empirical financial returns (we give a simple proof of this in C), the third one follows from the concavity condition (cfr. Subsec. 3.2.2 and references). Applying these conditions to Eq. (5.15), they become respectively (we report the explicit computation of the third condition in D)

$$\begin{cases} const = 0 \\ A = \dfrac{1}{2} - 8D - 4C - 2B \\ B = \dfrac{3C^2}{8D} \text{ with } D < 0, \end{cases} \tag{5.17}$$

[3] The third degree is ruled out by the concavity requirement.

so Eq. (5.15) can be rewritten as

$$\begin{cases} \zeta(q) = Dq^4 + Cq^3 + \dfrac{3C^2}{8D}q^2 + \left(\dfrac{1}{2} - 8D - 4C - \dfrac{3C^2}{4D}\right) q \\ D < 0, \end{cases} \tag{5.18}$$

which has only two degrees of freedom, *i.e.* C and D. As for the second degree polynomial fit, in its most general form it reads as

$$\zeta(q) = Bq^2 + Aq + const, \tag{5.19}$$

which then, enforcing conditions in Eq. (5.16), becomes

$$\begin{cases} \zeta(q) = Bq^2 + \left(\dfrac{1}{2} - 2B\right) q \\ B < 0, \end{cases} \tag{5.20}$$

having then only one degree of freedom. For each empirical time-series we chose between the two fits checking the maximum value of the adjusted coefficient of determination (see [174]). At this point we have then a shape for each of the three proposed autocorrelation lengths given in Subsec. 5.3.3. As a criterion to choose among them, we keep the fit which attains the least value of the root-mean-square error, in other words the one which leads to the least dispersion of the data around the fitted curve.

5.3.6 Summary of the method

1. Given one prescription for the autocorrelation length (see Subsec. 5.3.3), compute the value of τ_{max} for every measured q fixing then its value to be the maximum among them;

2. integrate the empirical scaling of the chosen qth absolute moments computed in $\tau \in [1, \tau_{max}]$;

3. for each moment fix the value of τ_{min} observing the behaviour of the term of degree zero of the parabolic fit (cfr. Eq. 5.14 and Subsec. 5.3.4);

4. infer the value of the scaling exponents via the best linear fit in the scaling regions $[\tau_{min}, \tau_{max}]$;

5. check that the filter function $g(x)$ converges to zero and that its integral converges to a constant;

6. perform a parabolic and a quartic fit, then decide the best among them checking the maximum adjusted coefficient of determination;

7. repeat steps from 1 to 6 for all three prescriptions for choosing τ_{max} (see Subse. 5.3.3) and select the one which gives the overall fit with the least root-mean-square error.

What it is left, is to prove that in the range $[\tau_{min}, \tau_{max}]$ chosen via this method, the filter function reaches a plateau, thus proving that its effect has been completely filtered out. This will be proved numerically in next sections. In particular we will show that this holds for the MRW, where the absolute moments scaling is computed for its increments (cfr. Eq. (3.37)), and afterwards for empirical data, where the absolute moments scaling is computed for the log-returns. We point out that for every τ we remove the mean from every return time-series since a non-zero mean would end up in the detection of spurious autocorrelations due also to possible non-stationarities. We report that this operation is justified by the financial assumption of zero returns on average.

5.4 Application to synthetic data: validation of the method

In this section we show the application of the method on a MRW, which has known multifractal properties, proving the capability of our method to capture, for example, the expected values of $H(-0.5)$, $H(-0.3)$, $H(-0.1)$, $H(0.1)$, $H(0.5)$ and $H(1)$. As an example, in Fig. 5.4 are reported all the relevant steps of the application of the method for the computation of $H(1)$ to a MRW made of $N = 10^7$ steps, $\lambda = 0.3$, $L = 5000$ and $\sigma = 10^{-5}$. The length of the time-series was chosen to reduce as much as possible the noise, the value

of λ to show clearly the convergence issues caused by the interplay between the power law tails and the volatility clustering while L and σ were chosen in order to be comparable with their value measured on empirical tick-by-tick financial data. In particular we report, from left to right from top to bottom, the integrated measured scaling (cfr. Eq. (5.11)), the whole shape of $c(\tau^*)$ and the maximum where the best parabolic fit is attained (cfr. Eqs. (5.13) and (5.14)), a zoom of the behaviour of $c(\tau^*)$ around the maximum where the best parabolic fit is attained (cfr. Eqs. (5.13) and (5.14)), the plain scaling with the asymptotic inferred scaling (cfr. Eqs. (5.8) and (5.10)), the filter function $g(x)$ and the integrated filter function (cfr. Eq. (5.12)). In order to choose the value of τ_{max} we fix it independently for each value of q using the cut of the autocorrelation at the 99% confidence level. As it appears evident from the figures, $c(\tau^*)$ reaches a first maximum and then starts to oscillate. The left bottom figures proves that the filter function converges to zero for high values of $x = \ln \tau$ while the right bottom one that its integral actually converges, thus filling the gaps left opened in the previous section at least for this particular process. The numerically computed scaling (blue solid line in the middle right figure) appears to settle on the asymptotic inferred scaling from above (dashed red line). In Fig. 5.5 we report instead the whole spectrum. In order to make a quantitative assessment we generated 10^4 MRWs made of 10^6 points and $\lambda = 0.3,\ 0.4, 0.5$, $L = 5000$, $\sigma = 10^{-5}$ as before. On each of them we applied our method in order to compute $H(-0.5)$, $H(-0.3)$, $H(-0.1)$, $H(0.1)$, $H(0.5)$, $H(1)$ and, since we found the estimators distributions are skewed, we report their median and median absolute deviation. We report the results in Tab. 5.1 along with the theoretical values between parenthesis in boldface under the measured values. The notation of the hat means the estimator of the quantity under it.

The measured values are in perfect agreement with the expected ones. In

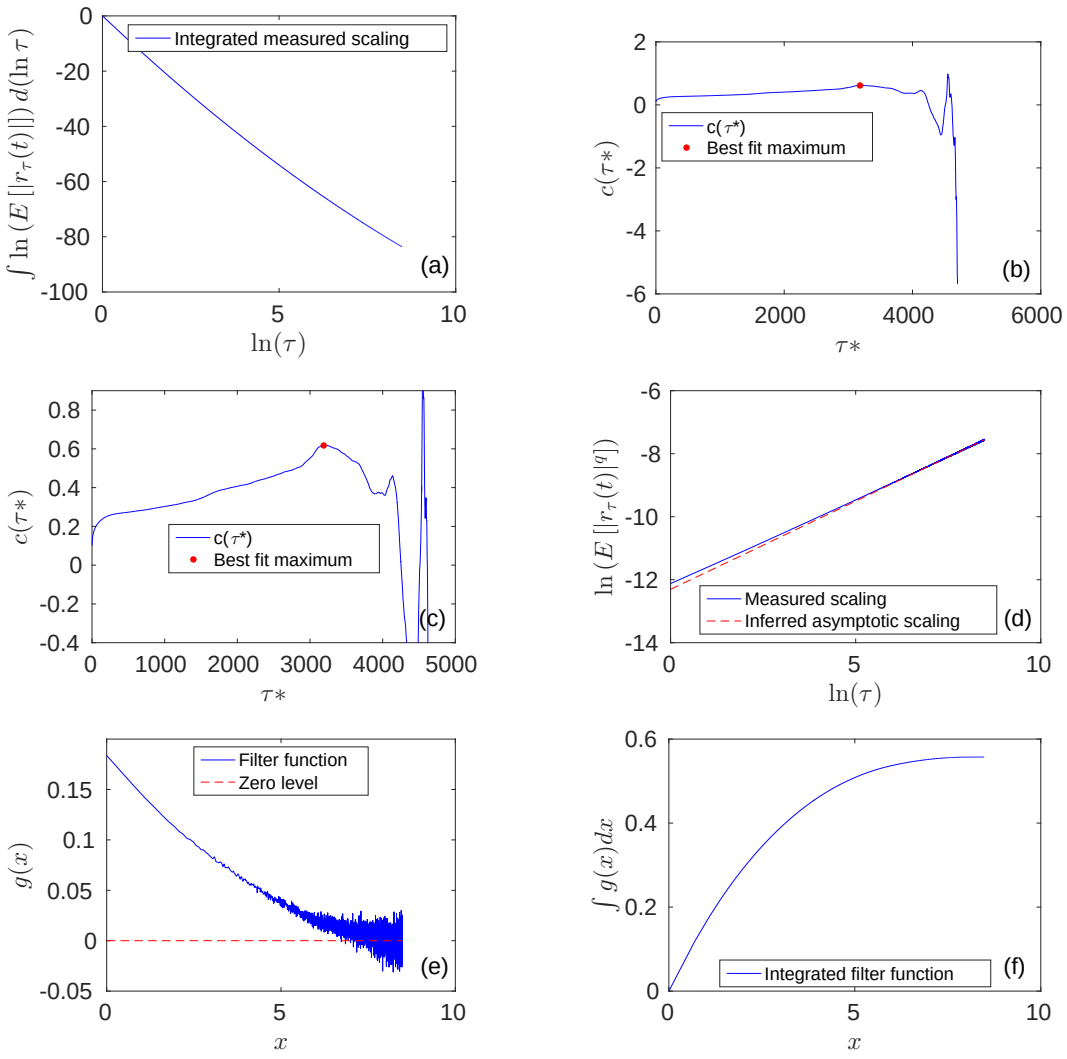

Figure 5.4: (a) integrated measured scaling (cfr. Eq. (5.11)). (b) in blue solid line $c(\tau^*)$ and the maximum where the best parabolic fit is attained marked with a red or shaded dot (cfr. Eqs. (5.13) and (5.14)). (c) zoom of the behaviour of $c(\tau^*)$ around the maximum where the best parabolic fit is attained (red or shaded dot) (cfr. Eqs. (5.13) and (5.14)). (d) plain scaling in blue solid line and the asymptotic inferred scaling in red dashed line (cfr. Eqs. (5.8) and (5.10)). (e) filter function $g(x)$ in blue solid line and the zero level in red dashed line. (f) integrated filter function (cfr. Eq. (5.12)).

the next section we turn our attention to empirical data.

5.5 Application to real financial data

In this section we discuss the application to real financial data. In particular we make few observations concerning the choice of the dataset, we illustrate

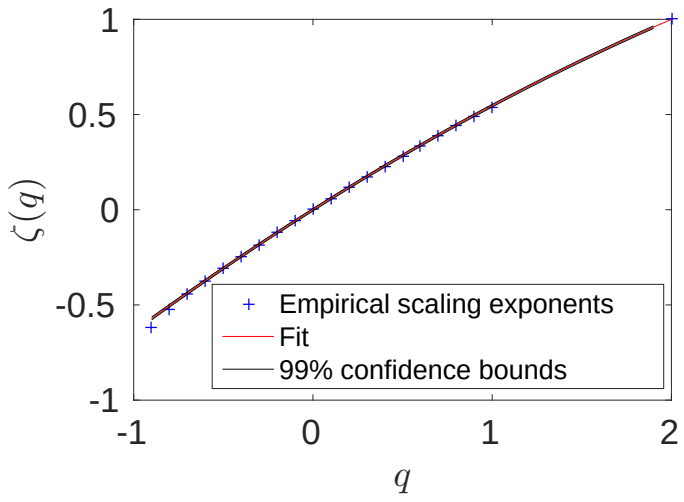

Figure 5.5: Fitted measured scaling exponents for a realization of a MRW. Blue crosses: measured scaling exponents. Red solid line: polynomial fit. Black solid lines: 99% confidence intervals of the values of the fitted curve.

MRW	$\lambda = 0.3$	$\lambda = 0.4$	$\lambda = 0.5$
$\hat{H}(-0.5)$	0.612 ± 0.028 (**0.6125**)	0.696 ± 0.033 (**0.7**)	0.795 ± 0.042 (**0.8125**)
$\hat{H}(-0.3)$	0.607 ± 0.035 (**0.6035**)	0.680 ± 0.043 (**0.684**)	0.770 ± 0.047 (**0.7875**)
$\hat{H}(-0.1)$	0.597 ± 0.033 (**0.5945**)	0.665 ± 0.038 (**0.668**)	0.748 ± 0.042 (**0.7625**)
$\hat{H}(0.1)$	0.589 ± 0.031 (**0.5855**)	0.648 ± 0.033 (**0.652**)	0.725 ± 0.037 (**0.7375**)
$\hat{H}(0.5)$	0.569 ± 0.026 (**0.5675**)	0.617 ± 0.023 (**0.62**)	0.679 ± 0.029 (**0.6875**)
$\hat{H}(1)$	0.545 ± 0.023 (**0.545**)	0.577 ± 0.022 (**0.58**)	0.618 ± 0.024 (**0.625**)

Table 5.1: Results of the application of the method in order to compute $H(-0.5)$, $H(-0.3)$, $H(-0.1)$, $H(0.1), H(0.5)$ and $H(1)$ of a MRW with parameters $\lambda = 0.3, 0.4, 0.5$ $L = 5000$, $\sigma = 10^{-5}$.

the method step by step on a specific dataset while we show the final outcome of its application to various other datasets.

5.5.1 The choice of the dataset

Nowadays trading takes place at high frequency speed which means that in a trading day may occur order of hundred thousands transactions. Moreover the number of transactions differs from day to day. As an example let us report the case of the trade log-price of the *American Express Company* (AXP), taken tick-by-tick from 12/10/2015 to 11/11/2015 traded on working days between 9:30 and 16:30 at the New York Stock Exchange (NYSE) made of 626710 points. The trading days in the given time-span are 23 and we can check for example how many trades occurred in the day with the minimum amount of trades and how many trades occurred in the day with the maximum amount of trades:

$$\begin{aligned} &\text{minimum } \# \text{ of trades} = 10110 \\ &\text{maximum } \# \text{ of trades} = 100133. \end{aligned} \tag{5.21}$$

In general we can say that, within a day, the secondly, minutely, hourly etc. log-returns are the result of the aggregation of the tick-by-tick log-returns (relative to the trading price). Thus if we consider the log price taken at a fixed time rate, say for example every second, it becomes a subordinated process which inherits the statistical properties of its subordinator (the trading time) (cfr. [176]), which we are in general not granted to be stationary. Moreover intraday data taken at a fixed time interval have strong seasonalities (cfr. [3]), which are instead almost absent in their tick-by-tick version. In order to clarify this point, let us show in Fig. 5.6 the comparison between the autocorrelation function of the absolute value of the log-returns of the AXP time-series on a tick-by-tick basis (left panel) and rearranged on a secondly basis (right panel). In the tick-by-tick case, the impact of the seasonalities is almost removed. Seasonalities actually can also be avoided analysing daily data, however the subordination feature mentioned above still holds and also a long time span is required in order to proper measure the multifractal scaling (cfr. [8]). For example in order to obtain a time-series of roughly 25000 steps, around 100

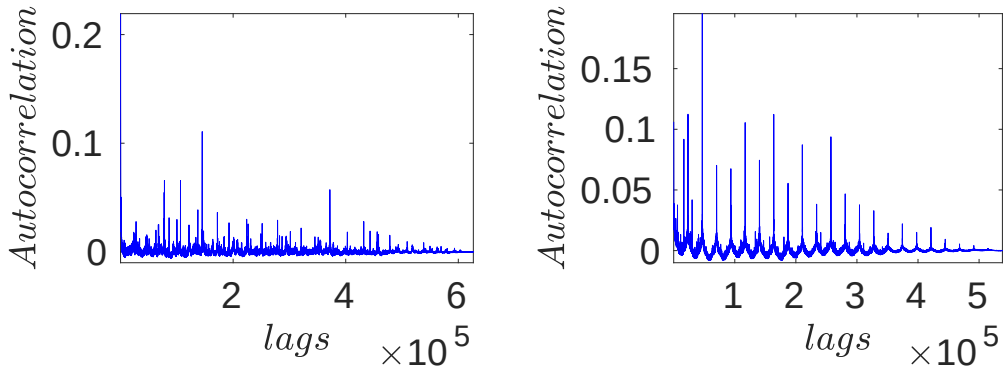

Figure 5.6: Left panel: autocorrelation function of the absolute values of the log-returns of AXP taken on a tick-by-tick basis. Right panel: autocorrelation function of the absolute values of the log-returns of AXP rearranged on a secondly basis.

years are needed, which heavily clashes with the assumption of stationarity. We add also that, according to our analyses, in order to reach a level of aggregation informative of the asymptotic behaviour, time-series made of at least 200000 steps are needed with an autocorrelation length of at least 1500 lags. Since these requirements are easily met by tick-by-tick data, we found quite a natural choice to limit our analysis to them. One last word has to be spent on the fact that in the tick-by-tick regime data are intrinsically discrete since in markets there is a lower bound to the fraction of the currency we trade with. We notice however that our analysis focuses on the high aggregation regime where the returns are supposed to take continuous values (cfr. Subsec. 5.2.2).

5.5.2 Numerical results: AXP

In this subsection we report the result of the application of our method for the computation of the scaling exponents of the AXP time-series, focusing in particular on $H(0.1)$ and $H(1)$ as an example. Given the prescription in Subsec. 5.3.3, the possible values of τ_{max} are

$$\begin{aligned} \tau_{max}^{99\%} &= 2798, \\ \tau_{max}^{95\%} &= 3507, \\ \tau_{max}^{50\%} &= 4201. \end{aligned} \tag{5.22}$$

According to the prescription of Subsec. 5.3.5 the one which minimizes the dispersion of the data around the fitted curve is the first one, *i.e.* $\tau_{max} = 2798$. In Figs. 5.7 and 5.8 we report all the relevant steps for the computation of $H(0.1)$ and $H(1)$ as described in Sec. 5.3.2 with the figures arranged as in Fig. 5.4.

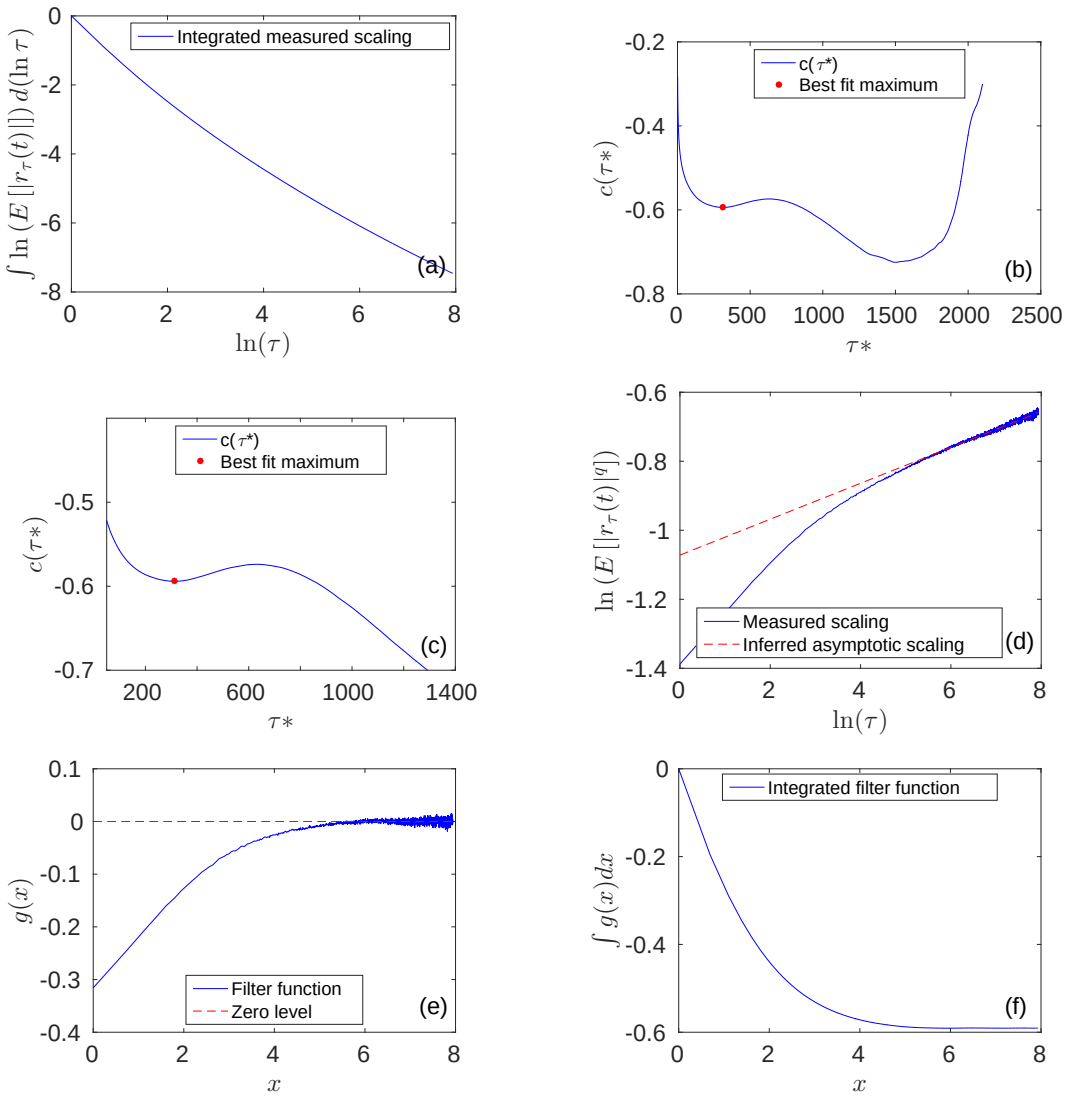

Figure 5.7: Step by step application of the method for the scaling of $H(0.1)$ for AXP. (a) integrated measured scaling (cfr. Eq. (5.11)). (b) in blue solid line $c(\tau^*)$ and the maximum where the best parabolic fit is attained marked with a red or shaded dot (cfr. Eqs. (5.13) and (5.14)). (c) zoom of the behaviour of $c(\tau^*)$ around the maximum where the best parabolic fit is attained (red or shaded dot) (cfr. Eqs. (5.13) and (5.14)). (d) plain scaling in blue solid line and the asymptotic inferred scaling in red dashed line (cfr. Eqs. (5.8) and (5.10)). (e) filter function $g(x)$ in blue solid line and the zero level in red dashed line. (f) integrated filter function (cfr. Eq. (5.12)).

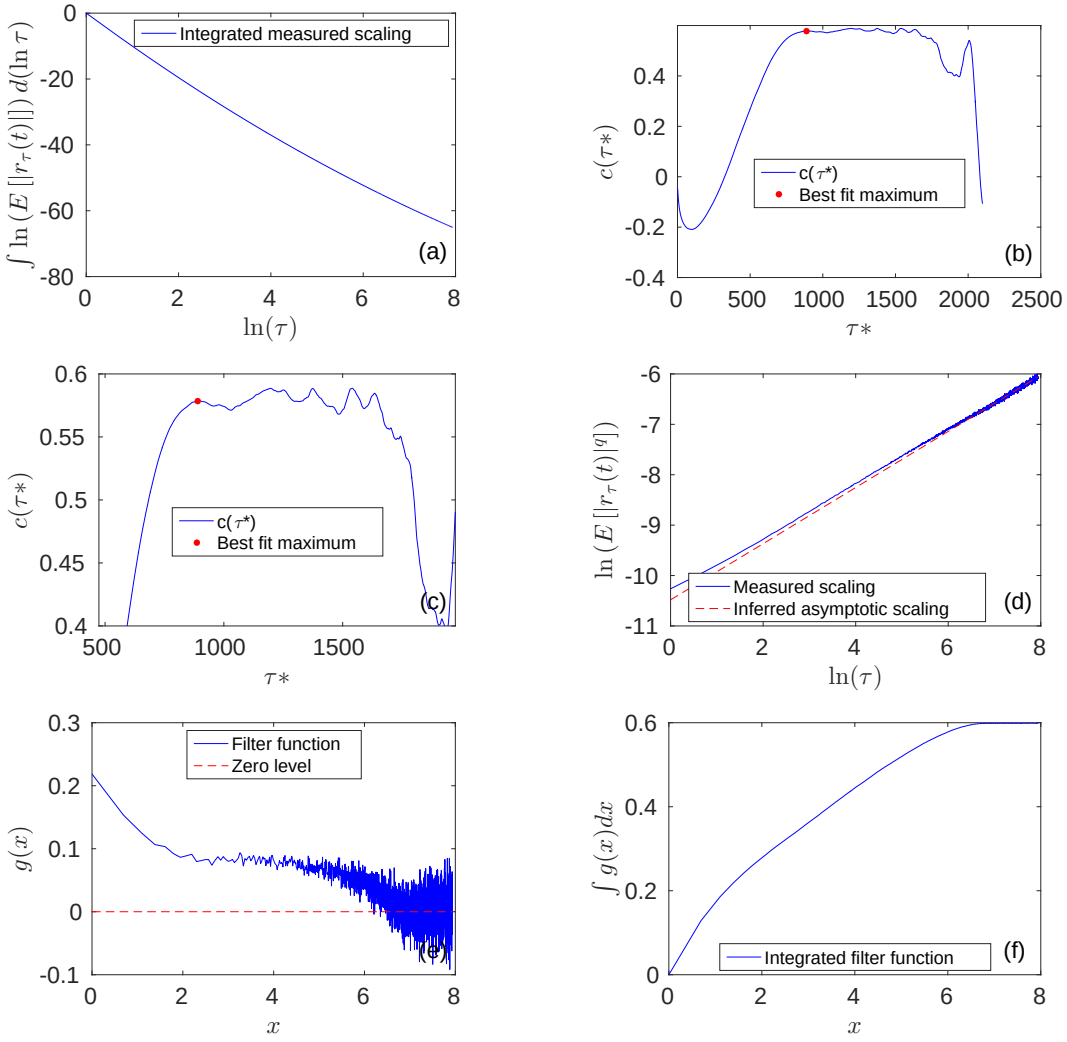

Figure 5.8: Step by step application of the method for the scaling of $H(1)$ for AXP. (a) integrated measured scaling (cfr. Eq. (5.11)). (b) in blue solid line $c(\tau^*)$ and the maximum where the best parabolic fit is attained marked with a red or shaded dot (cfr. Eqs. (5.13) and (5.14)). (c) zoom of the behaviour of $c(\tau^*)$ around the maximum where the best parabolic fit is attained (red or shaded dot) (cfr. Eqs. (5.13) and (5.14)). (d) plain scaling in blue solid line and the asymptotic inferred scaling in red dashed line (cfr. Eqs. (5.8) and (5.10)). (e) filter function $g(x)$ in blue solid line and the zero level in red dashed line. (f) integrated filter function (cfr. Eq. (5.12)).

The empirical scaling appears to settle in both cases on the asymptotic straight line found by the algorithm (see Figs. 5.7 and 5.8) and the values of τ_{min} found are

$$\hat{\tau}_{min}^{H(0.1)} = 255, \quad \hat{\tau}_{min}^{H(1)} = 815. \tag{5.23}$$

Again subfigures (e) and (f), in both cases, prove that, also for this empirical

dataset, for high values of $x = \ln \tau$ the filter function $g(x)$ oscillates around zero and that its integral converges. We notice also that in Fig. 5.8 the choice of the local maximum may seem puzzling, since other apparently better candidates appear on its right. However we recall that the local maximum is chosen in order to achieve the best parabolic fit of the integrated scaling in the adjusted coefficient of determination sense. In order to complete our analysis of the scaling properties of the AXP time-series we report in Fig. 5.9 the fit of all the scaling exponents we measured. In this case we found a second degree

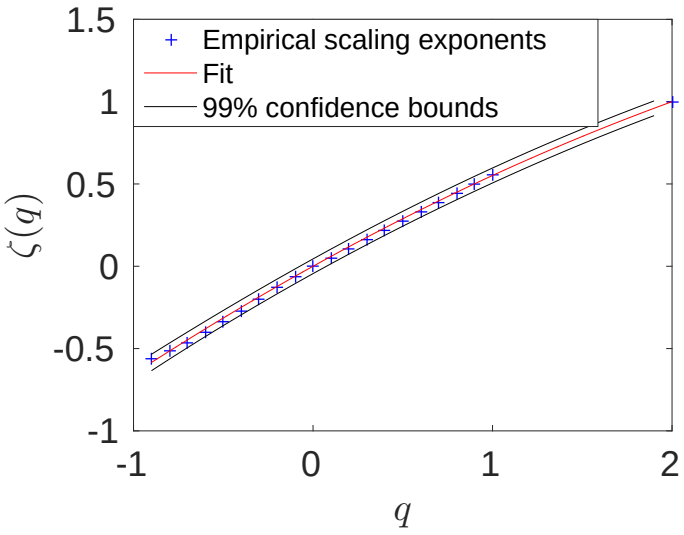

Figure 5.9: Blue crosses: empirical scaling exponents. Red solid line: polynomial fit. Black solid lines: 99% confidence intervals of the values of the fitted curve.

polynomial fit to be appropriate with the coefficients equal to:

$$\hat{B} = -0.052 \quad (-0.058, -0.045), \tag{5.24}$$

where we reported in parenthesis the 95% confidence interval of the estimated coefficients.

5.5.3 Other data

In this section we report the application of the method to the following empirical time-series: Abbott Laboratories (ABT), AECOM (ACM), Adobe Systems

(ADBE), American International Group (AIG), Advanced Micro Devices Inc. (AMD), Google (GOOGL), Honeywell International Inc. (HON), Marriott International (MAR), 3M Company (MMM), Procter & Gamble (PG). All time-series are taken between 12/10/2015 and 11/11/2015 on a tick-by-tick basis and traded on the NYSE. Details concerning the length of each time-series, the values of τ_{max} and the application of the method are reported in Tab. 5.2, along with the results of AXP discussed in the previous subsection. If we found a parabolic fit appropriate, the value of $\hat{B}$ is given, otherwise if we found a quartic fit appropriate, the values of $\hat{D}$ and $\hat{C}$ are given (see Subsec. 5.3.5) in both cases along with the 95% interval. In Figs. 5.10-5.19 we report instead for each empirical time-series the measured scaling exponents in blue crosses, the fitted polynomial in red solid line and the 99% confidence interval of the fitted functions in black solid lines. From Tab. 5.2 it appears that there is no clear preference for the parabolic or the quartic polynomial fit which is in turn linked to the complexity of the underlying generating process. For four time-series out of six for which the fourth degree polynomial is more suitable, we notice that the value of $\hat{C}$ can be assumed to be zero, which reflects in a symmetric Singularity Spectrum (cfr. Sec. 3.2).

Ticker	$\hat{D}$	$\hat{C}$	$\hat{B}$	τ_{max}	# of points
ABT	/	/	$-0.0314(-0.0330, -0.0298)$	4761	733160
ACN	/	/	$-0.0185(-0.0198, -0.0173)$	2297	288564
ADBE	/	/	$-0.0125\ (-0.0157, -0.0092)$	3254	361922
AIG	$-0.0149(-0.0274, -0.0024)$	$0.0049(-0.02811, 0.038)$	/	8323	979380
AMD	$-0.0353(-0.0411, -0.0294)$	$0.1424(0.1325, 0.1523)$	/	1831	283456
AXP	/	/	$-0.0515(-0.0578, -0.0452)$	2798	626710
GOOGL	$-0.0524(-0.0535, -0.0512)$	$0.1404(0.1380, 0.1429)$	/	1904	237276
HON	/	/	$-0.0254(-0.0273, -0.0236)$	4692	444198
MAR	$-0.0055(-0.0077, -0.0032)$	$-0.0185(-0.0192, -0.0177)$	/	3504	317754
MMM	$-0.0091(-0.0121, -0.0061)$	$0.0065(-0.0028, 0.0158)$	/	2138	305018
PG	/	/	$-0.0622(-0.0642, -0.0601)$	4661	946435

Table 5.2: Numerical results of the application of the method to empirical data. For each time-series is reported the ticker, the value of $\hat{D}$ and $\hat{C}$ or $\hat{B}$, whether we found more appropriate a second or a fourth degree polynomial fit, along with the 95% confidence interval, the value of τ_{max} and its length.

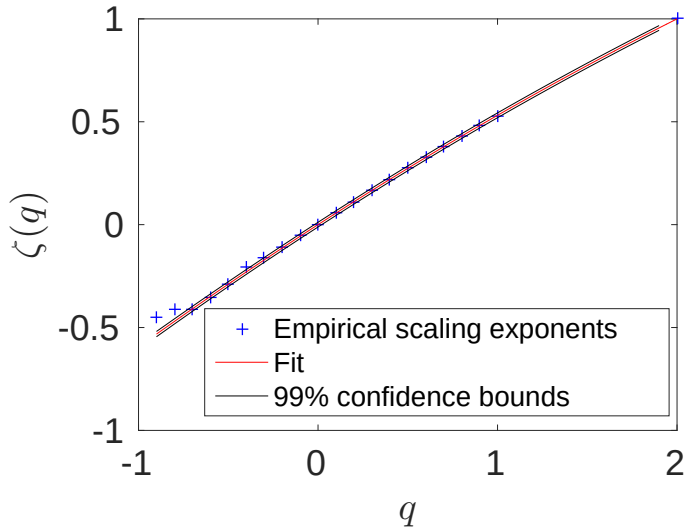

Figure 5.10: Fitted empirical scaling exponents for ABT time-series. Blue crosses: empirical scaling exponents. Red solid line: polynomial fit. Black solid lines: 99% confidence intervals of the values of the fitted curve.

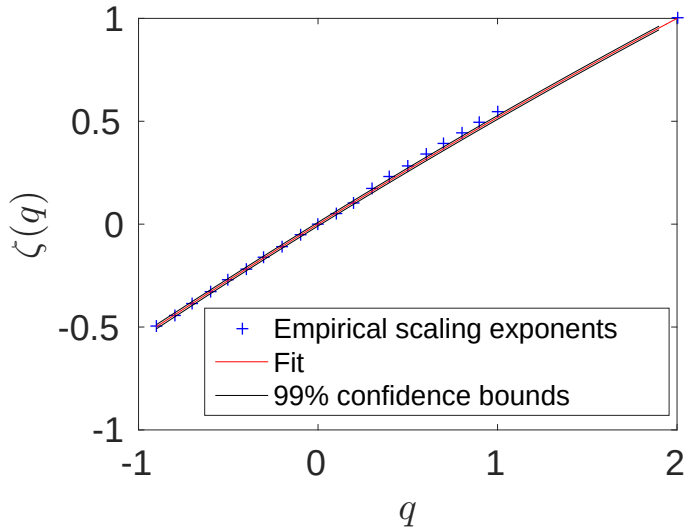

Figure 5.11: Fitted empirical scaling exponents for ACN time-series. Blue crosses: empirical scaling exponents. Red solid line: polynomial fit. Black solid lines: 99% confidence intervals of the values of the fitted curve.

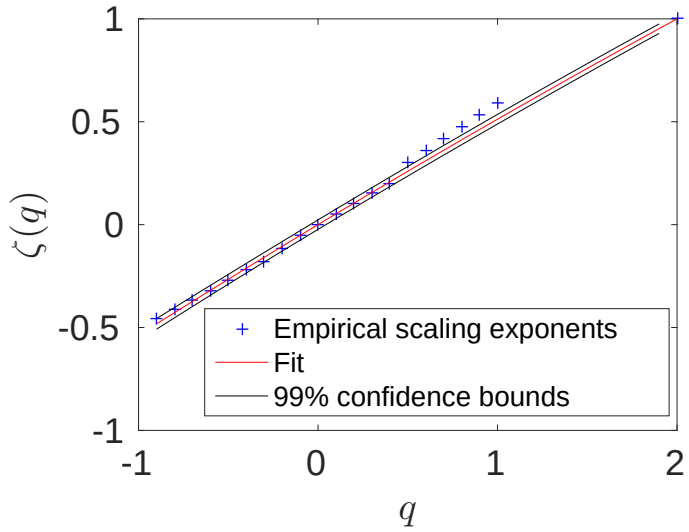

Figure 5.12: Fitted empirical scaling exponents for ADBE time-series. Blue crosses: empirical scaling exponents. Red solid line: polynomial fit. Black solid lines: 99% confidence intervals of the values of the fitted curve.

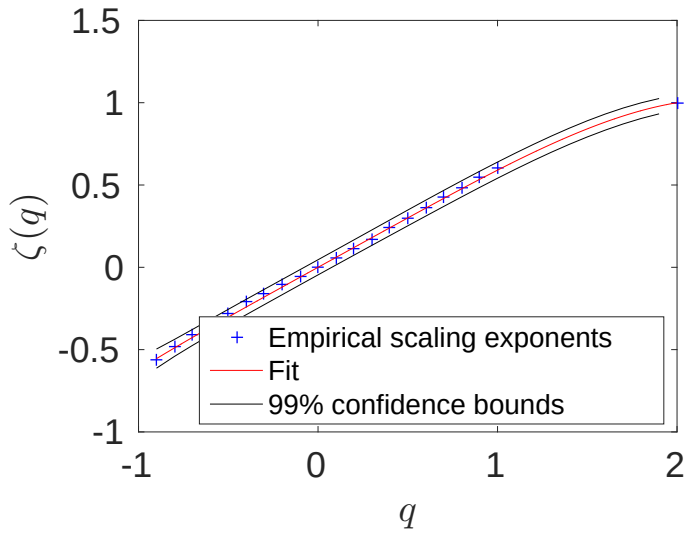

Figure 5.13: Fitted empirical scaling exponents for AIG time-series. Blue crosses: empirical scaling exponents. Red solid line: polynomial fit. Black solid lines: 99% confidence intervals of the values of the fitted curve.

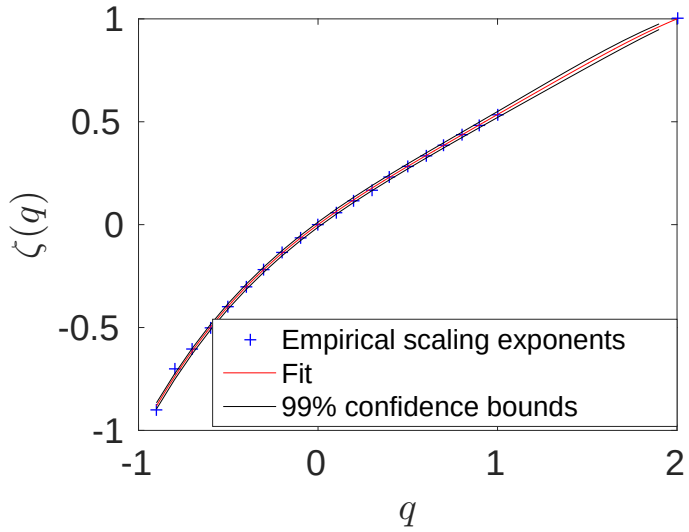

Figure 5.14: Fitted empirical scaling exponents for AMD time-series. Blue crosses: empirical scaling exponents. Red solid line: polynomial fit. Black solid lines: 99% confidence intervals of the values of the fitted curve.

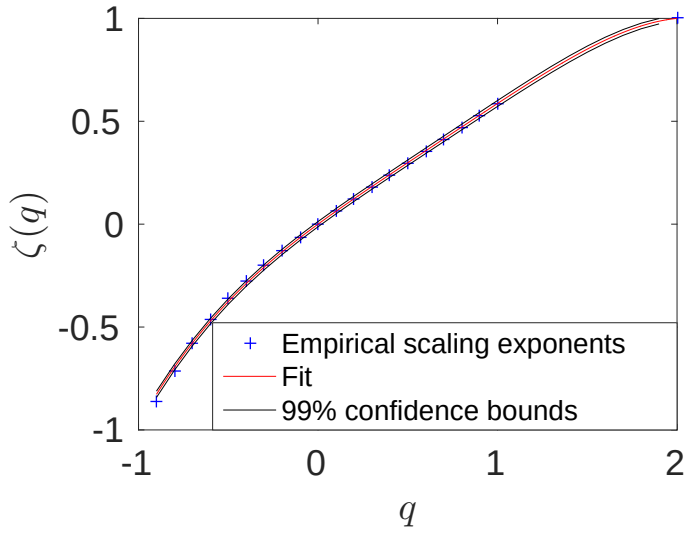

Figure 5.15: Fitted empirical scaling exponents for GOOGL time-series. Blue crosses: empirical scaling exponents. Red solid line: polynomial fit. Black solid lines: 99% confidence intervals of the values of the fitted curve.

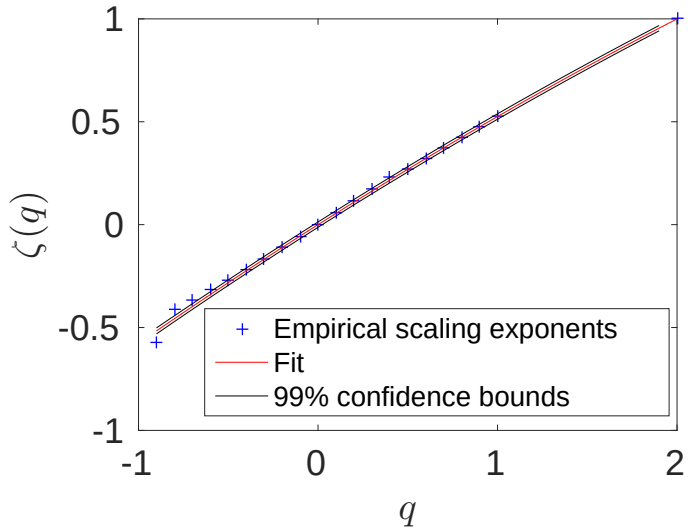

Figure 5.16: Fitted empirical scaling exponents for HON time-series. Blue crosses: empirical scaling exponents. Red solid line: polynomial fit. Black solid lines: 99% confidence intervals of the values of the fitted curve.

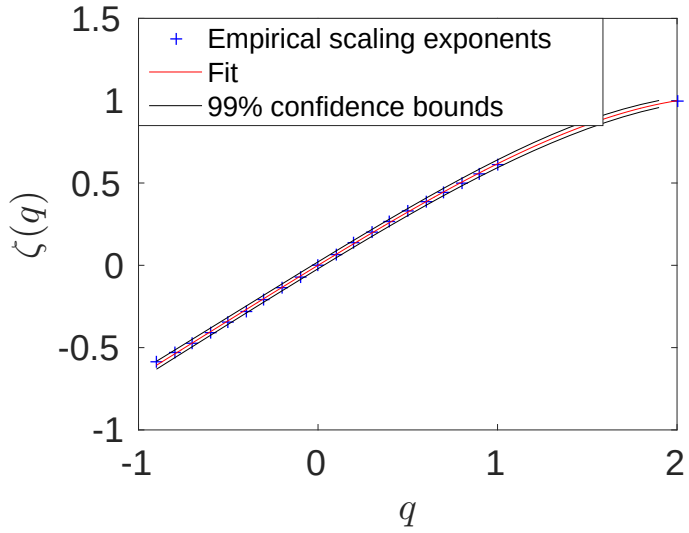

Figure 5.17: Fitted empirical scaling exponents for MAR time-series. Blue crosses: empirical scaling exponents. Red solid line: polynomial fit. Black solid lines: 99% confidence intervals of the values of the fitted curve.

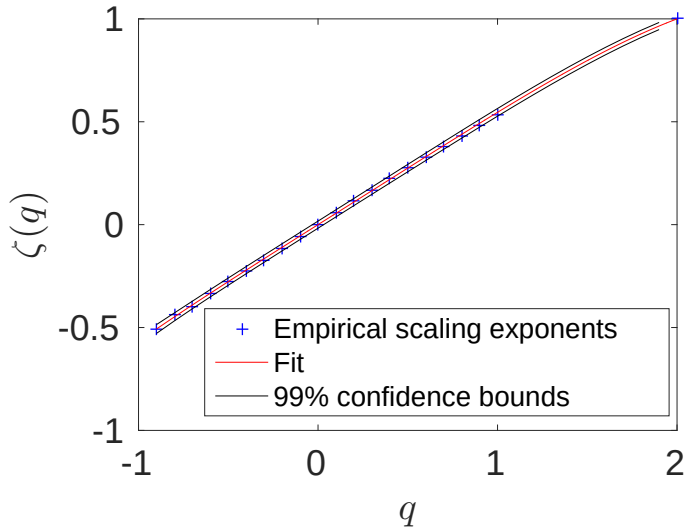

Figure 5.18: Fitted empirical scaling exponents for MMM time-series. Blue crosses: empirical scaling exponents. Red solid line: polynomial fit. Black solid lines: 99% confidence intervals of the values of the fitted curve.

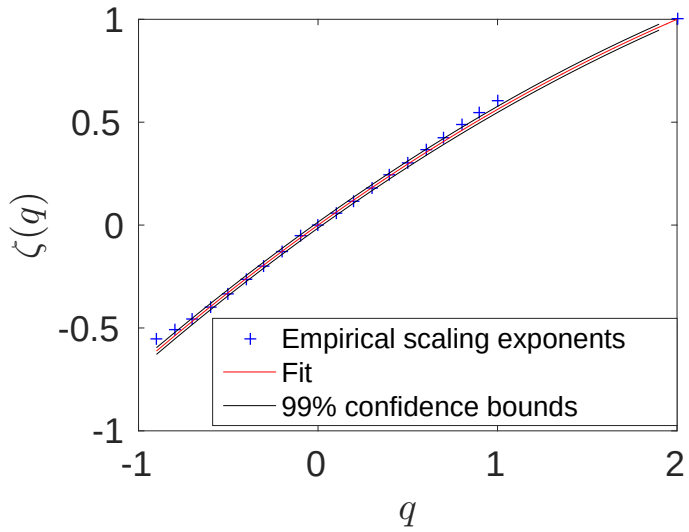

Figure 5.19: Fitted empirical scaling exponents for PG time-series. Blue crosses: empirical scaling exponents. Red solid line: polynomial fit. Black solid lines: 99% confidence intervals of the values of the fitted curve.

5.6 Summary

We proposed a new method to measure the scaling exponents of financial time-series, discussing how the discreteness of the available datasets, both for

synthetic and real time-series, affects the scaling measures. In particular we showed that the exact power law scaling of the moments holds for multi/uni-scaling processes continuous in time, while it does not for their discrete counterparts and it appears to be recovered only in the high aggregation limit. We argued then that the scaling of discrete processes, which corresponds to a multi/uni-scaling process continuous in time, whether synthetic or real, should be corrected via a filter function. According to our interpretation of the results, the need of this filter function arises when a process is not stable under aggregation, which means that, for discrete processes, the distribution of the increments at the finest scale is different with respect to the one at gross scale *i.e.* in the continuous time limit. In order to circumvent this problem we devised a numerical method to subtract the filter function from the underlying linear scaling, without the need of knowing its exact functional form. Finally we smoothed the measured scaling exponents by fitting them with either a second or a fourth degree polynomial, which, taking into account the theoretical requirement of the multifractal picture, reduce to have respectively one and two degrees of freedom. In general terms, a higher degree corresponds to a higher degree of complexity of the underlying generating process.

We found that there are few qualitative features common to all stocks concerning the behaviour of the filter function. For positive moments, almost always the scaling clearly converges to the asymptotic behaviour found by our algorithm from above. However a different behaviour of the overall shape of the convergence is found for values of q near zero and values of q near one, with a transient between the two regimes. In particular for values of q near zero the empirical scaling crosses its asymptotic inferred behaviour from below finally settling on it from above, while, for all but one time-series (ABT), for q near one the empirical scaling stays always above the asymptotic one before settling on it again from above. From another perspective it means that positive abso-

lute moments near to the first one tend to be always overestimated, whatever the aggregation, while small absolute moments tend to be underestimated for small aggregations while overestimated otherwise. As for the negative absolute moments the convergence pattern is stock-wise: in some cases the scaling lies always above the asymptotic scaling converging from above, in others it starts above, then it crosses the asymptotic scaling and finally converges from below. We report that this change of behaviour dependent on the order of the measured moment is absent for the MRW, where the convergence, for positive absolute moments, happens from above, while for negative ones it happens from below. We argue that this difference may arise from the fact that the innovations of a MRW, also at its finest scale, are (conditionally Gaussian) random variables continuous in value, whereas real financial tick-by-tick data are intrinsically discrete, due to the presence of a minimum tick size (cfr. for example [172]). It is worth noting that this feature of tick-by-tick data does not affect the coherence of our work since the goal of our method is to measure the scaling behaviour in a high aggregation regime, where returns can be considered continuous in value. We stress that this convergence has been found in the so-called trading time, which is inhomogeneous. Different approaches has been developed to deal with time inhomogeneity of tick-by-tick data (see for example [3, 177, 178]), however we decided to avoid to introduce such techniques both because we performed a univariate analysis and because we preferred to avoid to introduce a source of arbitrariness coming from the choice of a specific procedure. We also report that as for the overall shape of the function $\zeta(q)$, we found that in our dataset there is no clear preference between the second or the fourth degree considered polynomials, despite in four cases out of six, where the fourth degree polynomial fit was found more suitable, the coefficient of the third degree term can be assumed to be zero within the error bounds. In light of these observations the filter function can be seen

as a measure of the stability of the considered process under aggregation.

Chapter 6

On the interplay between scaling properties and cross-correlation

In this chapter we find a nonlinear dependence between an indicator of the degree of multiscaling[1] of log-return time-xseries of a stock and the average correlation of it with the other stocks traded in the same market. This result is a robust stylized fact holding for different financial markets. We investigate the relationship of this result with the stocks' capitalization and we show that a linear dependence from the logarithm of the capitalization does not explain the observed stylized fact.

6.1 Introduction

Financial time-series are characterized by the presence of so-called stylized facts [15, 14]. The most famous ones are the power law tails [101], the volatility clustering [21] the multiscaling [18, 3, 101, 102, 103, 110, 179, 134] and the presence of a dependency structure between stocks [44, 180, 181, 5, 47, 182]. The first three refer to univariate properties of financial time-series, and since

[1] In this chapter we use the term multiscaling in place of multifractal. In the literature the two are used interchangeably and in Mandelbrot papers the multifractal picture seems to be only a geometrical interpretation of the multiscaling property. As will be clarified in the course of this chapter we are here not measuring the multifractal scaling discussed in the previous one, but the biased, non-asymptotic one. Following the results of previous chapters and in order to fix the terminology, we distinguish the meaning of multiscaling and multifractal, by defining as multiscaling a time-series whose innovation distribution change under aggregation, which is clearly more general than multifractal.

the introduction of the Nobel prize winning ARCH model [16], they have been modelled in many ways via the introduction of more and more complex models [52, 54, 56, 71, 74, 78, 127].

On one hand there is the multiscaling property of financial time-series which has been widely studied in the last two decades. The research on this topic developed either on the empirical side [18, 3, 101, 102, 103, 105, 106, 107, 108, 115, 116, 117] and on the theoretical one [103, 121, 127, 129, 130]. Multiscaling models proved to be valuable tools for volatility and Value-at-Risk forecasting [122, 123, 124, 131, 132]. Moreover, the multiscaling property of financial log-returns has proven to be useful to monitor the stability of firms and markets [133, 115], where different agents interact at different frequencies [3].

On the other hand, there is the dependency structure of the markets which has been observed across different industries and asset classes[18]. Its presence is probably due to the fact that traders react simultaneously to new information and also share accidentally same trading strategies [18]. The study of the cross dependence, became particularly important since the introduction of the Nobel prize winning Markovitz portfolio selection [12] based on the cross-correlation matrix. In the Markovitz procedure, the optimal estimation of this matrix is paramount, thus a sweeping amount of papers have been published since then, dealing with the problem of de-noising the cross-correlations matrix [39, 40]. Also, once the importance of the proper modelling of the cross-dependence appeared clear, multivariate models with different specifications of the cross-correlation structure were developed [58, 60, 62, 65, 66, 85, 86, 158].

In this chapter we find a new stylized fact showing a robust statistical relationship between the multiscaling property of a stock log-returns and the average correlation of the stock with the log-returns of many other stocks traded in the same financial market. We verify that this relationship holds in several leading stock markets and we investigate about its origin. Theoretical

attempts in similar directions can be found for example in [158, 6]. However empirical evidence has been still lacking so far. It is worth noting that Ref. [49] goes in the same spirit of this paper. In fact in [49] the author observes a relationship between the volatility clustering in time and the cross-correlation of volatility with volatility of other stocks traded in the same market.

The structure of the chapter is as follows: in Sec. 6.2 we introduce the dataset and the tools we use to perform the analysis, in Sec. 6.3 we report the main result of the paper and in Sec. 6.4 we draw the conclusions.

6.2 Dateset and tools

In this section we describe the dataset we use to perform our empirical analyses and the methods we use to estimate the univariate and multivariate properties of the time series. Let us first fix the notation by calling the prices time series $p(t)$ and the log-return over a τ time horizon $r_\tau(t) = \ln[p(t+\tau)/p(t)]$, where $\tau = 1$ day in this paper. In what follows we remove the mean from every log-return time-series [18].

6.2.1 Dataset

The data we use for our analyses is made of six different sets of stocks. In particular we investigate log-returns time-series of the *London Stock Exchange* (LSE), *Frankfurt Stock Exchange* (FWB), *Tokyo Stock Exchange* (TSE) and *Hong Kong Stock Exchange* (HKSE). To these four sets of data we add another set of data obtained by merging stocks traded at the *New York Stock Exchange*, at the *Nasdaq Stock Market*, and at the *NYSE MKT LLC*. We address this dataset as NYSE17. For these five sets of data, we consider the closure price of stocks recorded on a daily basis from the 03/01/2000 up the 12/05/2017. A last dataset comprises the closure price recorded on a daily basis of the stocks traded at the *New York Stock Exchange* from the 02/01/1985 the 31/12/1999.

We address this dataset with the acronym NYSE99. Within the former (latter) time period we chose to consider only the stocks traded throughout the whole period of time, with an Initial Public Offer date earlier than the 03/01/2000 (02/01/1985) and traded at least up to the 15/07/2016 (31/12/1999). The number of stocks in each market with these properties is summarised in Tab. 6.1. For each stock in each market we also considered the capitalization time-series.

Stock Exchange	# of stocks
NYSE17	1270
LSE	145
FWB	126
TSE	958
HKSE	404
NYSE99	336

Table 6.1: Summary of the dataset used before the cleaning.

6.2.2 Data cleaning

Since our aim is to perform also a cross-correlation analysis, our dataset cannot be used as it is, because the price time-series are not aligned due to the fact the some of them have not been traded on certain days. The rationale behind the cleaning procedure we describe below is that we do not want to remove a stock just because it was not traded on few days in the given time-span. The main idea is then to fill the gaps dragging the last available price and assuming that a gap in the price time-series corresponds to a zero log-return. At the same time we do not want to drag too many prices because a log-returns time-series filled with zeros would not be statistically significant. In light of this we remove from our dataset the time-series which are too short in a certain statistical sense. The detailed procedure goes as follows:

1. Remove from the dataset the price time-series with length less than p times the longest one;

2. Find the common earliest day among the remaining time-series;

3. Create a reference time-series of dates when at least one of the stocks has been traded starting from the earliest common date found in the previous step;

4. Compare the reference time-series of dates with the time-series of dates of each stock and fill the gaps dragging the last available price.

In this analysis we chose $p = 0.90$, however we report that the results do not change if we pick a higher value of p, thus trying to keep as much as possible unmodified time-series. A summary of the number of stocks in each market after the cleaning can be found in Tab. 6.2. As for the capitalization, we

Stock Exchange	# of stocks
NYSE17	1202
LSE	144
FWB	126
TSE	724
HKSE	340
NYSE99	313

Table 6.2: Summary of the dataset.

considered the capitalization time-series for each stock and we took the median capitalization over the considered time-span. We chose the median and not the mean because we want to keep the most representative capitalization value of the capitalization over the given time-period. For few stocks the capitalization is not available. In this case, when a capitalization analysis is involved, we simply remove those stocks.

6.2.3 Multiscaling proxy

As discussed in Ch. 3, the multiscaling property of a time-series is detected via the non-linearity of the scaling exponents of the absolute moments of its

increments, which we report here for clarity keeping the notation unchanged:

$$E\left[|r_\tau(t)|^q\right] = K(q)\tau^{qH(q)}. \tag{6.1}$$

Following the prescription of Ch. 4, a possible way to define a multiscaling proxy is by quantifying the degree of non-linearity of the function $qH(q)$. In order to do so, first the scaling exponents $qH(q)$ have to be computed, which is done again via a linear regression in loglog scale of Eq. (6.1). Then the multiscaling proxy can be defined by fitting the measured scaling exponent with a second degree polynomial fit [8], namely

$$qH(q) = Bq^2 + Aq, \tag{6.2}$$

where we fixed the constant to zero for theoretical reasons (see for example [9] and Ch. 5) and $\hat{B}$ is the non-linearity proxy. Together with $\hat{B}$, also $\hat{A}$ gives information about the analysed process. In particular, when $\hat{B} < 0$, we expect $\hat{A} > 0.5$ for concavity, while when $\hat{B} \approx 0$, we expect $\hat{A} \approx 0.5$ since empirical log-returns taken on a daily basis are uncorrelated [14, 15].

6.2.4 Cross-correlation proxy

Concerning the market effect, we used three types of cross-correlation. The first one is the average of the standard cross-correlation between stocks, $\bar{\rho}_i$ for the ith stock in the following. The second is the average cross correlation between the signs of the log-returns, $\bar{R}_i$ for the ith stock in the following, which estimates the tendency of a stock to co-move with the rest of the market. The third one is the absolute log-returns average cross correlation, $\bar{S}_i$ for the ith stock in the following, as in [49], which estimates the tendency of a stock to display a big/small variation if the rest of the market does so. Calling $\rho_{ij} = \mathrm{Corr}\left[r_i, r_j\right]$ the standard cross-correlation matrix, $R_{ij} = \mathrm{Corr}\left[sign(r_i), sign(r_j)\right]$ the sign cross correlation matrix of the plain log-returns and $S_{ij} = \mathrm{Corr}\left[|r_i|, |r_j|\right]$ the cross correlation matrix of the absolute log-returns, the proxies can be written

as

$$\bar{\rho}_i = \frac{1}{N-1} \sum_{j \neq i=1}^{N} \rho_{ij}, \tag{6.3}$$

$$\bar{R}_i = \frac{1}{N-1} \sum_{j \neq i=1}^{N} R_{ij}, \tag{6.4}$$

$$\bar{S}_i = \frac{1}{N-1} \sum_{j \neq i=1}^{N} S_{ij}, \tag{6.5}$$

where the minus one means that we do not use the correlation of a stock with itself, which is one, when we compute the averages. We associate a p-value to each entry of the matrices ρ_{ij}, R_{ij} and S_{ij}. In our analyses, we consider the correlation coefficient compatible with a null hypothesis of uncorrelated log-returns each correlation coefficient that has a p-value of less than 5% [183]. We report that an alternative measure of sign correlation can be found, for example, in [184], defined as the probability that two discrete time-series have an innovation with the same-sign. Despite we found that this measure has a correlation close to one with ours, we chose the proxy in Eq. (6.4) since Eqs. (6.4) and (6.5) give a clear decomposition of the usual cross correlation matrix. Before moving on we report an intriguing dependence we found on our dataset. In particular we found an overall dependence between the sign cross-correlation, described by the $\bar{R}$ proxy, and the amplitudes cross-correlation, described by $\bar{S}$. We report the scatter plot of these two quantities in Fig. 6.1. There is evidence for a strong correlation between them, in order to make a quantitative assessment we report in Tab. 6.3 their Pearson correlation r up to two significant figures and the p-value up to three significant figures. We report also that the relationship found in [49] between volatility clustering and volatility cross-correlation on intraday data is confirmed also on our dataset made of daily data.

market	r	p-value
NYSE17	0.78	0.000
LSE	0.91	0.000
FWB	0.85	0.000
TSE	0.87	0.000
HKSE	0.85	0.000
NYSE99	0.81	0.000

Table 6.3: Pearson correlation r and p-value between $\bar{\rho}$ and $\bar{S}$.

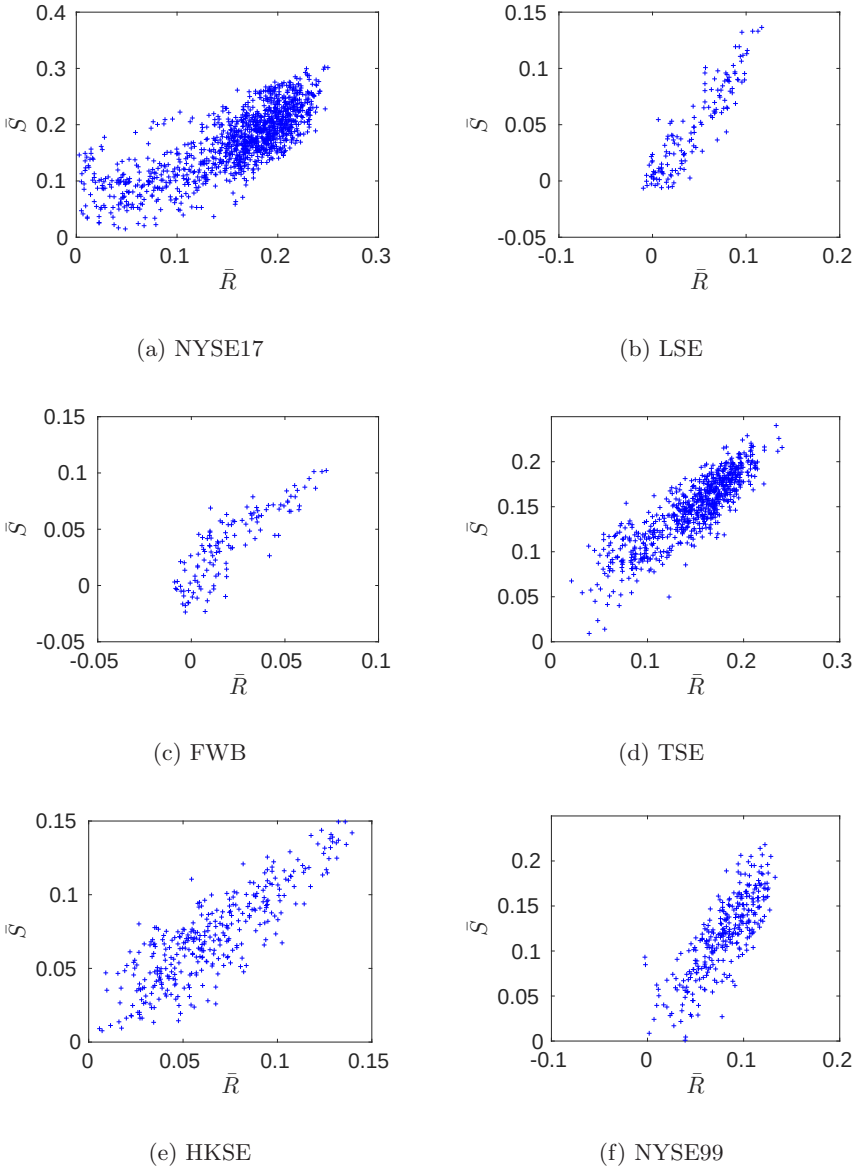

(a) NYSE17 (b) LSE

(c) FWB (d) TSE

(e) HKSE (f) NYSE99

Figure 6.1: Dependence between $\bar{R}$ and $\bar{S}$.

6.3 Relationship between scaling and standard cross-correlation

6.3.1 Main result

We present here empirical evidence of a new stylized fact. We find a relationship between the scaling property of a log-return financial time series and the average correlation of the stock with other stock log-returns traded in the same market. Specifically, in Fig. 6.2 we show the scatter plot of $\hat{B}$ as a function of $\bar{\rho}$. The range of the parameter τ_s over which the scaling is computed is chosen to be $\tau_s \in [1, 19]$ [133, 134] since an approximate linearity is present in this region, while the range of q is set as $q \in [0.1, 1]$, with steps of 0.1, following the prescription used in [8]. In Fig. 6.2 the color of the dot indicates the capitalization with increasing value ranging from dark blue to red in a log scale. We use a log scale since the interval in capitalization between the most capitalized stocks and the lowest capitalized one is covering many orders of magnitudes. A nonlinear relationship between $\hat{B}$ and $\bar{\rho}$ can be seen in the scatter plots of Fig. 6.2. It is worth noting that there is also a monotonic relationship between the market capitalization and the average cross correlation and between the market capitalization and the degree of multiscaling. In order to make a quantitative assessment about these relationships, we report in Tab. 6.4 the Kendall τ correlation [185] with two significant figures between the two quantities[2] along with the corresponding p-values up to the three significant figures. We observe that the dependence is statistically significant in all cases. The next section is dedicated to the investigation of the robustness of this result.

6.3.2 Validation of the empirical results

Ref. [8] found that the scaling of the moments at a low aggregation horizon is strongly affected by bias with respect to the expected asymptotic behaviour.

[2] We chose the Kendall due to the pronounced non-linearity of the dependence.

market	τ	p-value
NYSE17	0.30	0.000
LSE	0.65	0.000
FWB	0.74	0.000
TSE	0.46	0.000
HKSE	0.54	0.000
NYSE99	0.53	0.000

Table 6.4: Kendall τ correlation between $\hat{B}$ and $\bar{\rho}$.

The bias comes either from the presence of the power law tails of log-return probability density function and from the presence of the memory of the log-return time series. Hereafter, we want to understand whether the behaviour displayed in Fig. 6.2 is mainly due to the power law tails or to the time memory of log-return. In order to uncover the origin of the multiscaling property reported in Fig. 6.2, we shuffle the time-series in every market in a synchronous way, so that the autocorrelation structure of each time series is destroyed whereas the cross-correlation structure is preserved. In Fig. 6.3 we show the relationship between $\hat{B}$ and $\hat{\rho}$, computed on shuffled time series, while in Tab. 6.5 we report the Kendall τ correlation up to two significant figures between the two quantities along with the corresponding p-values. It appears evident that the relationship still holds almost unchanged after shuffling.

market	τ	p-value
NYSE17	0.30	0.000
LSE	0.66	0.000
FWB	0.74	0.000
TSE	0.58	0.000
HKSE	0.59	0.000
NYSE99	0.52	0.000

Table 6.5: Kendall τ correlation between $\hat{B}$ and $\bar{\rho}$ when the log-returns are shuffled but preserving the cross-correlation.

In order instead to preserve the memory structure of the time-series but removing the effect of the shape of distribution we use the normalization tech-

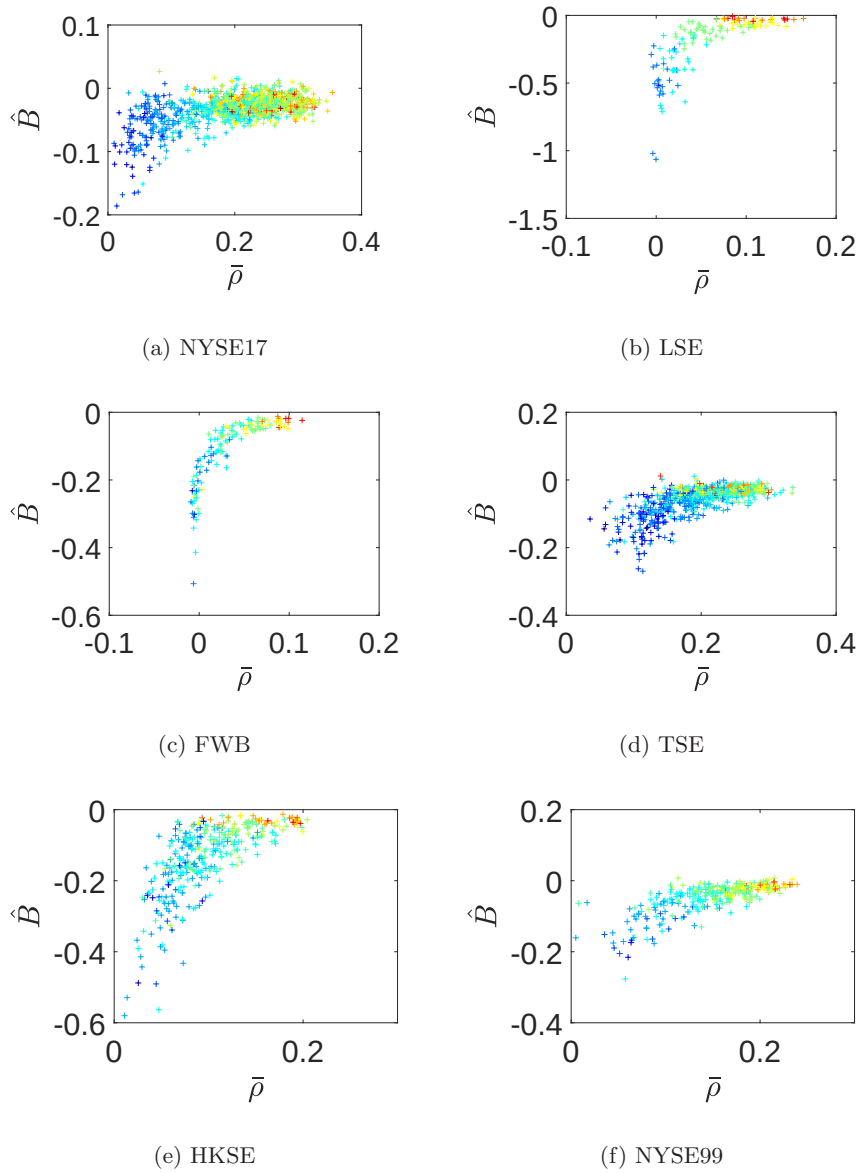

(a) NYSE17 (b) LSE

(c) FWB (d) TSE

(e) HKSE (f) NYSE99

Figure 6.2: Empirical evidence of the dependence between the degree of multiscaling measured by the proxy $\hat{B}$ of log-return and its average correlation $\bar{\rho}$ with the log-return of other stocks traded in the same market. The color represents the increasing capitalization from blue to red.

nique used already in [160, 8]. We limit ourself to report here that, once the shape effects are removed, the dependence is completely destroyed. We refer the interested reader to Appendix F for further details. Since this result shows that the main contribution to the multiscaling indicator comes from the tail, we should find that the value of $\hat{A}$ (cfr. Eq. 6.2) converges to 0.5 for stocks with $\hat{B} \approx 0$ for consistency. This observation is confirmed by plotting the

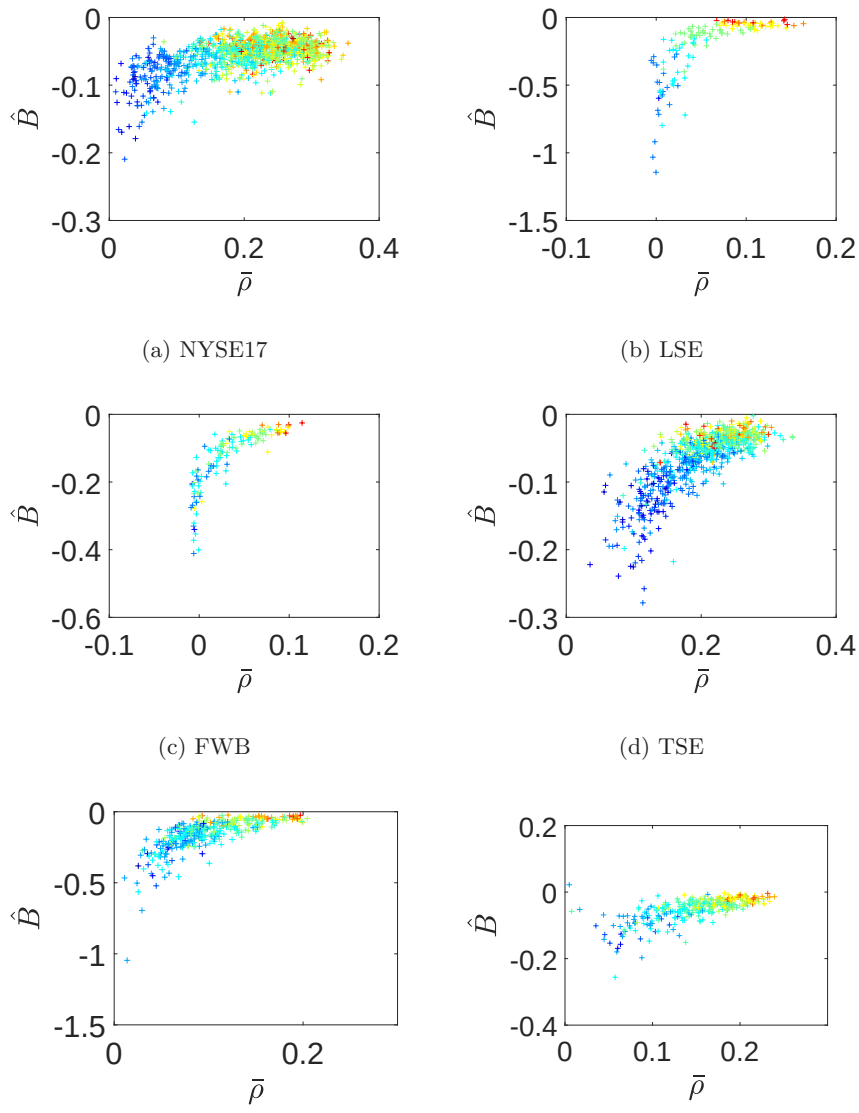

(a) NYSE17 (b) LSE

(c) FWB (d) TSE

(e) HKSE (f) NYSE99

Figure 6.3: Multiscaling properties, represented by the proxy $\hat{B}$, of a time-series plotted against its average cross-correlation $\bar{\rho}$ for shuffled log-returns, but preserving the cross-correlation. The color represents the increasing capitalization from blue to red.

scatter plot of $\hat{A}$ against $\bar{\rho}$ as we report in Fig. 6.4. In fact, this figure shows that $\hat{A}$ tends to 0.5 when $\hat{B}$ assumes values near zero, i.e. for highly capitalized stocks. In Tab. 6.6 we report the Kendall τ correlation up to two significant figures between the two quantities along with the corresponding p-values.

market	τ	p-value
NYSE17	-0.31	0.000
LSE	-0.64	0.000
FWB	-0.34	0.000
TSE	-0.43	0.000
HKSE	-0.54	0.000
NYSE99	-0.49	0.000

Table 6.6: Kendall τ correlation between the multiscaling proxy $\hat{A}$ and $\bar{\rho}$ along with the p-value.

6.3.3 Role of the capitalization

As pointed out in Subsec. 6.3.1 the scatter plots of Fig. 6.2 suggest that $\hat{B}$ and $\bar{\rho}$ depend on the logarithm of the capitalization. To confirm this observation and to quantify the effect we report in Tab. 6.7 the correlation between $\hat{B}$ and the logarithm of the capitalization (up to two significant figures and with the associated p-value) and in Tab. 6.8 the correlation between $\bar{\rho}$ and the logarithm of the capitalization (with the same degree of accuracy). Tabs. 6.7

ticker	ρ	p-value
NYSE17	0.29	0.000
LSE	0.73	0.000
FWB	0.48	0.000
TSE	0.45	0.000
HKSE	0.47	0.000
NYSE99	0.53	0.000

Table 6.7: Pearson's correlation coefficient between the the multiscaling proxy $\hat{B}$ and the logarithm of capitalization along with the p-value.

ticker	ρ	p-value
NYSE17	0.69	0.000
LSE	0.83	0.000
FWB	0.74	0.000
TSE	0.58	0.000
HKSE	0.67	0.000
NYSE99	0.77	0.000

Table 6.8: Pearson's correlation coefficient between the the average cross correlation $\bar{\rho}$ and the logarithm of capitalization along with the p-value.

and 6.8 show that the correlation is quite pronounced in both cases. Given this result, we want to verify if the dependence between the average correlation and the multiscaling proxy is driven only by the logarithm of the capitalization. In order to assess this we compute the partial correlation [186] between $\bar{\rho}$ and

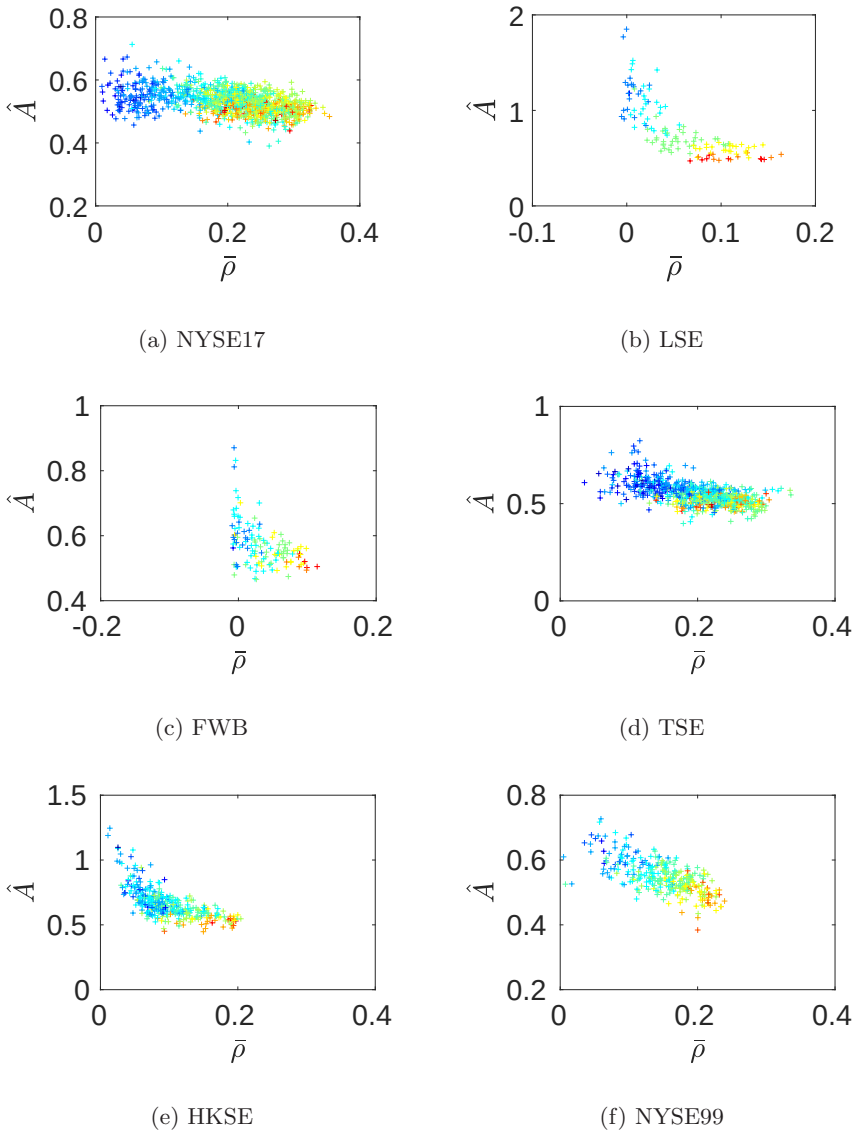

(a) NYSE17 (b) LSE

(c) FWB (d) TSE

(e) HKSE (f) NYSE99

Figure 6.4: Empirical evidence of the dependence between the multiscaling properties, represented by the proxy $\hat{A}$, of a time-series and its average cross-correlation $\bar{\rho}$. The color represents the increasing capitalization from blue to red.

$\hat{B}$ using as control variable the logarithm of the capitalization, *i.e.* Pearson's correlation between the residuals of $\hat{B}$ and $\bar{\rho}$ once they are regressed against the logarithm of the capitalization. We report in Tab. 6.9 the result of this analysis along with the coefficient of determination [187] of the linear fit between $\bar{\rho}$ and $\hat{B}$ and the logarithm of the capitalization, which is an estimate of the goodness of the fit. As we can see the correlation remains significant even

after the removal of the control variable, meaning that the interplay between scaling and cross-correlation has a deeper origin than just a linear relationship between the two variables and the logarithm of the capitalization.

ticker	ρ_{par}	p-value	$R^2_{\bar{\rho}}$	$R^2_{\hat{B}}$
NYSE17	0.34	0.000	0.47	0.22
LSE	0.25	0.000	0.69	0.57
FWB	0.68	0.000	0.54	0.30
TSE	0.52	0.000	0.33	0.33
HKSE	0.50	0.000	0.45	0.32
NYSE99	0.44	0.000	0.60	0.46

Table 6.9: Partial Pearson correlation ρ_{par} between the average cross-correlation $\bar{\rho}$ and $\hat{B}$, along with their respective p-value,. The coefficients of determination $R^2_{\bar{\rho}}$ and $R^2_{\hat{B}}$ are also reported for the linear fit between the logarithm of the capitalization and respectively $\bar{\rho}$ and $\hat{B}$.

6.4 Discussion and conclusion

We find an empirical relationship which links a univariate property, i.e. the degree of multiscaling behaviour of log-return, with a multivariate one, i.e. the average correlation of the stock log-return with log-return of many other stocks traded in the same market. Since the scaling measured for low aggregation horizons is biased by the presence of log-return tails and time autocorrelation [8], we investigated which of the two gives the major contribution to the degree of multiscaling behaviour of log-return. In order to do so we used the shuffling technique to isolate the tails contribution and the normalization technique to isolate the autocorrelation contribution (see for example [160, 8]). It turns out that the dependence found is due almost exclusively to the tails of log-return distribution. However, we also found that either $\bar{\rho}$ and $\hat{B}$ are correlated with the logarithm of capitalization of the analysed stock. In order to understand if the dependence from the logarithm of capitalization is fully explaining the stylized fact we find, we investigated the partial correlation between $\bar{\rho}$ and $\hat{B}$

using the logarithm of capitalization as a control variable. It turned out that removing the contribution due to the linear correlation with the logarithm of capitalization of the two variables does not fully explain the nonlinear dependence observed between $\bar{\rho}$ and $\hat{B}$. We interpret this finding as an evidence of the fact that the observed relationship must have a deeper origin.

According to the observations in [8, 9], a shuffled empirical log -return time series should scale asymptotically as a Brownian Motion due to the Central Limit Theorem [8, 9]. The reason why the scaling at small aggregation regimes for discrete time series disagrees with respect to the asymptotic one has been found in the instability under aggregation of the empirical distribution of log-returns [9]. We thus interpret the stocks with a value of $\hat{B}$ near to zero as more stable under aggregation, since the transient of the scaling differs less from the asymptotic one. Since the only stable distribution with finite variance is the Gaussian distribution, we find that the most capitalized and most cross-correlated stocks are those which are less volatile. This observation gives a statistical motivation to the fact that highly capitalized stocks are those which are less risky from an investor point of view. In particular, if a stock is characterized by $\hat{B}$ tending to 0 and $\hat{A}$ tending to 0.5, it means that the stock's behaviour differs less from the behaviour of a Brownian Motion than stocks with negative values of $\hat{B}$ and values of $\hat{A}$ larger than 0.5. This can be seen also from an economical point of view. In particular a stock with a high capitalization implies that a large number of market participants own that stock. A large number of participants is in turn linked to a higher liquidity. As observed in many studies (see for example [188]), an increased liquidity affects positively the market efficiency, which coincides with prices following a Brownian Motion.

Chapter 7

Conclusions

In this thesis we focused our attention on different aspects of the scaling behaviour of financial time-series, focusing in particular on its proper estimation. It turned out that the inherent discreteness of real data makes the use of the multifractal analysis not straightforward. A transient between a low aggregation regime, where the effect of the discrete nature of real processes is still present, and the high aggregation regime, where the continuity approximation can be assumed more safely, holds. We managed to devise a method to filter out this transient and to link the low aggregation behaviour to the cross dependence among different stocks in the same market unveiling a new stylized fact. The main results are the following:

- we solved an open debate in the literature about the source of the multiscaling behaviour of the log-price time-series;
- we pointed out that the scaling measures at small aggregation regimes are heavily biased, but that at the same time these biases convey important information about the statistical properties of the analysed time-series;
- we proposed a new algorithm able to tame the biases and filter them out, without the need of knowing the exact functional form these biases manifest themselves in;
- we found that the presence of the bias is a transient state and that finan-

cial log-returns under high aggregation tend to behave as a multifractal random variable;

- we linked the transient of each time-series to a cross dependence properties and also to a variables of economic interest, namely, the capitalization, and we reinterpret this result in terms of the efficiency of the considered stock.

Our analysis of the scaling properties started in Ch. 4 where the true source of the multifractal scaling of financial log-price time-series, namely the autocorrelation, is discovered, unfolding a debate in the literature where several works did not agree on the solution. In doing so we unveiled that the scaling measures are strongly affected by biases, especially in the short time-horizon, which may have caused the lack of agreement in previous approaches to the problem of the source of the multifractal behaviour. We studied and quantified these biases in a systematic way, managing to determine their specific sources. These results point toward the corollary that financial log-returns are not multifractal in the usual sense presented in Ch. 3. In particular the main problem was identified in their discreteness in both time and value which is at odd with the very first assumptions of the multifractal picture. However, it came as a surprise that the scaling of the absolute moments of log-returns, despite being evidently non linear in log-log scale at low aggregations regimes, becomes asymptotically linear at high ones. This observation led us to the conclusion that a method which filters out the transient behaviour at low aggregations regimes and reliably measures the asymptotic scaling exponents at high ones was needed. We then devised a method which, by means of a filter function whose role is to model the transient behaviour, shows that the asymptotic behaviour is indeed linear and measures it. It is worth stressing that the knowledge of the exact functional shape of the filter function is not needed in order for the method to work. Following these results, we realized that the

transient actually gathers information about the generating process underlying the financial log-returns making then the bias potentially very informative. In fact, in Ch. 6 we showed how its size is linked to a multivariate property of financial time-series, namely the cross correlation. This in particular helped us to infer that highly correlated stocks are those that are more stable under aggregation and in turn also more capitalized and efficient.

As for future studies, let us first of all observe that the results presented in Chs. 4 and 5 raise the question whether the bias in the estimation affects also other methods present in the literature for the estimation of the scaling exponents. In our opinion the reason is twofold: first, to the best of our knowledge there are not multifractal estimation methods which deal with the proper estimation of the scaling region; second not dealing with the scaling region means disregarding the asymptotic scaling which is the only where there is hope of finding a multifractal scaling according to our analysis.
Also, as briefly mentioned at the end of Ch. 4, these results are not confined to the financial area, but they apply to any time-series where a multifractal analysis is performed. There have been studies reporting the presence of a supposed multifractal scaling in many fields like biology, medicine, earthquakes analysis (see for example [189, 190, 191]). Given the possible presence of estimation biases, a review of these studies might be appropriate and the conclusions drawn potentially revised.

As for the empirical scaling behaviour found in Ch. 5 for real time-series, it would be interesting to understand, in terms of properties of the finest scale generating process, why we almost always observe the same qualitatively behaviour in the way the moments converge to the asymptotic scaling and why the ABT time-series differs from the others. Also, the fact that the

scaling of the absolute moments of empirical data converges asymptotically to linearity is in itself puzzling. In particular, different real time-series can be safely regarded as generated by different stochastic processes which in turn have a different memory structure. In light of this, it seems all but obvious that they have to converge asymptotically to a multifractal random process. This observation might open that door to a generalized version of the central limit theorem where numbers characterized by long-memory, under certain assumptions, necessarily converge to a multifractal variable[1].

We also observe that the method proposed in Ch. 5 can be easily generalized to the case of the bivariate multifractal exponents, which we reviewed in Sec. 3.4. In particular the scaling of the product of two different random variable with long memory, may potentially have completely different behaviours at low and at high aggregation horizon. On one side because the long memory leads the convergence rate, on the other because at low aggregation horizon there is still the presence of the biases. This in particular could lead to problems where an investor wants to asses the performances of a portfolio at different scales. Thus via a bivariate measure of scaling, a generalized cross-correlation matrix could be introduced which takes into account these issues and in turn perform more reliable portfolio performance estimations for different time-scales.

As for the empirical results found in Ch. 6 we regard the map we draw of the stocks, according to the average-cross correlation and scaling, relevant for the construction of new models. In particular, the empirical behaviour we found, from a qualitative point of view, seems to be the same in every market, thus a good multivariate model should be able to reproduce it.

[1] We report that a similar speculation is reported in [159]

Appendix A

Estimation of the β exponent

In this Appendix we want to give a proof of Eq. (2.13). Let us recall that

$$\chi_t(L,\gamma) = \frac{1}{L}\sum_{i=0}^{L-1} |r_\tau(t+i)|^\gamma, \tag{A.1}$$

and that the autocovariance of $|r_\tau(t)|^\gamma$ is assumed to follow

$$\mathrm{Cov}\left[|r_\tau(t+L)|, |r_\tau(t)|\right] \propto \sigma^2_{|r|^\gamma} L^{-\beta(\gamma)}, \qquad \beta(\gamma) \leq 1, \tag{A.2}$$

where $\sigma^2_{|r|^\gamma}$ is the variance of $|r_\tau(t)|^\gamma$. Our aim is to compute the quantity

$$\delta(L,\gamma) = \sqrt{\mathrm{Var}\left[\chi_t(L,\gamma)\right]} = \sqrt{E\left[\chi^2_t(L,\gamma)\right] - E^2\left[\chi_t(L,\gamma)\right]}. \tag{A.3}$$

First we notice that

$$\begin{aligned} E\left[\chi^2_t(L,\gamma)\right] &= \frac{1}{L^2} E\left[\left(\sum_{i=0}^{L-1} |r_\tau(t+i)|^\gamma\right)^2\right] \\ &= \frac{1}{L^2}\left\{\sum_{i=0}^{L-1} E\left[|r_\tau(t+i)|^{2\gamma}\right] + 2\sum_{i<j=0}^{L-1} E\left[|r_\tau(t+i)|^\gamma |r_\tau(t+j)|^\gamma\right]\right\}, \end{aligned} \tag{A.4}$$

and that

$$\begin{aligned} E^2\left[\chi_t(L,\gamma)\right] &= \frac{1}{L^2} E^2\left[\sum_{i=0}^{L-1} |r_\tau(t+i)|^\gamma\right] \\ &= \frac{1}{L^2}\left\{\sum_{i=0}^{L-1} E^2\left[|r_\tau(t+i)|^\gamma\right] + 2\sum_{i<j=0}^{L-1} E\left[|r_\tau(t+i)|^\gamma\right] E|r_\tau(t+j)|^\gamma\right\}. \end{aligned} \tag{A.5}$$

From Eqs. (A.2-A.5) it follows that

$$\begin{aligned} \mathrm{Var}\left[\chi_t(L,\gamma)\right] &= \frac{1}{L^2}\left\{\sum_{i=0}^{L-1}\mathrm{Var}\left[|r_\tau(t+i)|^\gamma\right] + 2\sum_{i<j=0}^{L-1}\mathrm{Cov}\left[|r_\tau(t+i)|^\gamma, |r_\tau(t+j)|^\gamma\right]\right\} \\ &\simeq \frac{\sigma^2_{|r|^\gamma}}{L^2}\left\{L + 2\sum_{i<j=0}^{L-1}(j-i)^{-\beta(\gamma)}\right\}. \end{aligned} \tag{A.6}$$

Let us now focus on the last term of the last equation:

$$\begin{aligned} \textstyle\sum_{i<j=0}^{L-1}(j-i)^{-\beta(\gamma)} &= (1^{-\alpha(\gamma)}) + (1^{-\alpha(\gamma)} + 2^{-\alpha(\gamma)}) + (1^{-\alpha(\gamma)} + 2^{-\alpha(\gamma)} + 3^{-\alpha(\gamma)}) + ... \\ &+ (1^{-\alpha(\gamma)} + ... + (L-1)^{-\alpha(\gamma)}) \\ &= (L-1)1^{-\alpha(\gamma)} + (L-2)2^{-\alpha(\gamma)} + (L-3)3^{-\alpha(\gamma)} + ... + 1(L-1)^{-\alpha(\gamma)} \\ &= \textstyle\sum_{i=1}^{L-1}(L-i)i^{-\alpha(\gamma)}. \end{aligned} \tag{A.7}$$

Since Eq. (A.2) is supposed to hold for large lags, we can impose $L \gg 1$ and so approximate the last sum by an integral, *i.e.*

$$\sum_{i<j=0}^{L-1}(j-i)^{-\beta(\gamma)} = \sum_{i=1}^{L-1}(L-i)i^{-\alpha(\gamma)} \simeq \int_0^L (L-x)x^{-\alpha(\gamma)}dx = \frac{L^{2-\beta(\gamma)}}{[1-\beta(\gamma)]\,[2-\beta(\gamma)]}. \tag{A.8}$$

Using now Eq. (A.8) into Eq. (A.6) and keeping only leading terms in L, we obtain the result

$$\delta(L,\gamma) = \sqrt{\mathrm{Var}\left[\chi_t(L,\gamma)\right]} = \frac{\sqrt{2}\sigma_{|r|^\gamma}}{\sqrt{[1-\beta(\gamma)]\,[2-\beta(\gamma)]}}L^{-\frac{\beta(\gamma)}{2}} \tag{A.9}$$

Appendix B

Explicit computation of Eq. 5.4

In order to understand the scaling properties of the moments of S_N in the continuous time limit we need first to know its pdf S_N, namely $p_s(S_N)$. From the probability theory we know that this pdf is given by the convolution of the single pdfs. For example

$$\begin{aligned} p_s(S_2) = p(x_1) * p(x_2) = \int_{\mathbb{R}} dx_1 p(x_1) p(S_2 - x_1), \\ p_s(S_3) = p(x_1) * p(x_2) * p(x_3) = \int_{\mathbb{R}} dS_2 \int_{\mathbb{R}} dx_1 p(x_1) p(S_2 - x_1) p(S_3 - S_2). \end{aligned} \tag{B.1}$$

In general, defining $S_0 = 0$,

$$p_s(S_N) = \prod_{i=1}^{N-1} \int_{\mathbb{R}} dS_i p(S_i - S_{i-1}) p(S_N - S_{N-1}). \tag{B.2}$$

If we consider the discrete case what we usually compute after shuffling is

$$\begin{aligned} E[|S_N|^q] &= \int_{\mathbb{R}} dS_N |S_N|^q p_s(S_N) \\ &= \int_{\mathbb{R}} dS_N |S_N|^q \prod_{i=1}^{N-1} \int_{\mathbb{R}} dS_i p(S_i - S_{i-1}) p(S_N - S_{N-1}). \end{aligned} \tag{B.3}$$

It is evident that the dependence of $E[|S_N|^q]$ from the time time-horizon $\tau = N\Delta t$ is certainly far from being a simple power law as requested by the multifractal picture (see Eq. (3.5)). Thus, this is why the numerical estimations are horizon-dependent. However analytically, in order to infer something about the multi/uni-scaling nature of the process x_i, we are interested in the continuous time limit of Eq. (B.3), in line with the underling assumptions

of multifractality. In particular we want to compute the simultaneous limits $\Delta t \to 0$, $N \to \infty$, but keeping the product $N\Delta t = \tau$ fixed, in order to have finite time horizons. In formulas we want to compute

$$\lim_{\substack{\Delta t\to 0\\ N\to\infty\\ N\Delta t=\tau}} E[|S_N|^q] = E[|S_\infty|^q] = \lim_{\substack{\Delta t\to 0\\ N\to\infty\\ N\Delta t=\tau}} \int_{\mathbb{R}} dS_N |S_N|^q p_s(S_N). \tag{B.4}$$

Due to the CLT the following equality holds:

$$E[|S_\infty|^q] = \lim_{\substack{\Delta t\to 0\\ N\to\infty\\ N\Delta t=\tau}} \int_{\mathbb{R}} dS_N |S_N|^q \frac{e^{-\frac{S_N^2}{2\sigma^2 N\Delta t}}}{\sqrt{2\pi}\sigma\sqrt{N\Delta t}}. \tag{B.5}$$

Using now the variable $z = \dfrac{S_N}{\sqrt{\sigma^2 N\Delta t}}$, Eq. (B.5) becomes

$$E[|S_\infty|^q] = \lim_{\substack{\Delta t\to 0\\ N\to\infty\\ N\Delta t=\tau}} \int_{\mathbb{R}} dz \sigma^q (N\Delta t)^{\frac{q}{2}} |z|^q \frac{e^{-\frac{z^2}{2}}}{\sqrt{2\pi}}; \tag{B.6}$$

Performing then the limit, taking out the constants and solving the integral (which is known), the solution is finally

$$E[|S_\infty|^q] = \sigma^q \frac{2^{\frac{q}{2}}\Gamma(\frac{q+1}{2})}{\sqrt{\pi}} \tau^{\frac{q}{2}}. \tag{B.7}$$

Appendix C

Computation of the value of $H(2)$ of real financial processes

In this appendix we show that for empirical financial time-series $H(2) = 0.5$. As noted in [8], on empirical financial datasets the estimator of $H(2)$ cannot be reliably measured because the second moment of the empirical distributions is finite, but the fourth momentum is often infinite (cfr. [14, 15]).Using empirical evidence is however possible to infer its value in the limit of infinite aggregation. This simple result follows from the following properties of financial time-series, calling $r_\tau(t)$ the log-returns:

$$\begin{cases} E[r_\tau(t)] = 0 \\ Var[r_\tau(t)] < \infty \\ Corr[r_\tau(t_1), r_\tau(t_2)] = 0 \qquad t_1 \neq t_2. \end{cases} \tag{C.1}$$

where by $Corr$ we mean the correlation function. We notice that in the high frequency domain the third property is true after few lags ([14, 3]) thus it does not affect the asymptotic properties of the scaling. Let us call then $\varepsilon_{\Delta t}(k)$ the elementary increments of a process satisfying the properties listed in Eq. (C.1) with variance $Var[\varepsilon_{\Delta t}(k)] = \sigma^2 \Delta t$, where σ is a fixed scalar and Δt the discretization step. The returns of this process under aggregation can be written on scale τ as

$$r_\tau(t) = \sum_{k=\frac{t}{\Delta t}+1}^{\frac{t+\tau}{\Delta t}} \varepsilon_{\Delta t}(k). \tag{C.2}$$

The following chain of equalities hold

$$\begin{aligned} E[|r_\tau(t)|^2] &= Var[r_\tau(t)] = Var[\textstyle\sum_{k=\frac{t}{\Delta t}+1}^{\frac{t+\tau}{\Delta t}} \varepsilon_{\Delta t}(k)] \\ &= \sum_{k=\frac{t}{\Delta t}+1}^{\frac{t+\tau}{\Delta t}} Var[\varepsilon_{\Delta t}(k)]] + \sum_{k_1<k_2=\frac{t}{\Delta t}+1}^{\frac{t+\tau}{\Delta t}} 2Cov[\varepsilon_{\Delta t}(k_1), \varepsilon_{\Delta t}(k_2)] \\ &= \sigma^2\tau, \end{aligned} \tag{C.3}$$

where the first and fourth equality follow from Eq. (C.1). Thus, with the notation of Eq. (3.5), it can be written that

$$E[|r_\tau(t)|^2] = K(2)\tau^{2H(2)} = \sigma^2\tau; \tag{C.4}$$

which in turn implies that $H(2) = 0.5$.

Appendix D

Effect of the concavity on the scaling exponents fitting function

In this appendix we derive the third condition in Eq. (5.17). The second derivative of Eq. (5.15) reads as

$$\zeta''(q) = 12Dq^2 + 6Cq + 2B. \tag{D.1}$$

To ensure that the condition $\zeta''(q) < 0$ holds for every q the roots of (D.1) must coincide and $D < 0$. In particular the roots of (D.1) are

$$q_{\pm} = \frac{-3C \pm \sqrt{9C^2 - 24BD}}{12D}, \tag{D.2}$$

which, in order to coincide, must satisfy

$$B = \frac{3C^2}{8D}. \tag{D.3}$$

Appendix E

Other measures of cross-correlation

In this subsection we show that the dependence holds also for other measures of cross-correlations, namely the sign cross-correlation and the amplitudes cross-correlation. Using the notation of Subsec. 6.2.4, we report in Figs. E.1 and E.2 the value of $\hat{B}$ respectively against $\bar{R}$ and $\bar{S}$. In Tabs are instead reported the τ correlations along with the p-values. It appears evident that the dependence is still strongly present.

market	τ	p-value
NYSE17	0.28	0.000
LSE	0.61	0.000
FWB	0.64	0.000
TSE	0.44	0.000
HKSE	0.57	0.000
NYSE99	0.56	0.000

Table E.1: Kendall τ correlation between $\hat{B}$ and $\bar{R}$.

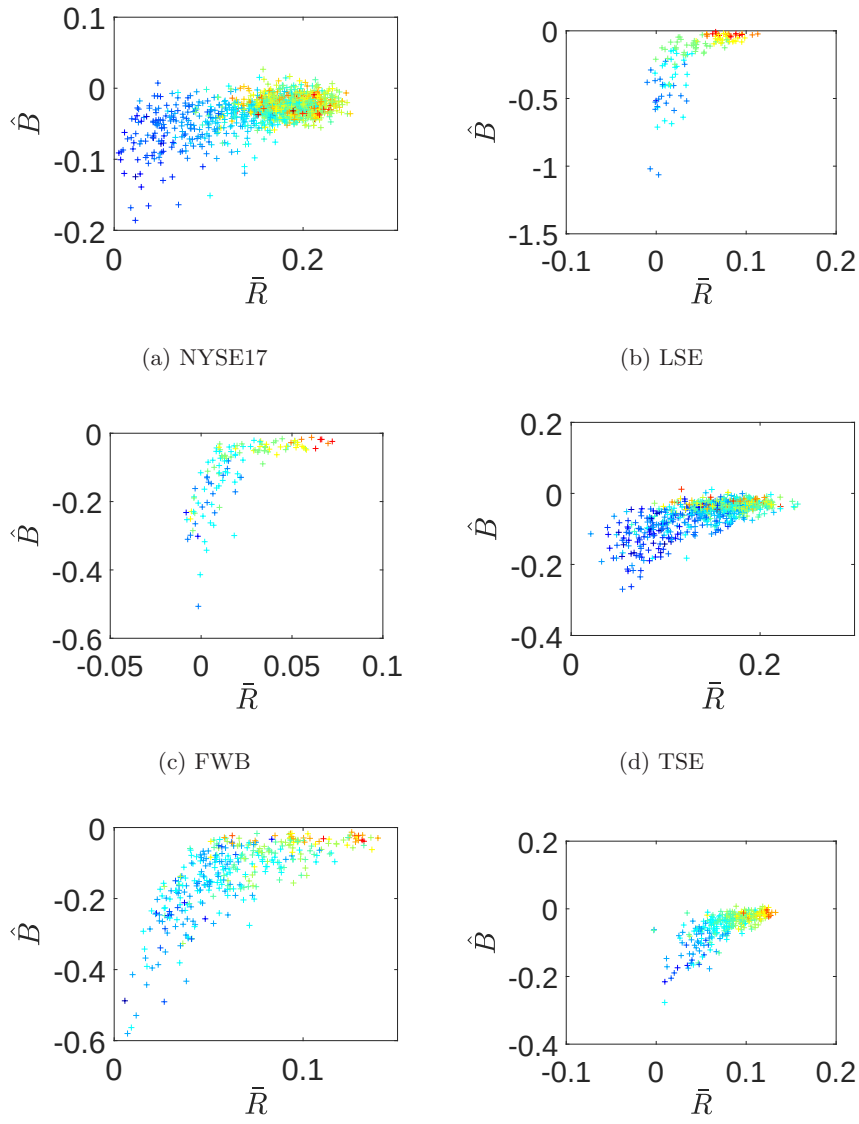

(a) NYSE17 (b) LSE

(c) FWB (d) TSE

(e) HKSE (f) NYSE99

Figure E.1: Empirical evidence of the dependence between the degree of multiscaling measured by the proxy $\hat{B}$ of log-return and its sign correlation $\bar{R}$ with the log-return of other stocks traded in the same market. The color represents the increasing capitalization from blue to red.

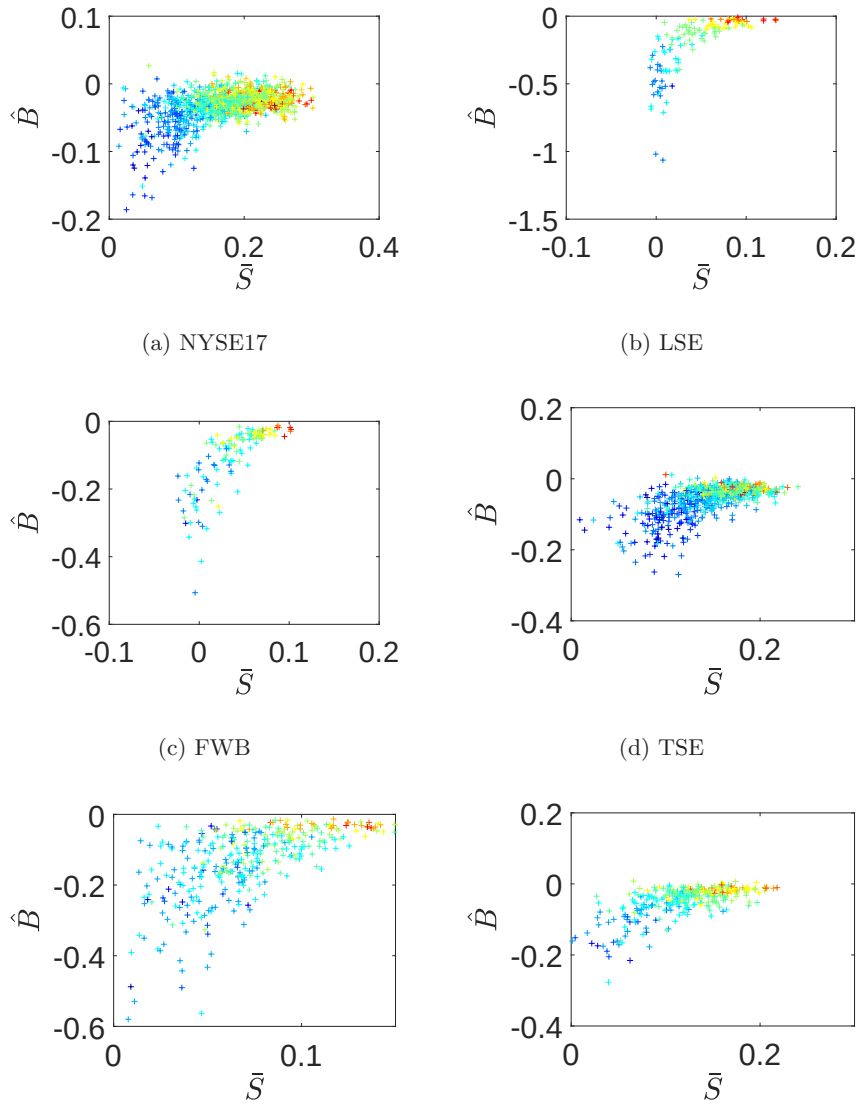

(a) NYSE17 (b) LSE

(c) FWB (d) TSE

(e) HKSE (f) NYSE99

Figure E.2: Empirical evidence of the dependence between the degree of multiscaling measured by the proxy $\hat{B}$ of log-return and its absolute values correlation $\bar{S}$ with the log-return of other stocks traded in the same market. The color represents the increasing capitalization from blue to red.

market	τ	p-value
NYSE17	0.30	0.000
LSE	0.65	0.000
FWB	0.66	0.000
TSE	0.41	0.000
HKSE	0.46	0.000
NYSE99	0.44	0.000

Table E.2: Kendall τ correlation between $\hat{B}$ and $\bar{S}$.

Appendix F

Normalization effect

We summarize here the result of the effect of the normalization procedure [160, 8] on the dependency between $\hat{B}$ and $\bar{\rho}$. The graphical results is reported in Fig. F.1 while the numerical ones in Tab. F.1. We see that after normalization the effect disappears completely in four cases out of six and in the the remaining two is strongly lessened.

market	τ	p-value
NYSE17	-0.02	0.405
LSE	0.02	0.760
FWB	0.22	0.000
TSE	-0.05	0.069
HKSE	0.12	0.001
NYSE99	0.14	0.000

Table F.1: Kendall τ correlation between $\hat{B}$ and $\bar{\rho}$ when the log-returns are normalized.

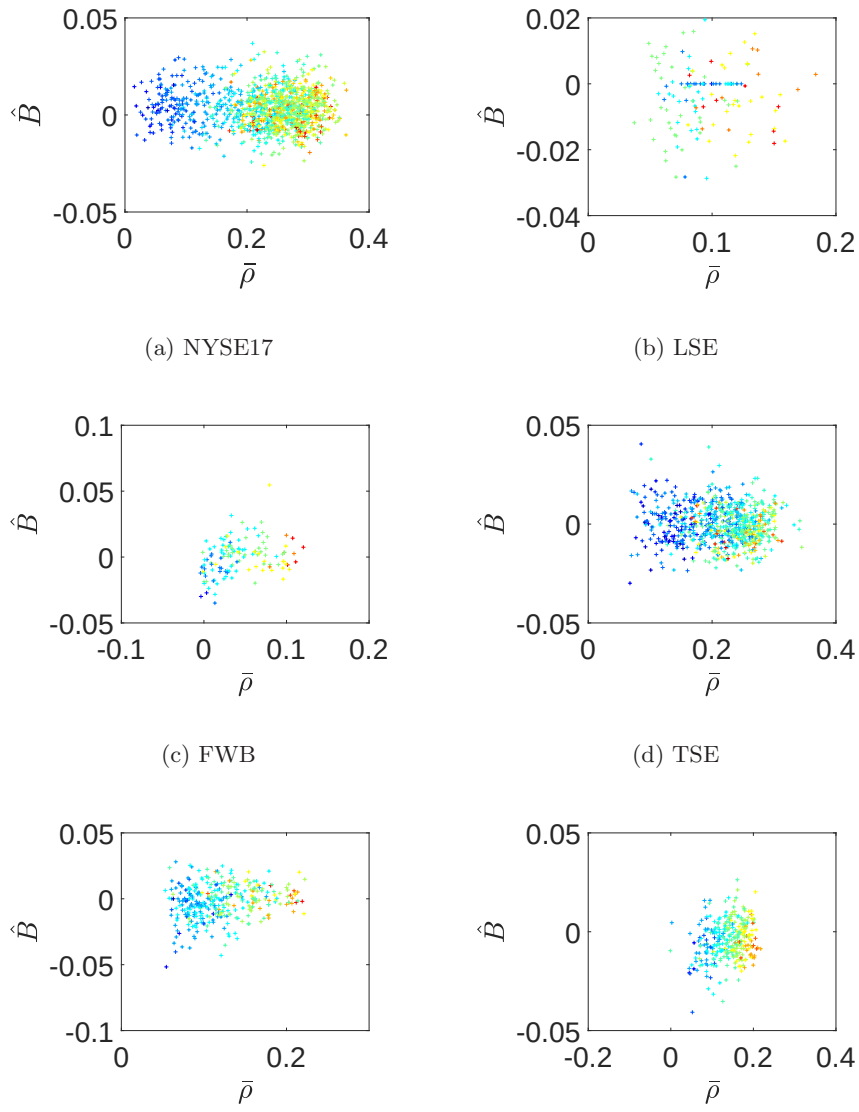

(a) NYSE17 (b) LSE

(c) FWB (d) TSE

(e) HKSE (f) NYSE99

Figure F.1: Scatter plot between the degree of multiscaling measured by the proxy $\hat{B}$ of log-return and its average correlation $\bar{\rho}$ with the log-return of other stocks traded in the same market when the log-returns are normalized. The color represents the increasing capitalization from blue to red.

Bibliography

[1] Giorgio Parisi. Complex systems: a physicist's viewpoint. Physica A: Statistical Mechanics and its Applications, 263(1-4):557–564, 1999.

[2] Riccardo Junior Buonocore, Nicolò Musmeci, Tomaso Aste, and Tiziana Di Matteo. Two different flavours of complexity in financial data. The European Physical Journal Special Topics, 225(17-18):3105–3113, 2016.

[3] Michel M. Dacorogna, Ramazan Gençay, Ulrich A. Müller, Richard B. Olsen, and Olivier V. Pictet. An Introduction to High-Frequency Finance. Academic Press, San Diego, 2001.

[4] Thomas Lux and Michele Marchesi. Scaling and criticality in a stochastic multi-agent model of a financial market. Nature, 397(6719):498, 1999.

[5] Tomaso Aste and Tiziana Di Matteo. Introduction to complex and econophysics systems: A navigation map. Complex physical, biophysical and econophysical systems, pages 1–35, 2010.

[6] Raffaello Morales, Tiziana Di Matteo, and Tomaso Aste. Dependency structure and scaling properties of financial time series are related. Scientific reports, 4, 2014.

[7] Benoit B. Mandelbrot. The variation of certain speculative prices. The journal of business, 36(4):394–419, 1963.

[8] Riccardo J. Buonocore, Tomaso Aste, and Tiziana Di Matteo. Measuring multiscaling in financial time-series. Chaos, Solitons & Fractals, 88:38 – 47, 2016. Complexity in Quantitative Finance and Economics.

[9] Riccardo J. Buonocore, Tomaso Aste, and Tiziana Di Matteo. Asymptotic scaling properties and estimation of the generalized hurst exponents in financial data. Phys. Rev. E, 95:042311, Apr 2017.

[10] Riccardo Junior Buonocore, Rosario N. Mantegna, and Tiziana Di Matteo. On the interplay between scaling properties and cross-correlation. in preparation, 2017.

[11] Louis Bachelier. Théorie de la spéculation. Gauthier-Villars, 1900.

[12] Harry Markowitz. Portfolio selection. The journal of finance, 7(1):77–91, 1952.

[13] Fischer Black and Myron Scholes. The pricing of options and corporate liabilities. Journal of political economy, 81(3):637–654, 1973.

[14] Rama Cont. Empirical properties of asset returns: stylized facts and statistical issues. Quantitative Finance, 1(2):223–236, 2001.

[15] Anirban Chakraborti, Ioane Muni Toke, Marco Patriarca, and Frédéric Abergel. Econophysics review: I. empirical facts. Quantitative Finance, 11(7):991–1012, 2011.

[16] Robert F. Engle. Autoregressive conditional heteroscedasticity with estimates of the variance of united kingdom inflation. Econometrica, 50(4):987–1007, 1982.

[17] Andrew Clare, James Seaton, Peter N. Smith, and Stephen Thomas. The trend is our friend: Risk parity, momentum and trend following in

global asset allocation. Journal of Behavioral and Experimental Finance, 9:63–80, 2016.

[18] Rosario N. Mantegna and H. Eugene Stanley. Introduction to Econophysics: Correlations and Complexity in Finance. Cambridge University Press, 1999.

[19] Aaron Clauset, Cosma Rohilla Shalizi, and Mark EJ Newman. Power-law distributions in empirical data. SIAM review, 51(4):661–703, 2009.

[20] Yogesh Virkar, Aaron Clauset, et al. Power-law distributions in binned empirical data. The Annals of Applied Statistics, 8(1):89–119, 2014.

[21] Zhuanxin Ding, Clive W.J. Granger, and Robert F. Engle. A long memory property of stock market returns and a new model. Journal of Empirical Finance, 1(1):83 – 106, 1993.

[22] Michele Pasquini and Maurizio Serva. Multiscale behaviour of volatility autocorrelations in a financial market. Economics Letters, 65(3):275–279, 1999.

[23] Barry C. Arnold and Richard A. Groeneveld. Measuring skewness with respect to the mode. The American Statistician, 49(1):34–38, 1995.

[24] John C. Cox and Stephen Ross. The valuation of options for alternative stochastic processes. Journal of Financial Economics, 3(1-2):145–166, 1976.

[25] Jean-Philippe Bouchaud, Andrew Matacz, and Marc Potters. Leverage effect in financial markets: The retarded volatility model. Phys. Rev. Lett., 87:228701, Nov 2001.

[26] Vasiliki Plerou, Parameswaran Gopikrishnan, Bernd Rosenow, Luís A. Nunes Amaral, and H. Eugene Stanley. Universal and nonuniversal

properties of cross correlations in financial time series. Physical Review Letters, 83(7):1471, 1999.

[27] Andrew W. Lo and A. Craig MacKinlay. When are contrarian profits due to stock market overreaction? The Review of Financial Studies, 3(2):175–205, 1990.

[28] Vincenzo Tola, Fabrizio Lillo, Mauro Gallegati, and Rosario N. Mantegna. Cluster analysis for portfolio optimization. Journal of Economic Dynamics and Control, 32(1):235–258, 2008.

[29] Michele Tumminello, Tomaso Aste, Tiziana Di Matteo, and Rosario N. Mantegna. A tool for filtering information in complex systems. Proceedings of the National Academy of Sciences of the United States of America, 102(30):10421–10426, 2005.

[30] Tomaso Aste, Tiziana Di Matteo, and Stephen T. Hyde. Complex networks on hyperbolic surfaces. Physica A: Statistical Mechanics and its Applications, 346(1):20–26, 2005.

[31] Vincenzo Tola, Fabrizio Lillo, Mauro Gallegati, and Rosario N. Mantegna. Cluster analysis for portfolio optimization. Journal of Economic Dynamics and Control, 32(1):235–258, 2008.

[32] Tomaso Aste, Ruggero Gramatica, and Tiziana Di Matteo. Exploring complex networks via topological embedding on surfaces. Physical Review E, 86(3):036109, 2012.

[33] Guido Previde Massara, Tiziana Di Matteo, and Tomaso Aste. Network filtering for big data: triangulated maximally filtered graph. Journal of complex Networks, 5(2):161–178, 2016.

[34] Won-Min Song, Tiziana Di Matteo, and Tomaso Aste. Hierarchical information clustering by means of topologically embedded graphs. PLoS One, 7(3):e31929, 2012.

[35] Won-Min Song, Tiziana Di Matteo, and Tomaso Aste. Nested hierarchies in planar graphs. Discrete Applied Mathematics, 159(17):2135–2146, 2011.

[36] Giuseppe Buccheri, Stefano Marmi, and Rosario N. Mantegna. Evolution of correlation structure of industrial indices of us equity markets. Physical Review E, 88(1):012806, 2013.

[37] Jukka-Pekka Onnela, Anirban Chakraborti, Kimmo Kaski, and Janos Kertesz. Dynamic asset trees and black monday. Physica A: Statistical Mechanics and its Applications, 324(1):247–252, 2003.

[38] Wooseok Jang, Junghoon Lee, and Woojin Chang. Currency crises and the evolution of foreign exchange market: Evidence from minimum spanning tree. Physica A: Statistical Mechanics and its Applications, 390(4):707–718, 2011.

[39] Nicolo Musmeci, Tiziana Di Matteo, and Tomaso Aste. Risk diversification: a study of persistence with a filtered correlation-network approach. Journal of Network Theory in Finance, 1(1):1–22, 3 2015.

[40] Francesco Pozzi, Tiziana Di Matteo, and Tomaso Aste. Spread of risk across financial markets: better to invest in the peripheries. Scientific reports, 3, 2013.

[41] Jukka-Pekka Onnela, Anirban Chakraborti, Kimmo Kaski, Janos Kertesz, and Antti Kanto. Dynamics of market correlations: Taxonomy and portfolio analysis. Physical Review E, 68(5):056110, 2003.

[42] Petter Holme and Jari Saramäki. Temporal networks. Physics reports, 519(3):97–125, 2012.

[43] Hakan Kaya. Eccentricity in asset management. Network Theory in Finance, 1(1):1–32, 2015.

[44] Rosario N. Mantegna. Hierarchical structure in financial markets. The European Physical Journal B-Condensed Matter and Complex Systems, 11(1):193–197, 1999.

[45] Tomaso Aste, W. Shaw, and Tiziana Di Matteo. Correlation structure and dynamics in volatile markets. New Journal of Physics, 12(8):085009, 2010.

[46] Tomaso Aste and Tiziana Di Matteo. Dynamical networks from correlations. Physica A: Statistical Mechanics and its Applications, 370(1):156–161, 2006.

[47] Michele Tumminello, Fabrizio Lillo, and Rosario N. Mantegna. Correlation, hierarchies, and networks in financial markets. Journal of Economic Behavior & Organization, 75(1):40–58, 2010.

[48] Brian S. Everitt, Sabine Landau, Morven Leese, and Daniel Stahl. Hierarchical clustering. Cluster Analysis, 5th Edition, pages 71–110, 2011.

[49] Salvatore Miccichè. Empirical relationship between stocks' cross-correlation and stocks' volatility clustering. Journal of Statistical Mechanics: Theory and Experiment, 2013(05):P05015, 2013.

[50] Anshul Verma, Riccardo Junior Buonocore, and Tiziana Di Matteo. A DBHT-driven log-volatility factor model: a deepening on the source of the volatility clustering. in preparation, 2017.

[51] George E. P. Box, Gwilym M. Jenkins, Gregory C. Reinsel, and Greta M. Ljung. Time Series Analysis: Forecasting and Control. Wiley Series in Probability an. Wiley, 2015.

[52] Tim Bollerslev. Generalized autoregressive conditional heteroskedasticity. Journal of Econometrics, 31(3):307–327, 1986.

[53] Robert F. Engle and Victor K. NG. Measuring and testing the impact of news on volatility. The Journal of Finance, 48(5):1749–1778, 1993.

[54] Enrique Sentana. Quadratic arch models. The Review of Economic Studies, 62(4):639–661, 1995.

[55] Lawrence R. Glosten, Ravi Jagannathan, and David E. Runkle. On the relation between the expected value and the volatility of the nominal excess return on stocks. Journal of Finance, 48(5):1779–1801, 1993.

[56] Daniel B. Nelson. Conditional heteroskedasticity in asset returns: A new approach. Econometrica, 59(2):347–70, 1991.

[57] Luc Bauwens, Sébastien Laurent, and Jeroen V. K. Rombouts. Multivariate garch models: a survey. Journal of Applied Econometrics, 21(1):79–109, 2006.

[58] Tim Bollerslev, Robert F. Engle, and Jeffrey M. Wooldridge. A capital asset pricing model with time-varying covariances. Journal of Political Economy, 96(1):116–131, 1988.

[59] Zhuanxin Ding and Robert F. Engle. Large scale conditional covariance matrix modeling, estimation and testing. NYU Working Paper No. S-DRP-01-07, 2001.

[60] Robert F. Engle and Kenneth F. Kroner. Multivariate simultaneous generalized arch. Econometric Theory, 11(1):122–150, 1995.

[61] Eugene F. Fama and Kenneth R. French. Common risk factors in the returns on stocks and bonds. Journal of Financial Economics, 33(1):3 – 56, 1993.

[62] Robert F. Engle, Victor K. Ng, and Michael Rothschild. Asset pricing with a factor-arch covariance structure. Journal of Econometrics, 45(1):213 – 237, 1990.

[63] Kariya T. Mtv model and its application to the prediction of stock prices. In Tarmo Pukkila and Simo Puntanen, editors, Proceedings of the Second International Tampere Conference in Statistics : University of Tampere. Dept. of Mathematical Sciences/Statistics, University of Tampere, 1987.

[64] Carol Alexander and Aubrey Chibumba. Multivariate orthogonal factor garch. University of Sussex, Mimeo, 1997.

[65] Tim Bollerslev. Modelling the Coherence in Short-run Nominal Exchange Rates: A Multivariate Generalized ARCH Model. The Review of Economics and Statistics, 72(3):498–505, August 1990.

[66] Yiu K. Tse and Albert K. C. Tsui. A multivariate generalized autoregressive conditional heteroscedasticity model with time-varying correlations. Journal of Business & Economic Statistics, 20(3):351–362, 2002.

[67] Robert Engle. Dynamic conditional correlation: A simple class of multivariate generalized autoregressive conditional heteroskedasticity models. Journal of Business & Economic Statistics, 20(3):339–350, 2002.

[68] Roger B. Nelsen. An Introduction to Copulas. Lecture notes in statistics. Springer, 1999.

[69] Andrew J. Patton. Modelling time-varying exchange rate dependence using the conditional copula. University of California at San Diego,

Economics Working Paper Series qt01q7j1s2, Department of Economics, UC San Diego, June 2001.

[70] Eric Jondeau and Michael Rockinger. The copula-garch model of conditional dependencies: An international stock market application. Journal of International Money and Finance, 25(5):827–853, 2006.

[71] Stephen J. Taylor. Financial returns modelled by the product of two stochastic processes, a study of daily sugar prices 1961-79. In O.D. Anderson, editor, Time Series Analysis, Theory and Practice, volume 1, pages 203–226. North-Holland, 1981.

[72] Roman Liesenfeld and Robert C. Jung. Stochastic volatility models: conditional normality versus heavy-tailed distributions. Journal of Applied Econometrics, 15(2):137–160, 2000.

[73] Siddhartha Chib, Federico Nardari, and Neil Shephard. Markov chain monte carlo methods for stochastic volatility models. Journal of Econometrics, 108(2):281 – 316, 2002.

[74] Bjø rn Eraker, Michael Johannes, and Nicholas Polson. The impact of jumps in volatility and returns. The Journal of Finance, 58(3):1269–1300, 2003.

[75] David S. Bates. Post-'87 crash fears in s&p 500 futures options. Working Paper 5894, National Bureau of Economic Research, January 1997.

[76] Darrell Duffie, Jun Pan, and Kenneth Singleton. Transform analysis and asset pricing for affine jump-diffusions. Econometrica, 68(6):1343–1376, 2000.

[77] Kenneth R. French, G. William Schwert, and Robert F. Stambaugh. Expected stock returns and volatility. Journal of Financial Economics, 19(1):3 – 29, 1987.

[78] Andrew C. Harvey and Neil Shephard. Estimation of an asymmetric stochastic volatility model for asset returns. Journal of Business & Economic Statistics, 14(4):429–434, 1996.

[79] Gleb Sandmann and Siem Jan Koopman. Estimation of stochastic volatility models via monte carlo maximum likelihood. Journal of Econometrics, 87(2):271 – 301, 1998.

[80] Eric Jacquier, Nicholas G. Polson, and Peter E. Rossi. Bayesian analysis of stochastic volatility models. Journal of Business & Economic Statistics, 12(4):371–389, 1994.

[81] Nikolaus Hautsch and Yangguoyi Ou. Discrete-Time Stochastic Volatility Models and MCMC-Based Statistical Inference. SFB 649 Discussion Papers SFB649DP2008-063, Sonderforschungsbereich 649, Humboldt University, Berlin, Germany, September 2008.

[82] F. Jay Breidt, Nuno Crato, and Pedro De Lima. The detection and estimation of long memory in stochastic volatility. Journal of econometrics, 83(1):325–348, 1998.

[83] Andrew C. Harvey. Long-memory in stochastic volatility. In Stephen Satchell and John Knight, editors, Forecasting Volatility in the Financial Markets, pages 351 – 364. Elsevier, 3 edition, 2007.

[84] Josu Arteche. Gaussian semiparametric estimation in long memory in stochastic volatility and signal plus noise models. Journal of Econometrics, 119(1):131 – 154, 2004.

[85] Andrew Harvey, Esther Ruiz, and Neil Shephard. Multivariate stochastic variance models. The Review of Economic Studies, 61(2):247–264, 1994.

[86] Eric Jacquier, Nicholas G. Polson, and Peter Rossi. Stochastic volatility: Univariate and multivariate extensions. Computing in Economics and Finance 1999 112, Society for Computational Economics, 1999.

[87] Mark Pitt and Neil Shephard. Time varying covariances: a factor stochastic volatility approach. Bayesian statistics, 6:547–570, 1999.

[88] Omar Aguilar and Mike West. Bayesian dynamic factor models and portfolio allocation. Journal of Business & Economic Statistics, 18(3):338–357, 2000.

[89] Benoit B. Mandelbrot. Intermittent turbulence in self-similar cascades: divergence of high moments and dimension of the carrier. Journal of Fluid Mechanics, 62(2):331–358, 1974.

[90] J-P Kahane and Jacques Peyriere. Sur certaines martingales de benoit mandelbrot. Advances in mathematics, 22(2):131–145, 1976.

[91] Richard Holley and Edward C. Waymire. Multifractal dimensions and scaling exponents for strongly bounded random cascades. The Annals of Applied Probability, pages 819–845, 1992.

[92] Kenneth J. Falconer. The multifractal spectrum of statistically self-similar measures. Journal of Theoretical Probability, 7(3):681–702, 1994.

[93] Matthias Arbeiter and Norbert Patzschke. Random self-similar multifractals. Mathematische Nachrichten, 181(1):5–42, 1996.

[94] Julien Barral. Moments, continuité, et analyse multifractale des martingales de mandelbrot. Probability Theory and Related Fields, 113(4):535–569, 1999.

[95] Benoit B Mandelbrot. Multifractal measures, especially for the geophysicist. Pure and applied geophysics, 131(1-2):5–42, 1989.

[96] Benoit B. Mandelbrot. Limit lognormal multifractal measures. In E. Dotsman, Y. Ne'eman, and A. Voronel, editors, Frontiers of Physics: Landau Memorial Conference, pages 309–340, New York, 1989. Pergamon.

[97] J. Christos Vassilicos, Antonis Demos, and Fidelio Tata. No evidence of chaos but some evidence of multifractals in the foreign exchange and the stock markets. In Applications of Fractals and Chaos, pages 249–265. Springer, 1993.

[98] Shoaleh Ghashghaie, Wolfgang Breymann, Joachim Peinke, Peter Talkner, and Yadollah Dodge. Turbulent cascades in foreign exchange markets. Nature, 381(6585):767–770, 1996.

[99] Stefano Galluccio, Guido Caldarelli, Matteo Marsili, and Y-C Zhang. Scaling in currency exchange. Physica A: Statistical Mechanics and its Applications, 245(3-4):423–436, 1997.

[100] Francois Schmitt, Daniel Schertzer, and Shaun Lovejoy. Multifractal analysis of foreign exchange data. Applied stochastic models and data analysis, 15(1):29–53, 1999.

[101] Rosario N. Mantegna and H. Eugene Stanley. Scaling behaviour in the dynamics of an economic index. Nature, 376(6535):46–49, 1995.

[102] Tiziana Di Matteo. Multi-scaling in finance. Quantitative finance, 7(1):21–36, 2007.

[103] Laurent E. Calvet and Adlai J. Fisher. Multifractality in asset returns: Theory and evidence. Review of Economics and Statistics, 84(3):381–406, 2002.

[104] Laurent E. Calvet and Adlai J. Fisher. Multifractal volatility: theory, forecasting, and pricing. Academic Press, 2008.

[105] Ruipeng Liu, Tiziana Di Matteo, and Thomas Lux. Multifractality and long-range dependence of asset returns: The scaling behaviour of the markov-switching multifractal model with lognormal volatility components. Advances in Complex Systems, 11:669 – 684, 2008.

[106] Marco Bartolozzi, Christopher Mellen, Tiziana Di Matteo, and Tomaso Aste. Multi-scale correlations in different futures markets. The European Physical Journal B-Condensed Matter and Complex Systems, 58(2):207–220, 2007.

[107] Marco Bartolozzi, Christopher Mellen, Francis Chan, David Oliver, Tiziana Di Matteo, and Tomaso Aste. Applications of physical methods in high-frequency futures markets. Proc. SPIE, 6802:680203–680203–14, 2007.

[108] Ladislav Kristoukek. Fractal markets hypothesis and the global financial crisis: scaling, investment horizons and liquidity. Advances in Complex Systems, 15(06):1250065, 2012.

[109] Zhi-Qiang Jiang and Wei-Xing Zhou. Multifractality in stock indexes: Fact or fiction? Physica A: Statistical Mechanics and its Applications, 387(14):3605–3614, 2008.

[110] Thomas Lux. Detecting multi-fractal properties in asset returns: The failure of the scaling estimator. International Journal of Modern Physics C, 15(04):481–491, 2004.

[111] Dariusz Grech and Zygmunt Mazur. On the scaling ranges of detrended fluctuation analysis for long-term memory correlated short series of data. Physica A: Statistical Mechanics and its Applications, 392(10):2384–2397, 2013.

[112] Dariusz Grech and Zygmunt Mazur. Scaling range of power laws that originate from fluctuation analysis. Physical Review E, 87(5):052809, 2013.

[113] Luis G. Moyano, Jeferson De Souza, and S. M. Duarte Queirós. Multifractal structure of traded volume in financial markets. Physica A: Statistical Mechanics and its Applications, 371(1):118–121, 2006.

[114] Jeferson De Souza and S. M. Duarte Queirós. Effective multifractal features of high-frequency price fluctuations time series and ℓ-variability diagrams. Chaos, Solitons & Fractals, 42(4):2512 – 2521, 2009.

[115] Raffaello Morales, Tiziana Di Matteo, Ruggero Gramatica, and Tomaso Aste. Dynamical generalized hurst exponent as a tool to monitor unstable periods in financial time series. Physica A: Statistical Mechanics and its Applications, 391(11):3180 – 3189, 2012.

[116] Wei-Xing Zhou. Multifractal detrended cross-correlation analysis for two nonstationary signals. Physical Review E, 77(6):066211, 2008.

[117] Gao-Feng Gu and Wei-Xing Zhou. Detrending moving average algorithm for multifractals. Physical Review E, 82(1):011136, 2010.

[118] Wei-Xing Zhou. Finite-size effect and the components of multifractality in financial volatility. Chaos, Solitons & Fractals, 45(2):147–155, 2012.

[119] Noemi Nava, Tiziana Di Matteo, and Tomaso Aste. Time-dependent scaling patterns in high frequency financial data. The European Physical Journal Special Topics, 225(10):1997–2016, 2016.

[120] Noemi Nava, Tiziana Di Matteo, and Tomaso Aste. Anomalous volatility scaling in high frequency financial data. Physica A: Statistical Mechanics and its Applications, 447:434 – 445, 2016.

[121] Benoit B. Mandelbrot, Adlai Fisher, and Laurent E. Calvet. A Multifractal Model of Asset Returns. Cowles Foundation Discussion Papers 1164, Cowles Foundation for Research in Economics, Yale University, September 1997.

[122] Laurent E. Calvet and Adlai Fisher. Forecasting multifractal volatility. Journal of Econometrics, 105(1):27–58, 2001.

[123] Thomas Lux. The markov-switching multifractal model of asset returns: Gmm estimation and linear forecasting of volatility. Journal of Business & Economic Statistics, 26(2):194–210, 2008.

[124] Thomas Lux and Leonardo Morales-Arias. Forecasting volatility under fractality, regime-switching, long memory and student- innovations. Computational Statistics & Data Analysis, 54(11):2676 – 2692, 2010. The Fifth Special Issue on Computational Econometrics.

[125] Mawuli Segnon and Thomas Lux. Multifractal Models in Finance: Their Origin, Properties, and Applications. Number 1860 in Kiel working paper. Institute for the World Economy, Kiel, 2013.

[126] Ruipeng Liu, Tiziana Di Matteo, and Thomas Lux. True and apparent scaling: The proximity of the markov-switching multifractal model to long-range dependence. Physica A: Statistical Mechanics and its Applications, 383(1):35–42, 2007.

[127] Emmanuel Bacry, Jean Delour, and Jean-François Muzy. Multifractal random walk. Physical Review E, 64(2):026103, 2001.

[128] Jean-François Muzy and Emmanuel Bacry. Multifractal stationary random measures and multifractal random walks with log infinitely divisible scaling laws. Physical Review E, 66(5):056121, 2002.

[129] Emmanuel Bacry and Jean François Muzy. Log-infinitely divisible multifractal processes. Communications in Mathematical Physics, 236(3):449–475, 2003.

[130] Emmanuel Bacry, Laurent Duvernet, and Jean-François Muzy. Continuous-time skewed multifractal processes as a model for financial returns. Journal of Applied Probability, 49(2):482–502, 2012.

[131] Laurent E. Calvet and Adlai J. Fisher. How to forecast long-run volatility: Regime switching and the estimation of multifractal processes. Journal of Financial Econometrics, 2(1):49–83, 2004.

[132] Emmanuel Bacry, Alexey Kozhemyak, and Jean-François Muzy. Continuous cascade models for asset returns. Journal of Economic Dynamics and Control, 32(1):156–199, 2008.

[133] Tiziana Di Matteo, Tomaso Aste, and Michel M. Dacorogna. Scaling behaviors in differently developed markets. Physica A: Statistical Mechanics and its Applications, 324(1):183–188, 2003.

[134] Tiziana Di Matteo, Tomaso Aste, and Michel M. Dacorogna. Long-term memories of developed and emerging markets: Using the scaling analysis to characterize their stage of development. Journal of Banking & Finance, 29(4):827–851, 2005.

[135] Laurent E. Calvet, Adlai J. Fisher, and Benoit B. Mandelbrot. Large deviations and the distribution of price changes. Cowles Foundation Discussion Paper No. 1165, 1997.

[136] Laurent E. Calvet, Adlai J. Fisher, and Benoit B. Mandelbrot. Multifractality of deutschemark/us dollar exchange rates. Cowles Foundation Discussion Papers 1166, Cowles Foundation for Research in Economics, Yale University, 1997.

[137] Thomas C. Halsey, Mogens H. Jensen, Leo P. Kadanoff, Itamar Procaccia, and Boris I. Shraiman. Fractal measures and their singularities: The characterization of strange sets. Phys. Rev. A, 33:1141–1151, Feb 1986.

[138] Roberto Benzi, Giovanni Paladin, Giorgio Parisi, and Angelo Vulpiani. On the multifractal nature of fully developed turbulence and chaotic systems. Journal of Physics A: Mathematical and General, 17(18):3521, 1984.

[139] Roberto Benzi, Giorgio Parisi, and Società italiana di fisica. Turbulence and Predictability in Geophysical Fluid Dynamics and Climate Dynamics: Proceedings of the International School of Physics "Enrico Fermi," Course LXXXVIII, Varenna on Lake Como, Villa Monastero, 14-24 June 1983. North-Holland, 1985.

[140] Albert-László Barabási and Tamás Vicsek. Multifractality of self-affine fractals. Physical Review A, 44(4):2730, 1991.

[141] Jozef Barunik and Ladislav Kristoufek. On hurst exponent estimation under heavy-tailed distributions. Physica A: Statistical Mechanics and its Applications, 389(18):3844–3855, 2010.

[142] Jan W. Kantelhardt, Stephan A. Zschiegner, Eva Koscielny-Bunde, Shlomo Havlin, Armin Bunde, and H. Eugene Stanley. Multifractal de-

trended fluctuation analysis of nonstationary time series. Physica A: Statistical Mechanics and its Applications, 316(1):87–114, 2002.

[143] C-K Peng, Sergey V. Buldyrev, Shlomo Havlin, Michael Simons, H. Eugene Stanley, and Ary L. Goldberger. Mosaic organization of dna nucleotides. Physical Review e, 49(2):1685, 1994.

[144] Alain Arneodo, Emmanuel Bacry, and Jean-François Muzy. The thermodynamics of fractals revisited with wavelets. Physica A: Statistical Mechanics and its Applications, 213(1):232–275, 1995.

[145] Pierre Goupillaud, Alex Grossmann, and Jean Morlet. Cycle-octave and related transforms in seismic signal analysis. Geoexploration, 23(1):85–102, 1984.

[146] Alexander Grossmann and Jean Morlet. Decomposition of hardy functions into square integrable wavelets of constant shape. SIAM Journal on Mathematical Analysis, 15(4):723–736, 1984.

[147] Emmanuel Bacry, Jean-François Muzy, and Alain Arnéodo. Singularity spectrum of fractal signals from wavelet analysis: Exact results. Journal of Statistical Physics, 70(3):635–674, 1993.

[148] Jean-François Muzy, Emmanuel Bacry, and Alain Arneodo. The multifractal formalism revisited with wavelets. International Journal of Bifurcation and Chaos, 04(02):245–302, 1994.

[149] Boris Podobnik and H. Eugene Stanley. Detrended cross-correlation analysis: A new method for analyzing two nonstationary time series. Phys. Rev. Lett., 100:084102, Feb 2008.

[150] Sergio Arianos and Anna Carbone. Cross-correlation of long-range correlated series. Journal of Statistical Mechanics: Theory and Experiment, 2009(03):P03037, 2009.

[151] Ladislav Kristoufek. Multifractal height cross-correlation analysis: A new method for analyzing long-range cross-correlations. EPL (Europhysics Letters), 95(6):68001, 2011.

[152] Zoltán Eisler and János Kertész. Multifractal model of asset returns with leverage effect. Physica A: Statistical Mechanics and its Applications, 343:603–622, 2004.

[153] Benoit Pochart and Jean-Philippe Bouchaud. The skewed multifractal random walk with applications to option smiles. Quantitative finance, 2(4):303–314, 2002.

[154] Emmanuel Bacry, Jean Delour, and Jean-François Muzy. Modelling financial time series using multifractal random walks. Physica A: Statistical Mechanics and its Applications, 299(1):84–92, 2001.

[155] Laurent E. Calvet, Adlai J. Fisher, and Samuel B. Thompson. Volatility comovement: a multifrequency approach. Journal of econometrics, 131(1):179–215, 2006.

[156] Ruipeng Liu. Multivariate multifractal models: Estimation of parameters and applications to risk management. PhD thesis, Christian-Albrechts Universität Kiel, 2008.

[157] Julien Idier. Long-term vs. short-term comovements in stock markets: the use of markov-switching multifractal models. The European Journal of Finance, 17(1):27–48, 2011.

[158] Jean-François Muzy, Didier Sornette, Jean Delour, and Alain Arneodo. Multifractal returns and hierarchical portfolio theory. Quantitative Finance, 1(1):131–148, 2001.

[159] Jean-Philippe Bouchaud, Marc Potters, and Martin Meyer. Apparent multifractality in financial time series. The European Physical Journal B-Condensed Matter and Complex Systems, 13(3):595–599, 2000.

[160] Wei-Xing Zhou. The components of empirical multifractality in financial returns. EPL (Europhysics Letters), 88(2):28004, 2009.

[161] Jozef Barunik, Tomaso Aste, Tiziana Di Matteo, and Ruipeng Liu. Understanding the source of multifractality in financial markets. Physica A, 391:4234, 2012.

[162] Elena Green, William Hanan, and Daniel Heffernan. The origins of multifractality in financial time series and the effect of extreme events. The European Physical Journal B, 87(6):1–9, 2014.

[163] Stanisław Drożdż, Jarosław Kwapień, Paweł Oświecimka, and Rafal Rak. Quantitative features of multifractal subtleties in time series. EPL (Europhysics Letters), 88(6):60003, 2010.

[164] Jarosław Kwapień and Stanisław Drożdż. Physical approach to complex systems. Physics Reports, 515(3):115–226, 2012.

[165] Norman L Johnson, Samuel Kotz, and Narayanaswamy Balakrishnan. Continuous univariate distributions. Number v. 2 in Wiley series in probability and mathematical statistics: Applied probability and statistics. Wiley & Sons, 1995.

[166] Hiroya Nakao. Multi-scaling properties of truncated lévy flights. Physics Letters A, 266(4):282–289, 2000.

[167] A. V. Chechkin and V. Yu Gonchar. Self and spurious multi-affinity of ordinary levy motion, and pseudo-gaussian relations. Chaos, Solitons & Fractals, 11(14):2379 – 2390, 2000.

[168] Karim Abadir and Jan Magnus. The central limit theorem for student's distribution. Econometric Theory, 20(6):1261–1263, 2004.

[169] Darko Stošić, Dusan Stošić, Tatijana Stošić, and H. Eugene Stanley. Multifractal analysis of managed and independent float exchange rates. Physica A: Statistical Mechanics and its Applications, 428:13–18, 2015.

[170] Raffaello Morales, Tiziana Di Matteo, and Tomaso Aste. Non-stationary multifractality in stock returns. Physica A: Statistical Mechanics and its Applications, 392(24):6470–6483, 2013.

[171] Ying-Hui Shao, Gao-Feng Gu, Zhi-Qiang Jiang, Wei-Xing Zhou, and Didier Sornette. Comparing the performance of fa, dfa and dma using different synthetic long-range correlated time series. Scientific reports, 2, 2012.

[172] Jean-Philippe Bouchaud, Marc Mézard, and Marc Potters. Statistical properties of stock order books: empirical results and models. Quantitative finance, 2(4):251–256, 2002.

[173] Maurice S. Bartlett. On the theoretical specification and sampling properties of autocorrelated time-series. Supplement to the Journal of the Royal Statistical Society, 8(1):27–41, 1946.

[174] Henri Theil. Economic forecasts and policy. Amsterdam : North-Holland Pub. Co, 2nd rev. ed edition, 1961. Includes bibliographical references.

[175] Peter Bloomfield and William Steiger. Least absolute deviations curve-fitting. SIAM Journal on Scientific and Statistical Computing, 1(2):290–301, 1980.

[176] Benoit B. Mandelbrot. Fractals and Scaling in Finance: Discontinuity, Concentration, Risk. Selecta Volume E. Springer Science & Business Media, 2013.

[177] Jeffrey R. Russell and Robert F. Engle. Analysis of high-frequency data. Handbook of financial econometrics, 1:383–426, 2009.

[178] Alexandre Dupuis and Richard B. Olsen. High Frequency Finance: Using Scaling Laws to Build Trading Models, pages 563–584. John Wiley & Sons, Inc., 2012.

[179] Thomas Lux and Michele Marchesi. Scaling and criticality in a stochastic multi-agent model of a financial market. Nature, 397(6719):498, 1999.

[180] Nicolò Musmeci, Tomaso Aste, and Tiziana Di Matteo. Relation between financial market structure and the real economy: Comparison between clustering methods. PloS one, 10(3):e0116201, 2015.

[181] Nicolò Musmeci, Tomaso Aste, and Tiziana Di Matteo. Interplay between past market correlation structure changes and future volatility outbursts. Scientific Reports, 6:36320, 2016.

[182] Christian Borghesi, Matteo Marsili, and Salvatore Micciche. Emergence of time-horizon invariant correlation structure in financial returns by subtraction of the market mode. Physical Review E, 76(2):026104, 2007.

[183] Jean Dickinson Gibbons. Nonparametric Statistical Inference. M. Dekker, New York, 1985.

[184] Valery A. Kalyagin, Panos M. Pardalos, and Themistocles M. Rassias. Network Models in Economics and Finance. Springer Optimization and Its Applications. Springer International Publishing, 2014.

[185] M. Hollander, D.A. Wolfe, and E. Chicken. Nonparametric Statistical Methods. Wiley Series in Probability and Statistics. Wiley, 2013.

[186] Kunihiro Baba, Ritei Shibata, and Masaaki Sibuya. Partial correlation and conditional correlation as measures of conditional independece. Australian & New Zealand Journal of Statistics, 46(4):657–664, 2004.

[187] Jan Kmenta. Elements of econometrics. Macmillan series in economics. Macmillan, 1971.

[188] Dennis Chung and Karel Hrazdil. Liquidity and market efficiency: A large sample study. Journal of Banking & Finance, 34(10):2346 – 2357, 2010.

[189] N. C. Kenkel and D. J. Walker. Fractals in the biological sciences. Coenoses, pages 77–100, 1996.

[190] Xiaodong Yang, Xinbao Ning, and Jun Wang. Multifractal analysis of human synchronous 12-lead ecg signals using multiple scale factors. Physica A: Statistical Mechanics and its Applications, 384(2):413 – 422, 2007.

[191] Luciano Telesca, Vincenzo Lapenna, and Maria Macchiato. Multifractal fluctuations in earthquake-related geoelectrical signals. New Journal of Physics, 7(1):214, 2005.